PIPELINE TRANSIENTS IN HIGHLY SATURATED FLUIDS WITH GASEOUS AND VAPOROUS CAVITATION

Thesis for the Degree of M. S.

MICHIGAN STATE UNIVERSITY

MARK J. SUNDQUIST

1977

ABSTRACT

PIPELINE TRANSIENTS IN HIGHLY SATURATED FLUIDS WITH GASEOUS AND VAPOROUS CAVITATION

By

Mark J. Sundquist

Recently, hydraulic transients in pipes which include multi-phase flows and gas release have received considerable attention. A lack of understanding of the gas release phenomena in turbulent pipe flow has resulted in difficulty to correctly model gas release during transient conditions. In addition, due to the variable wave speed associated with these mixtures, questions arise as to the selection of a numerical technique to accurately model the governing differential equations.

In this study a mathematical model is developed to simulate hydraulic transients in two-component, gas-liquid mixtures including distributed gas evolution. The numerical technique is the method of characteristics using specified distance and time intervals. Due to the variable wave speed, an interpolation scheme is developed which reduces the severity of interpolation errors as compared to the conventional interpolation scheme.

To obtain a quantitative understanding of the nature of gas release under turbulent conditions, the experimental phase of this study includes the measurement of the amount of gas released from agitated water saturated with carbon dioxide gas in a closed container. This experiment provides a basis from which a gas release model is developed for use in

the numerical simulation of transient pipe flow. Pressure transients are recorded from a 400 ft. copper pipeline in which water saturated with carbon dioxide is the transported fluid. Initial steady-state pressures are above the gas saturation pressure of the water resulting in essentially one-phase flow. A quick valve closure initiates the transient resulting in column separation and, owing to gas release, a developing two-component flow situation.

Numerical simulations are conducted for the laboratory conditions. Good agreement of peak pressures and timing of the primary pressure peaks are obtained; however, higher order pressure fluctuations traveling along the pipe are not simulated, possibly due to inaccuracies in predicting the evolution of gas along the pipe.

PIPELINE TRANSIENTS IN HIGHLY SATURATED FLUIDS WITH GASEOUS AND VAPOROUS CAVITATION

By

Mark J. Sundquist

A THESIS

Submitted to
Michigan State University
in partial fulfillment of the requirements
for the degree of

MASTER OF SCIENCE

Department of Civil and Sanitary Engineering

1977

ACKNOWLEDGMENTS

The writer wishes to express sincere appreciation to his major professor, Dr. David C. Wiggert, for his invaluable guidance, encouragement and support and to Dr. David A. McIntosh for his suggestions and interest. The writer also wishes to thank Dr. E. B. Wylie of the University of Michigan for his helpfulness and interest in this study. Appreciation is also expressed to the University of Michigan for their generosity in extending to this study the use of the Van Slyke apparatus, dead weight tester and copper coil.

This study was supported in part by the National Science Foundation, Grant No. 74-06653, and by the Department of Civil Engineering of Michigan State University. The writer expresses his appreciation of this financial support.

The writer also wishes to acknowledge the numerous friendships acquired over the past years for making the stay at this university a most memorable and enjoyable experience.

TABLE OF CONTENTS

Chapter Page

LIST OF TABLES

LIST OF FIGURES

NOMENCLATURE

A	pipe cross-sectional area	L^2
a	wave speed in pipe	LT^{-1}
a'	total height of oscillation	L
C	grid point on x-t plane	
C^+, C^-	characteristic curves	
C', C"	grid points on x-t plane	
c	pipe constraint factor	
c'	gas concentration in water	ML^{-3}
c'_o	gas concentration at bubble surface	ML^{-3}
c'_∞	gas concentration far away from the bubble	ML^{-3}
D	pipe diameter	L
D'	diffusion coefficient	L^2T^{-1}
E	pipe elastic modulus	$ML^{-1}T^{-2}$
e	pipe wall thickness	L
F_x	Force in the x-direction in the momentum equation	MLT^{-2}
f	Darcy-Weisbach friction factor	
H	hydraulic gradeline	L
K_g	bulk modulus of elasticity of the gas	$ML^{-1}T^{-2}$
K_ℓ	bulk modulus of elasticity of the liquid	$ML^{-1}T^{-2}$
k	universal gas constant	
L	grid point on x-t plane	
L	length of pipe segment	L

M	grid point on x-t plane	
N	moles of gas in bubble	
n, n"	number of distance increments used in interpolation scheme	
n'	polytropic gas constant	
P	grid point on x-t plane	
p	internal pipe pressure	$ML^{-1}T^{-2}$
p_o	reference pressure	$ML^{-1}T^{-2}$
p_f	fluid pressure	$ML^{-1}T^{-2}$
p_v	vapor pressure of fluid	$ML^{-1}T^{-2}$
Δp	difference between gas saturation pressure of the fluid and the instantaneous pressure	$ML^{-1}T^{-2}$
R	bubble radius	L
r	location on x-t grid where the C^+ characteristic intersects a distance line	
s	location on x-t grid where the C^- characteristic intersects a distance line	
T	fluid temperature	
T_o	reference temperature	
t	time	T
Δt	specified time increment of x-t grid	T
u	mixture velocity or velocity of right side of vapor void	LT^{-1}
u_L	velocity of left side of vapor void	LT^{-1}
u'	relative velocity of fluid to a gas bubble	LT^{-1}
V	volume	L^3
V_b	volume of gas bubble	L^3
v	velocity vector	LT^{-1}
X	grid point on x-t plane	
x	distance along pipe	L

Δx	specified distance increment of x-t grid	L
Y	location on the x-t grid where a characteristic curve intersects the boundary	
Z	grid point on x-t plane	
z	elevation above datum	L
α	void fraction	
β	Henry's Law solubility gas constant	
Γ	gas production rate	$MT^{-1}L^{-3}$
γ_{ℓ}	unit weight of liquid	$ML^{-2}T^{-2}$
γ_{m}	unit weight of mixture	$ML^{-2}T^{-2}$
ζ	interpolation location between fixed nodes	
ζ'	interpolation location used in conventional interpolation scheme	
θ	angle of pipe inclination	
λ	characteristic roots	
ρ_{g}	density of gas	ML^{-3}
ρ_{ℓ}	density of liquid	ML^{-3}
σ	surface tension	MT^{-2}
τ_{o}	pipe wall shear stress	$ML^{-1}T^{-2}$
ϕ	flow parameter or dummy variable of integration	
ω	frequency	T^{-1}

CHAPTER I

INTRODUCTION

1.1 Description of the Problem

The transient analysis of a piping system is of importance when designing for peak pressures and flows. Through the operation of system components such as valves and pumps, pressure wave propagation will take place in the system. This may result in the local pressure at some point reaching vapor pressure of the liquid initiating vapor cavity growth. This phenomenon is commonly referred to as column separation. The impending collapse of the cavity may result in large pressures which may damage the pipe or other system components.

The presence of even a small amount of entrained gas can significantly change the transient response. If any entrained gas is present or if the fluid has the capacity to release gas during the transient, an analysis which neglects this effect will predict transient pressures which are more severe than will actually occur.

In a pipe, two types of cavitation can be distingushed. According to Henry's Law, if at any time the pressure falls below the saturation pressure of the liquid, the dissolved gas will evolve out of solution in the form of free gas. Conversely, if the pressure is greater than the existing gas saturation pressure, any free gas will dissolve into solution until equilibrium is reached. However, the evolution rate is faster than the solution rate. Therefore, during a transient in which the pressure-time history oscillates about the gas saturation

pressure of the fluid, a condition of rectified diffusion will exist resulting in a net gain of free gas with each cycle. The presence of this free gas results in a two-phase flow situation. The celerity of this mixture is reduced due to the added compressibility of the gas and can be smaller than either the gas or liquid celerities. This reduced wave speed will lead to attentuated pressure peaks and phase changes. This process of evolution of free gas is called gaseous cavitation.

In addition to gaseous cavitation, if the fluid pressure falls to its vapor pressure, vaporous cavitation will occur. This is an explosive process which results from the vaporous growth of sub-macroscopic nuclei containing liquid vapor and free gas. This phenomenon accounts for the flashing behind a negative pressure wave and in the most severe situation, for column separation.

As outlined by Van Wijngaarden [22] the rate of growth for a single bubble neglecting viscous forces and assuming the growth is slow is estimated to be

$$\frac{dV_b}{dt} = \frac{kT}{p_f - p_v + (\frac{4}{3})(\sigma/R)} \frac{dN}{dt}$$

where V_b is the bubble volume, t is time, k is the universal gas constant, T is the temperature, p_f is the fluid pressure, p_v is the vapor pressure of the fluid, σ is the coefficient of surface tension, R is the bubble radius and N is the moles of gas in the bubble.

The quantity dN/dt is the molar flux of gas into the bubble and represents the diffusive process of gaseous cavitation. As described by Van Wijngaarden, this quantity is dependent upon the diffusion coefficient, the bubble radius, the transport velocity around the bubble

and the gas concentration gradient in the liquid.

If the denominator in the right-hand side of the above equation does not vanish, then the growth of the bubble is governed by the gaseous diffusion term. These growth rates will have finite values and can be termed gaseous cavitation.

If, however, the denominator is zero, which implies that

$$p_f = p_v - \frac{4}{3}\frac{\sigma}{R}$$

then the growth rate would become infinite. This pressure then marks the threshold for vaporous cavitation.

For an accurate description of vaporous cavitation, higher order terms should be included in the growth equation. Then a finite growth rate of the bubble at the threshold vaporous cavitation pressure would result. However, these growth rates would still be very large as compared to the gaseous cavitation growth rates.

Parkin and Kermeen [15] have found that the time required for vaporous cavitation is of the order of a few microseconds as compared with hundreds of milliseconds to achieve any significant gaseous cavitation. However, vaporous cavitation does enhance gaseous cavitation by creating large bubbles in which the mass transfer of gas can occur. Since portions of a pipe may experience vapor pressure conditions for extended periods, such as severe column separation cases, significant gas release can occur.

The importance of considering gaseous cavitation and its effects during a pressure transient depends upon the liquid being transported, the type of gas, and the extent to which it is dissolved into the liquid. In some cases, such as short lines transporting water which

has a small dissolved air content, unless steady state pressures are below the gas saturation pressure, it is probable that very little gas is released and essentially one-phase flow exists. In this case, a waterhammer analysis neglecting gas release should accurately predict the system response. In long lines where the transient pressures may exist below the gas saturation pressure for extended times, or in highly soluble solutions such as water and carbon dioxide, significant gas release may occur and should be considered to correctly model the physical system.

The effects of released gas on hydraulic transients has lacked rational interpretations. In part, this is caused by a lack of transient data which shows significant gas release. It is hoped that this study gives insight into the effects of released gas through the presentation of comprehensive laboratory data. In addition, the numerical aspects, which are concerned with accurately modeling the phenomena involved, are hoped to provide a reliable means of predicting gas release transients.

1.2 Literature Review

It is well accepted that the presence of submacroscopic nuclei is required to initiate vaporous and gaseous cavitation [6,15,17] . These nuclei can be small gas-filled pockets in the crevices of the container or gas pockets on particles within the free stream of the flow. Epstein and Plesset [4] developed solutions for the rate of growth of a bubble by diffusion neglecting translational motion of the bubble. Parkin and Kermeen [15] improved on their approach by deriving equations to handle bubble growth by convective diffusion. They established that the growth time is several orders of magnitude greater when considering the effects

of water transport around the bubble than without transport. They also noted that these growth times are very much greater than comparable vaporous growth.

Parkin and Kermeen also collected data on the growth of bubbles attached to a body submerged in a free stream. It was suggested that the diffusive growth of these small gas bubbles then served as nuclei for vaporous growth as they were swept downstream. They were able to predict the data within an order of magnitude. Also included in their experimental investigation was the measurement of the minimum pressure achieved by water just before vaporous cavitation inception. They found that ordinary water in the tunnel did experience a tensile stress. The tension required for inception increased as the free-stream velocity increased. Once cavitation occurred, the tension was relieved suggesting the possibility that tension in the water is required, if for only an instant, to initiate vaporous cavitation.

Van Wijngaarden [22] tried to improve the analytic approach to convective diffusion by including the effects of surface tension and vapor pressure. In his development he showed that tensile stresses can be reached before vaporous cavitation due to the surface tension of the nuclei. He obtained a slightly better agreement of the data obtained by Parkin and Kermeen.

Schweitzer and Szebehely [17] conducted experiments in which they measured gas release in a closed container with an agitated air-liquid interface. Using an indirect method in which the pressure of the air volume of the container was measured, they found that the gas released exponentially with time for a step decrease in pressure. Included in their formulations is the presence of an experimentally determined time constant which characterizes the rate of release. This time constant

is a function of the air-liquid volume ratio in the container.

In studying the transient pressures on the downstream side of a closing valve in a kerosene pipeline, Swaffield [20] included the influence of air release. He assumed that the volume of fluid to release air was just that which passed through the valve since closure began. He also assumed no resolution and a simple adiabatic compression and expansion of the air involved. His experimental data showed transient pressures that were always above vapor pressure indicating that vaporous cavitation did not occur and that the column separation void behind the valve contained mostly air caused by gas release. In his model he used a complicated boundary condition at the valve to handle the effects of the released gas at that point. The model incorporated the method of characteristics using a constant wave speed, and Henry's Law was used to calculate the volume of air released. He obtained better agreement with experimental data when including air release than with just a vapor-filled cavity.

To improve on Swaffield's model, Driels [3] used the results of Schweitzer and Szebehely in predicting transient pressures in a kerosene-filled pipeline. He utilized the same assumptions and boundary conditions as Swaffield but included Schweitzer's experimental time constant to determine the time-dependent nature of gas release. He was successful in predicting the first pressure rise but had less success in predicting the magnitude and timing of the secondary peaks.

Kranenburg [8,9] developed a model in which he accounted for gas release into existing nuclei. He describes two flow regimes, one being column separation which is characterized by free surface flow, the other as cavitating flow which is of a bubbly nature due to the

presence of dispersed gas and vapor bubbles. In his analytical development he considers the gas release which occurs into an individual nucleus; then assuming the number of nuclei present, their size, and relative velocity to the free stream, calculates the gas release occurring throughout the pipe during transient conditions. He utilizes a Lax-Wendroff scheme with a variable wavespeed due to its ability to spread a developing shock over a number of mesh points. He attained good agreement with experimental data from a long pipeline in which water with some dissolved air content was used as the working fluid. A pump failure and restart were used to initiate the transients. In studying the experimental results of Swaffield [20] and Baltzer [2], he concluded that gas release has no great influence in cases where only cavitating flow occurs, whereas the influence is considerable in cases where column separation combined with cavitating flow exist.

Martin, Padmanabhan and Wiggert [14] investigated hydraulic transients in two-phase, bubbly, air-water mixtures. Their laboratory experiments were concerned with initial void fractions that were large as compared to a developing, two-phase flow due to gas release. Included in their equation development is the provision for a gas release rate. In their study both the Lax-Wendroff scheme and the method of characteristics were used and compared. Due to the convergence of like characteristics during the formation of shocks, the Lax-Wendroff scheme was favored. However, the two schemes produced identical results in cases where no shock developed. Good agreement was obtained with two-phase experimental data where there was no gas production.

In a more recent study Tullis, Streeter and Wylie [21] developed two models to simulate gas release during pressure transients. To

account for the variable wave speed the method of characteristics using a characteristics grid was employed with occasional interpolations to straighten the grid. A constant gas release rate was assumed whenever the pressure dropped below the gas saturation pressure. In the second model, the air was concentrated at the computing sections while keeping the full liquid wave speed between the computing nodes, thereby allowing the method of specified time intervals to be used. The two models produced nearly identical transients in cases where the same amount of air was released. It was shown that by concentrating the air at computing points, the effective overall system wave speed can be reduced thereby correctly simulating the variable wave speed phenomenom. Thus, they concluded that the air does not have to be homogenously dispersed to accurately model gas release transients. They also concluded that in cases where little air is released there may be an apparent thermodynamic loss associated with the vaporization process. To account for this effect a linear dissipation was added to the model. With such dissipation, satisfactory agreement with experimental data in which only small amounts of air were released was attained.

1.3 Scope of Investigation

As cited in the literature review, little is known about the process and time rates of gas release occurring in a closed conduit. This can be seen by the large number of arbitrary values used in past models describing the rate of gas release. To attain a better understanding of this problem, a bench-top experiment was conducted in which a closed vessel completely filled with gas-saturated water was subjected to a step decrease in pressure under agitated conditions. Measurement of the amount of gas released provided insight for approximating a rate

of gas release function for turbulent flow conditons in a closed circuit.

A laboratory investigation was conducted to observe the effects of released gas on hydraulic transients. Tests were carried out in a 400 ft. long copper pipe of one inch diameter with a quick-closing solenoid-actuated valve. The transported fluid was water which was saturated with carbon dioxide. Since CO_2 is much more soluble in water than air, (approximately 47 times more soluble at $20^{o}C$ according to Henry's Law) significant gas release during the transient occurred. Systematic changes of pertinent variables, primarily the dissolved gas content and initial pressure provided important information regarding the effects of gas release on the system response.

The analytical aspects are concerned with the development of the governing partial differential equations which describe the transient flow regime, including the distributed evolution of gas and the subsequent two-phase flow. The method of characteristics is then used to numerically solve the governing equations. Attempts are then made to numerically predict the transient flows observed in the experiments.

CHAPTER II

EQUATION DEVELOPMENT

To describe the analytical nature of two-phase transients, the conservation of the mass of the liquid and gas phases along with the conservation of momentum of the mixture will be developed using the control volume approach. Unlike the usual waterhammer analysis where one is concerned with only the fluid, the presence of the gas entrained in the fluid requires the added consideration of its behavior in the control volume. In addition, the production or resolution of any free gas in the control volume must also be considered. These equations will then form a basis from which a numerical solution can proceed to obtain values for the dependent variables velocity, pressure and void fraction as functions of the independent variables distance and time.

The following assumptions are made with respect to the flow regime:

1. The flow is one dimensional.
2. The fluid mixture is of a homogeneous two-phase, bubbly nature.
3. The difference in pressure across a bubble surface can be ignored.
4. The momentum of the gas phase relative to the liquid phase is small and therefore neglected. Hence, the liquid and bubble velocities in the development are the same.
5. The average cross-sectional values of void fraction, mixture velocity and phase densities can be used, that is;

$$\langle\phi\rangle = \frac{1}{A}\int_A \phi \, dA$$

where A is the cross-sectional area and ϕ represents the fluid property. Henceforth, the symbol <> will be omitted and average properties will be assumed unless otherwise stated.

2.1 The Conservation of Mass of the Liquid Phase

The conservation of mass for the liquid component requires that the time rate of increase of mass within a control volume is just equal to the net rate of mass inflow to the control volume. Figure 1 shows the mass flow of liquid into a control volume of length δx. The flow is normal to the control surface at surfaces 1 and 2.

Applying the law of conservation of mass to the liquid in the control volume, as outlined by Yadigaroglu and Lahey [24], results in the differential form

$$\frac{\partial}{\partial t}[\rho_\ell(1-\alpha)A] + \frac{\partial}{\partial x}[\rho_\ell(1-\alpha)Au] = -\Gamma A \qquad (1)$$

where Γ is the gas production rate per unit volume of mixture, ρ_ℓ is the liquid density, A is the cross-sectional area, u is the liquid velocity and α is the void fraction, defined as the ratio of the volume of the gas to the control volume.

Expanding Equation (1) and grouping derivatives results in

$$\frac{\partial u}{\partial x} + \frac{1}{A}\left(u\frac{\partial A}{\partial x} + \frac{\partial A}{\partial t}\right) + \frac{1}{(1-\alpha)}\left[u\frac{\partial(1-\alpha)}{\partial x} + \frac{\partial(1-\alpha)}{\partial t}\right] +$$

$$\frac{1}{\rho_\ell}\left(u\frac{\partial \rho_\ell}{\partial x} + \frac{\partial \rho_\ell}{\partial t}\right) = \frac{-\Gamma}{\rho_\ell(1-\alpha)} \qquad (2)$$

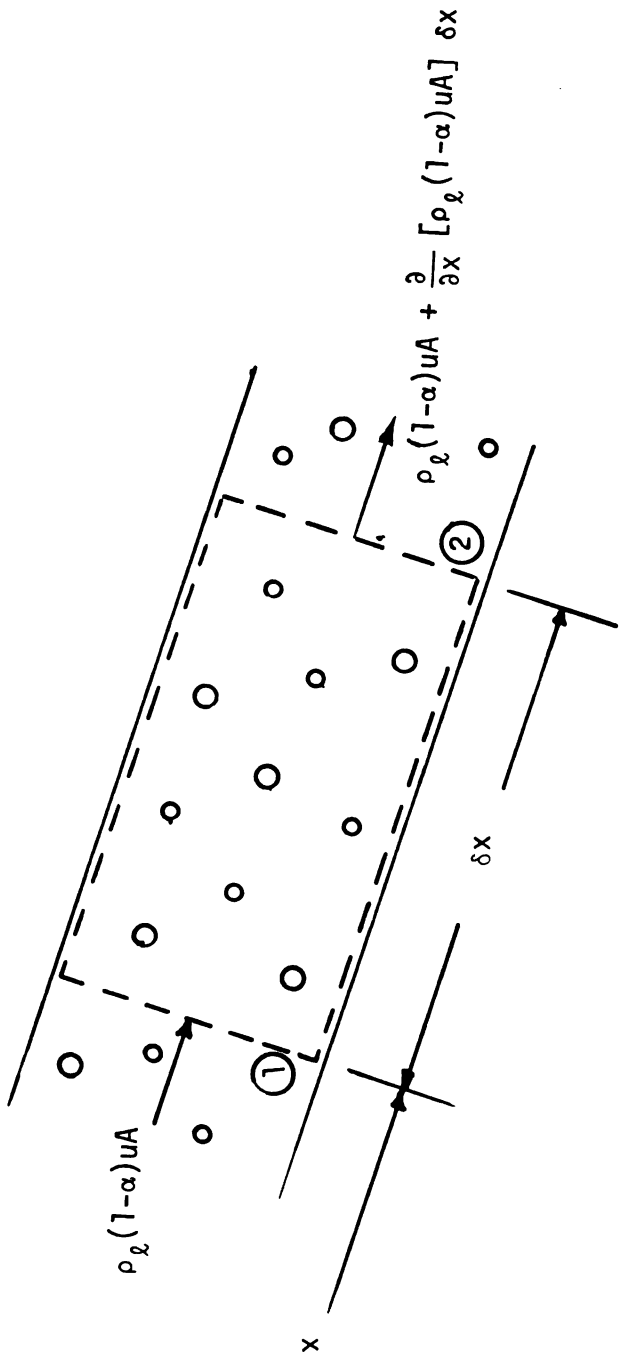

Figure 1. Control Volume for Conservation of Mass of Liquid.

Identifying the total derivative with respect to time as

$$\frac{d}{dt} = u \frac{\partial}{\partial x} + \frac{\partial}{\partial t} \tag{3}$$

Equation (2) becomes

$$\frac{\partial u}{\partial x} + \frac{1}{A}\frac{dA}{dt} + \frac{1}{(1-\alpha)}\frac{d(1-\alpha)}{dt} + \frac{1}{\rho_\ell}\frac{d\rho_\ell}{dt} = \frac{-\Gamma}{\rho_\ell(1-\alpha)} \tag{4}$$

Considering the bulk modulus of elasticity of the liquid as

$$K_\ell = \rho_\ell \frac{dp}{d\rho_\ell} = \rho_\ell \frac{dp/dt}{d\rho_\ell/dt} \tag{5}$$

where dp/dt is the total derivative of the pressure with respect to time, then from Equation (5) it is seen that

$$\frac{1}{\rho_\ell}\frac{d\rho_\ell}{dt} = \frac{1}{K_\ell}\frac{dp}{dt} \tag{6}$$

The second term of Equation (4) describes the radial deformation of the pipe. By considering the radial stresses and strains and using Poisson's ratio it can be shown [19] that

$$\frac{1}{A}\frac{dA}{dt} = \frac{Dc}{Ee}\frac{dp}{dt} \tag{7}$$

where D is the pipe diameter, c is the pipe constraint factor that characterizes the anchorage of the pipe, E is Young's modulus of the pipe and e is the thickness of the pipe wall.

Substitutions of Equations (6) and (7) into Equation (4) yields

$$\left[\frac{Dc}{Ee} + \frac{1}{K_\ell}\right]\frac{dp}{dt} + \frac{\partial u}{\partial x} - \frac{1}{(1-\alpha)}\frac{d\alpha}{dt} = \frac{-\Gamma}{\rho_\ell(1-\alpha)} \tag{8}$$

Equation (8) describes, in differential form, the conservation of mass of the liquid, including the compressibility of the liquid and pipe wall, of a two-phase gas-liquid mixture in which gas generation can occur.

2.2 The Conservation of Mass of the Gas Phase

Consider the control volume of length δx of Figure 2. Represented is the mass flow rate of gas into the control volume. Applying the law of conservation of mass to the gas in the control volume, as outlined by Yadigaroglu and Lahey [24], results in

$$\frac{\partial}{\partial t}\left(\rho_g \alpha A\right) + \frac{\partial}{\partial x}\left(\rho_g \alpha A u\right) = \Gamma A \tag{9}$$

Expanding Equation (9) and grouping derivatives results in

$$\frac{\partial u}{\partial x} + \frac{1}{A}\left[u\frac{\partial A}{\partial x} + \frac{\partial A}{\partial t}\right] + \frac{1}{\alpha}\left[u\frac{\partial \alpha}{\partial x} + \frac{\partial \alpha}{\partial t}\right] + \frac{1}{\rho_g}\left[u\frac{\partial \rho_g}{\partial x} + \frac{\partial \rho_g}{\partial t}\right] = \frac{\Gamma}{\rho_g \alpha} \tag{10}$$

Using Equation (3) to recognize the total derivatives with respect to time yields

$$\frac{\partial u}{\partial x} + \frac{1}{A}\frac{dA}{dt} + \frac{1}{\alpha}\frac{d\alpha}{dt} + \frac{1}{\rho_g}\frac{d\rho_g}{dt} = \frac{\Gamma}{\rho_g \alpha} \tag{11}$$

Substituting Equation (6) as it applies to the gas phase and Equation (7) into Equation (11) yields

$$\left[\frac{1}{Kg} + \frac{Dc}{Ee}\right]\frac{dp}{dt} + \frac{\partial u}{\partial x} + \frac{1}{\alpha}\frac{d\alpha}{dt} = \frac{\Gamma}{\rho_g \alpha} \tag{12}$$

Equation (12) describes, in differential form, the conservation of mass of the gas, including the compressibility of the gas and pipe wall, for

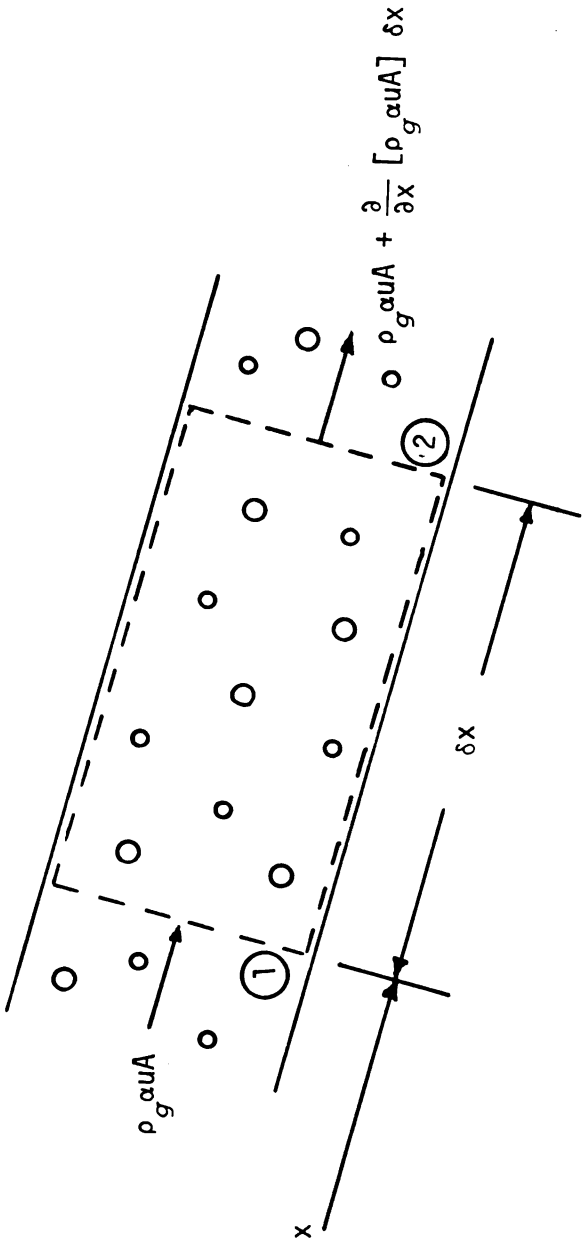

Figure 2. Control Volume for Conservation of Mass of Gas.

a two-phase, gas-liquid mixture in which gas generation can occur.

2.3 Mixture Momentum

In the development of the momentum equation the mass of the mixture will be considered. The equation of motion states that the resultant of the external forces acting on a control volume must be equivalent to the net flux of linear momentum from the control volume and the time rate of change of linear momentum within the volume. In integral form it is expressed as

$$\sum F_x = \frac{\partial}{\partial t} \int_{c.v.} \rho\, u\, dv + \int_{c.s.} \rho\, u^2\, dA \qquad (13)$$

Figure 3 shows a control volume of length δx and the external forces acting on it.

Evaluating Equation (13) over the control volume and recognizing that the mixture density is given by

$$\rho_m = \rho_\ell (1 - \alpha) + \rho_g\, \alpha \qquad (14)$$

results in the differential form of the mixture momentum equation as

$$-\frac{\partial}{\partial x}(pA)\delta x + \gamma_m A \sin \Theta\, \delta x - \tau_o \pi D\, \delta x + p \frac{\partial A}{\partial x} \delta x =$$

$$\frac{\partial}{\partial t}\left[\rho_m\, uA\delta x\right] + \frac{\partial}{\partial x}\left[\rho_m\, u^2 A\right] \delta x \qquad (15)$$

where τ_o is the wall shear stress, γ_m is the unit weight of the mixture and Θ is the angle of pipe inclination with the horizontal. Dividing

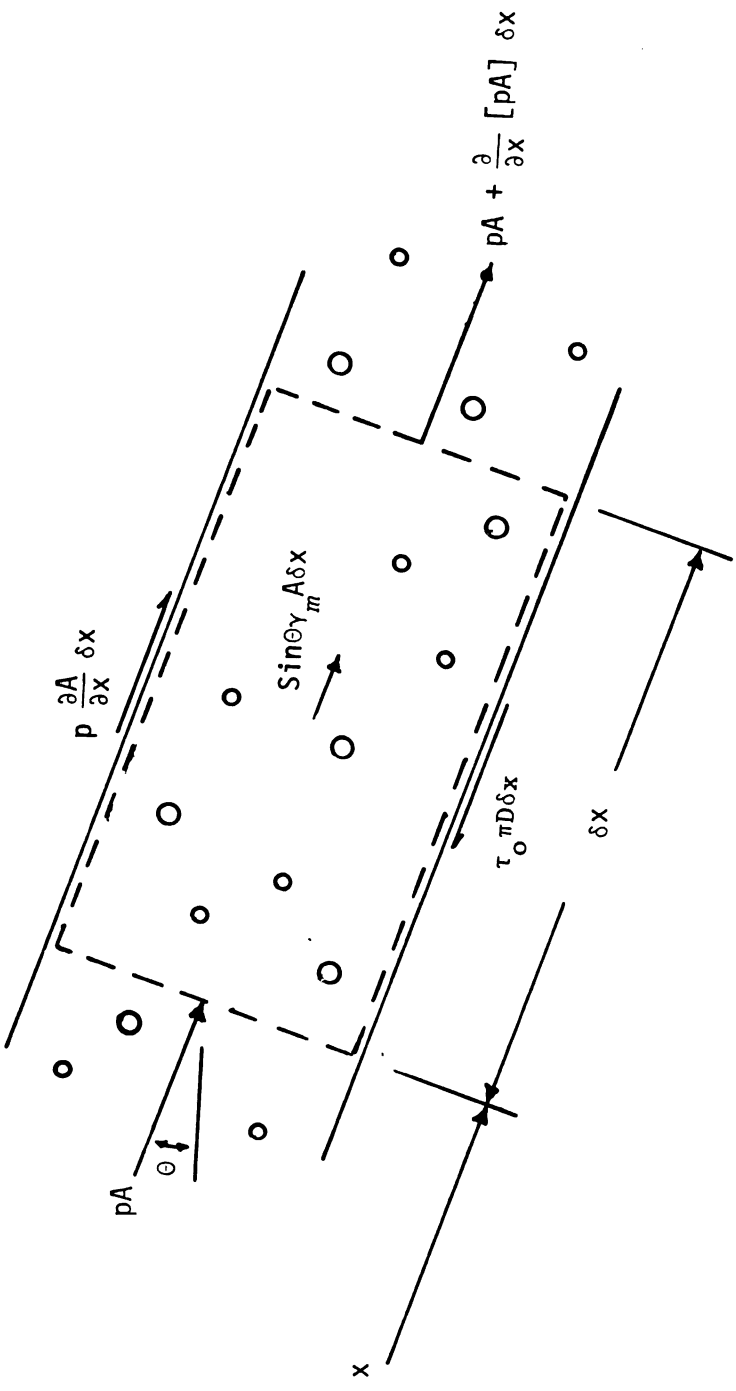

Figure 3. Control Volume for Mixture Momentum Equation.

Equation (15) by δx and expanding yields

$$- \frac{\partial}{\partial x}(pA) + \gamma_m A \sin\theta - \tau_o \pi D + p\frac{\partial A}{\partial x} = \rho_m A \frac{\partial u}{\partial t} + uA\rho_m \frac{\partial u}{\partial x}$$

$$+ u\frac{\partial}{\partial t}(A\rho_m) + u\frac{\partial}{\partial x}(u A\rho_m) \qquad (16)$$

By the combination of the continuity Equations (1) and (9), it can be shown that the last two terms on the right-hand side of Equation (16) sum to zero. In addition, since we are dealing with very low void fraction situations in which $\alpha << 1$, then $\rho_g \alpha << \rho_\ell(1 - \alpha)$ and the mixture density and mixture unit weight can be approximated by

$$\rho_m \cong \rho_\ell (1 - \alpha) \qquad (17)$$

$$\gamma_m \cong \rho_\ell (1 - \alpha)g \qquad (18)$$

The wall shear stress is generally taken as the steady-state shear stress for the same velocity;

$$\tau_o = \rho_\ell(1 - \alpha)\, f\, u\, |u|\, /8 \qquad (19)$$

where f is the Darcy-Weisbach friction factor based on one-component flow [13]. The absolute value of the velocity is taken such that the shear stress opposes the direction of the flow. Substituting Equations (17), (18) and (19) into Equation (16) and rearranging yields

$$\frac{du}{dt} + \frac{1}{\rho_\ell(1 - \alpha)}\frac{\partial p}{\partial x} + \frac{f\, u|u|}{2D} - g \sin\theta = 0 \qquad (20)$$

Equation (20) is the differential form of the conservation of momentum of the gas and liquid mixture. Together with the continuity equations for the gas and liquid, a set of three equations have been described which form a basis from which a numerical solution can proceed. The equations are recognized to be of the hyperbolic type, hence they can be transformed into total derivatives and integrated along characteristic lines. In this manner the equations can be solved simultaneously to obtain values for the dependent variables of velocity, pressure and void fraction.

CHAPTER III

NUMERICAL ANALYSIS

In the last chapter the governing differential equations for two-phase transient pipe flow including gas release were presented. The present task is to develop a numerical technique to obtain accurate values from the simultaneous solution of the governing equations while maintaining numerical errors within acceptable limits.

Except for the presence of nuclei, the initial flow in a piping system may be essentially single phase. As the transient pressures drop below the gas-saturation pressure, gas evolution takes place resulting in a two-phase flow regime. To numerically handle this situation, the grid of characteristics could be used to find explicit solutions, without interpolation errors, of pressure, velocity and void fraction. However, as the void fraction grows, the changing wave speed may badly distort the grid making the simultaneous intersection of the three characteristic equations almost impossible. Since we are dealing with a developing two-phase flow, the void fractions are probably small enough such that shock conditions do not occur. The convergence of like characteristics would signify shock development. If this does occur the Hugoniot relations must be incorporated into the model to handle this internal discontinuity thereby making the programming difficult.

The Lax-Wendroff two-step scheme has the capability to spread a developing shock over a number of mesh points by the introduction of

a numerical viscosity. This scheme is an explicit finite-difference technique of second-order accuracy which requires that the constitutive equations be written in so-called conservation form. Kranenburg [9] found that the amount of numerical damping introduced by this scheme to be acceptable in cases where the nonlinearity does not exceed certain bounds. However, in cases where the pressure dropped to vapor pressure or during shock conditions, additional numerical viscosity was needed to suppress oscillations and instabilities caused by the nonlinearity of the problem. This numerical viscosity was introduced by the addition of a smoothing operation to those nodes in which the solution oscillations were above a prescribed amount.

In light of the undesirable aspects of the two above schemes, the method of characteristics with specified distance and time increments is the numerical technique chosen for this study. Since the computing nodes are located at fixed distance locations, this technique has a particular advantage in the integration of the pathline characteristic along a time line. Ames [1] states that this method will pass weak shocks in a pseudo manner. However, interpolation errors resulting in numerical dissipation of the wavefront are inherent with this method if the cererity is changing in the pipe. To minimize these errors, an interpolation technique, similar to that proposed by Vardy [23], was developed which attempts to reduce them to an acceptable level. Evidence will be presented which demonstrates that interpolations taken outside of a distance increment may reduce the numerical damping associated with interpolations.

3.1 Determination of the Characteristics Equations

The governing equations developed in Chapter 2 form a system of

three quasi-linear, hyperbolic, partial differential equations. Due to their hyperbolic nature they can be transformed into ordinary differential equations along characteristic lines. To find these characteristic equations, the basic equations will first be put into a more suitable form.

With the substitutions

$$b_\ell = \frac{1}{K_\ell} + \frac{Dc}{Ee} \tag{21}$$

$$b_g = \frac{1}{K_g} + \frac{Dc}{Ec} \tag{22}$$

and eliminating dp/dt from Equations (8) and (12) results in

$$\frac{d\alpha}{dt} - \left(\frac{1}{b_\ell} - \frac{1}{b_g}\right)\left[\frac{1}{b_\ell(1-\alpha)} + \frac{1}{b_g\,\alpha}\right]^{-1}\frac{\partial u}{\partial x} = \Gamma\left[\frac{1}{\rho_\ell(1-\alpha)b_\ell} + \frac{1}{\rho_g\, b_g\alpha}\right]\left[\frac{1}{b_\ell(1-\alpha)} + \frac{1}{b_g\,\alpha}\right]^{-1} \tag{23}$$

Eliminating $\frac{\partial u}{\partial x}$ from Equations (8) and (12) yields

$$(b_\ell - b_g)\frac{dp}{dt} - \frac{d\alpha}{dt}\left[\frac{1}{(1-\alpha)} + \frac{1}{\alpha}\right] = -\Gamma\left[\frac{1}{\rho_\ell(1-\alpha)} + \frac{1}{\rho_g\alpha}\right] \tag{24}$$

The hydraulic gradeline H is defined as

$$H = p/\rho_\ell g + z \tag{25}$$

where z is the elevation above a reference datum. Solving Equation (25) for p and differentiating with respect to x and t gives

$$\frac{\partial p}{\partial x} = \rho_\ell g\left(\frac{\partial H}{\partial x} - \frac{\partial z}{\partial x}\right) \tag{26}$$

$$\frac{\partial p}{\partial t} = \rho_\ell g \left(\frac{\partial H}{\partial t} - \frac{\partial z}{\partial t} \right) = \rho_\ell g \frac{\partial H}{\partial t} \tag{27}$$

Equations (26) and (27) were attained assuming

$$g(H - z) \frac{\partial \rho_\ell}{\partial x} << \rho_\ell g \left(\frac{\partial H}{\partial x} - \frac{\partial t}{\partial x} \right) \tag{28}$$

$$g(H - z) \frac{\partial \rho_\ell}{\partial t} << \rho_\ell g \left(\frac{\partial H}{\partial t} - \frac{\partial z}{\partial t} \right) \tag{29}$$

Recognizing that $\partial z/\partial x = -\sin \theta$ and using Equations (26) and (27) the total derivative of p with respect to t is

$$\frac{dp}{dt} = \rho_\ell g \frac{dH}{dt} + u \rho_\ell g \sin \theta \tag{30}$$

Substituting Equation (30) into (24) and rearranging yields

$$\frac{dH}{dt} - \frac{d\alpha}{dt} \left[\frac{1}{1-\alpha} + \frac{1}{\alpha} \right] \left[\rho_\ell \, g(b_\ell - b_g) \right]^{-1} = - \Gamma \left[\frac{1}{\rho_\ell (1-\alpha)} + \frac{1}{\rho_g \alpha} \right]$$

$$\left[\rho_g \, g(b_\ell - b_g) \right]^{-1} - u \sin \theta \tag{31}$$

In addition, substituting Equation (26) into (20) and rearranging gives

$$\frac{du}{dt} + \frac{1}{(1-\alpha)} g \frac{\partial H}{\partial x} = g \sin \theta \left[1 - \frac{1}{(1-\alpha)} \right] - \frac{f u |u|}{2D} \tag{32}$$

Equations (23), (31), and (32) can now be written as

$$\frac{d\alpha}{dt} - \overline{A} \frac{\partial u}{\partial x} = \overline{B} \tag{33}$$

$$\frac{du}{dt} + \overline{C} \frac{\partial H}{\partial x} = \overline{D} \tag{34}$$

$$\frac{dH}{dt} + \overline{E} \frac{d\alpha}{dt} = \overline{F} \tag{35}$$

where the coefficients are

$$\overline{A} = \alpha(1-\alpha)\left(\frac{1}{K_g} - \frac{1}{K_\ell}\right)\left[\frac{Dc}{Ee} + \frac{\alpha}{K_g} + \frac{(1-\alpha)}{K_\ell}\right]^{-1} \tag{36}$$

$$\overline{B} = \Gamma\left[\rho_\ell(1-\alpha)\frac{Dc}{Ee} + \frac{\rho_g\alpha}{K_g} + \frac{\rho_\ell(1-\alpha)}{K_\ell}\right]\left[\rho_g\rho_\ell\left(\frac{Dc}{Ee} + \frac{\alpha}{K_g} + \frac{1-\alpha}{K_\ell}\right)\right]^{-1} \tag{37}$$

$$\overline{C} = \frac{g}{(1-\alpha)} \tag{38}$$

$$\overline{D} = g \sin\theta\left[1 - \frac{1}{(1-\alpha)}\right] - \frac{f\,u\,|u|}{2D} \tag{39}$$

$$\overline{E} = \left[\alpha(1-\alpha)(\rho_\ell g)\left(\frac{1}{K_g} - \frac{1}{K_\ell}\right)\right]^{-1} \tag{40}$$

$$\overline{F} = \Gamma\left[\frac{1}{\rho_\ell(1-\alpha)} + \frac{1}{\rho_g\,\alpha}\right]\left[\rho_\ell\, g\left(\frac{1}{K_g} - \frac{1}{K_\ell}\right)\right]^{-1} - u\sin\theta \tag{41}$$

Arranging Equations (33), (34) and (35) into matrix form yields

$$\begin{bmatrix} 1 & 0 & 0 \\ 0 & 1 & 0 \\ \overline{E} & 0 & 1 \end{bmatrix}\begin{Bmatrix} \alpha \\ u \\ H \end{Bmatrix}_t + \begin{bmatrix} u & -\overline{A} & 0 \\ 0 & u & \overline{C} \\ u\overline{E} & 0 & u \end{bmatrix}\begin{Bmatrix} \alpha \\ u \\ H \end{Bmatrix}_x = \begin{Bmatrix} \overline{B} \\ \overline{D} \\ \overline{F} \end{Bmatrix} \tag{42}$$

The system of Equations (42) is in a convenient form in which to determine the characteristic equations. The approach used will be that of the normal form as outlined by Forsythe and Wasow [5]. The details of this method as applied to Equation (42) can be found in Appendix A.

The eigenvalues or characteristic roots λ for the system of Equations (42) were determined to be

$$\lambda_1 = u \tag{43}$$

$$\lambda_{2,3} = u \pm (\bar{A}\ \bar{C}\ \bar{E})^{\frac{1}{2}} \tag{44}$$

Equations (43) and (44) represent the path lines in the time-distance domain in which the system Equation (42) can be transformed into ordinary differential equations.

It is of interest to expand the last term in Equation (44):

$$a = (\bar{A}\ \bar{C}\ \bar{E})^{\frac{1}{2}} = \left[\rho_\ell(1-\alpha)\left(\frac{Dc}{Ee} + \frac{\alpha}{K_g} + \frac{1-\alpha}{K_\ell}\right)\right]^{-\frac{1}{2}} \tag{45}$$

This is recognized to be the pressure wave propagation speed of a two-phase, bubbly mixture in a closed conduit [14]. In Figure 4 the dependence of the wavespeed upon the void fraction can be seen. Due to the density of the mixture being primarily influenced by the liquid phase and the compressibility governed by the gas phase, the mixture celerity quickly becomes smaller than either the gas or liquid wave speed even at very small void fractions.

Using the characteristic roots, the characteristic or compatibility relations for the system Equation (42) were determined to be

pathline

$$\bar{E}\frac{d\alpha}{dt} + \frac{dH}{dt} - \bar{F} = 0 \tag{46}$$

$$\frac{dx}{dt} = u \tag{47}$$

C^+

$$\frac{a}{\bar{C}}\ \frac{du}{dt} + \frac{dH}{dt} + \bar{E}\ \bar{B} - \frac{a\bar{D}}{\bar{C}} - \bar{F} = 0 \tag{48}$$

$$\frac{dx}{dt} = u + a \tag{49}$$

$$C^- \begin{cases} -\frac{\bar{a}}{\bar{C}} \frac{du}{dt} + \frac{dH}{dt} + \bar{E}\,\bar{B} + \frac{\bar{a}\bar{D}}{\bar{C}} - \bar{F} = 0 & (50) \\ \\ \frac{dx}{dt} = u - a & (51) \end{cases}$$

Equations (46), (48) and (50) are now ordinary differential equations which are valid in the time-distance grid along their respective characteristics, that is, along lines in the x-t domain defined by Equations (47), (49) and (51). It is interesting to note that Equations (48) and (50), which are concerned with the velocity and pressure, follow characteristics which describe the pressure wave propagation along the pipe. Equation (46), which is concerned with the relation between pressure and void fraction, follows a characteristic which describes the velocity of the mixture along the pipe. Figure 5 is a definition sketch of the characteristics in the x-t plane.

3.2 Finite Difference Relations

A finite-difference approach can be used to solve for the unknown values in Equations (48) and (50). If the time increment is small, a first-order approximation is

$$\int_{\phi_o}^{\phi_1} f(\phi)d\phi = f(\phi_o)[\phi_1 - \phi_o] \qquad (52)$$

Referring to Figure 5, the two compatibility relations, Equations (48) and (50), can be integrated along their characteristics to give the first-order approximations

$$\left(\frac{\bar{a}}{\bar{C}}\right)_r (u_p - u_r) + (H_p - H_r) + \bar{G}_r(t_p - t_r) = 0 \qquad (53)$$

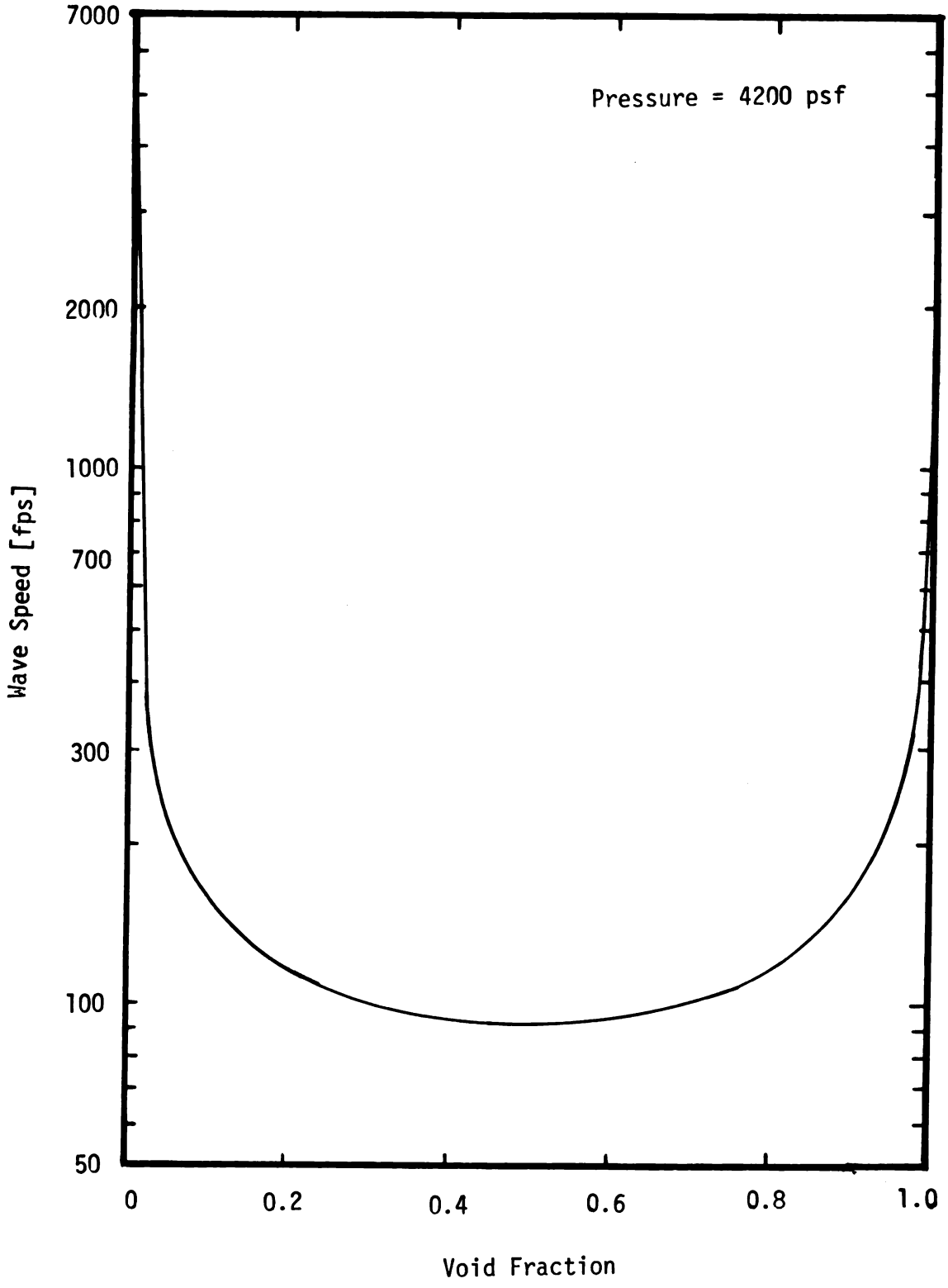

Figure 4. Wave Speed versus Void Fraction for Bubbly Two-Phase Flow in a One Inch Copper Pipe.

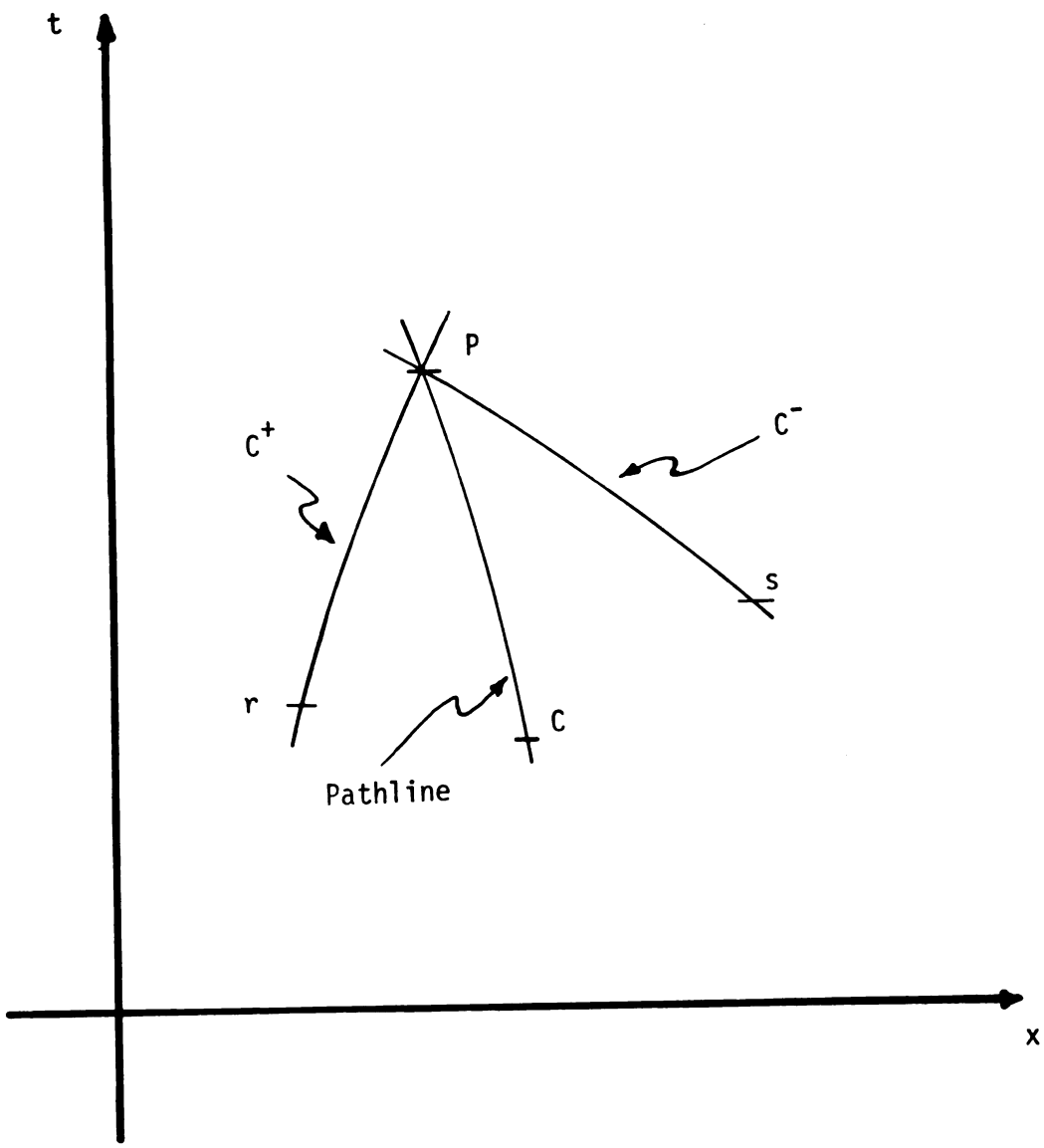

Figure 5. Definition Sketch Showing Intersection of C^+, C^- and Pathline Characteristic Curves in the x-t Plane.

$$-\left(\frac{a}{C}\right)_s (U_P - U_s) + (H_P - H_s) + \bar{H}_s(t_P - t_s) = 0 \tag{54}$$

where

$$\bar{G} = (\bar{E}\,\bar{B} - \bar{F} - a\,\bar{D} / \bar{C}) \tag{55}$$

$$\bar{H} = (\bar{E}\,\bar{B} - \bar{F} + a\,\bar{D} / \bar{C}) \tag{56}$$

To improve the numerical accuracy a second-order finite difference approximation can be used. The approximation, known as the trapazoid rule, is given by

$$\int_{\phi_o}^{\phi_1} f(\phi)d\phi = \frac{1}{2}[f(\phi_o) + f(\phi_1)][\phi_1 - \phi_o] \tag{57}$$

Integrating Equations (48) and (50) along their characteristics using Equation (57) results in the second-order finite difference equations:

$$\frac{1}{2}\left[\left(\frac{a}{C}\right)_r + \left(\frac{a}{C}\right)_p\right](u_P - u_r) + (H_P - H_r) + \frac{1}{2}\left[\bar{G}_r + \bar{G}_p\right]\Delta t = 0 \tag{58}$$

$$-\frac{1}{2}\left[\left(\frac{a}{C}\right)_s + \left(\frac{a}{C}\right)_p\right](u_P - u_s) + (H_P - H_s) + \frac{1}{2}\left[\bar{H}_s + \bar{H}_P\right]\Delta t = 0 \tag{59}$$

Consider a grid of fixed distance and time increments superimposed on the x-t plane, as in Figure 6. The objective is to determine values of the unknowns at a new time step. Since the wave speed is much greater than the velocities, approximations to the characteristic Equations (47), (49) and (51) will be made as dx/dt=0, dx/dt=a, dx/dt=-a, respectively. If at times t all values along the pipe are known, then since the characteristics pass through node P, the simultaneous solution of the three

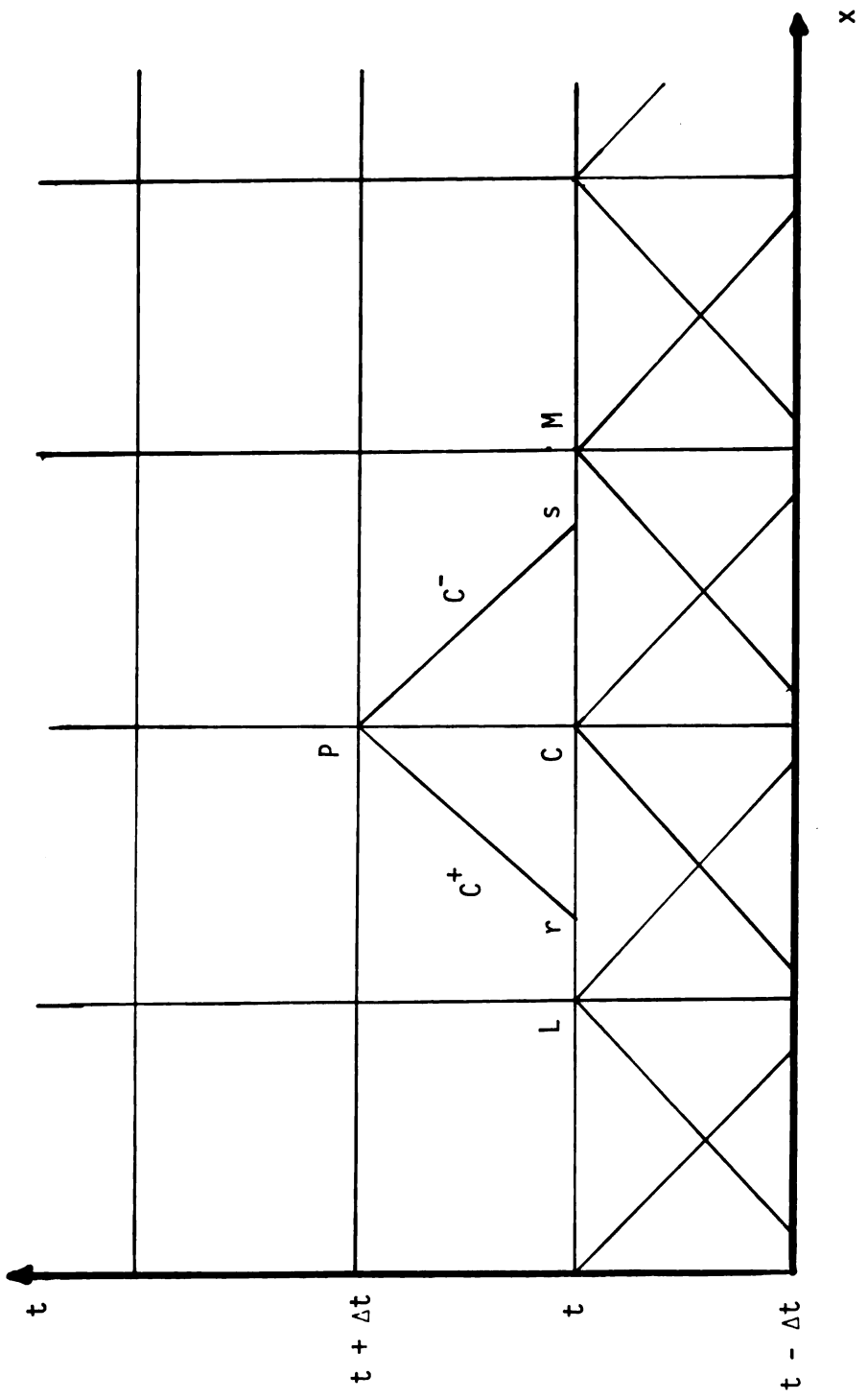

Figure 6. Characteristic Lines on the x-t Grid with Specified Distance and Time Intervals.

difference equations will lead to the solution of values at P.

Using the first-order Equations (53) and (54) and eliminating Hp yields

$$u_P = \left[\left(\frac{a}{C}\right)_r + \left(\frac{a}{C}\right)_s \right]^{-1} \left[\left(\frac{a}{C}\right)_r u_r + \left(\frac{a}{C}\right)_s U_s + H_r - H_s - \left(\bar{G}_r - \bar{H}_s\right)\Delta t \right] \tag{60}$$

Eliminating u_p from Equations (53) and (54) gives

$$H_P = \left[\left(\frac{\bar{C}}{a}\right)_r - \left(\frac{\bar{C}}{a}\right)_s \right]^{-1} \left[u_s \left(\frac{\bar{C}}{a}\right)_s - u_r \left(\frac{\bar{C}}{a}\right)_r - H_s \left(\frac{\bar{C}}{a}\right)_s + H_r \left(\frac{\bar{C}}{a}\right)_r - \bar{G}_r \Delta t \left(\frac{\bar{C}}{a}\right)_r - \bar{H}_s \Delta t \left(\frac{\bar{C}}{a}\right)_s \right] \tag{61}$$

To obtain second-order accuracy for the velocity at node P, Hp is eliminated from Equations (58) and (59) to yield

$$U_P = \left[\left(\frac{a}{C}\right)_r + 2\left(\frac{a}{C}\right)_P + \left(\frac{a}{C}\right)_s \right]^{-1} \left\{ \left[\left(\frac{a}{C}\right)_r + \left(\frac{a}{C}\right)_P \right] u_r + \left[\left(\frac{a}{C}\right)_s + \left(\frac{a}{C}\right)_P \right] u_s + 2(H_r - H_s) - \Delta t \left(\bar{G}_r + \bar{G}_P - \bar{H}_s - \bar{H}_P \right) \right\} \tag{62}$$

Second-order accuracy for the head at P can be obtained from either Equation (58) or (59). Solving for H_p in Equation (59) results in

$$H_P = H_s + \frac{1}{2} \left[\left(\frac{a}{C}\right)_s + \left(\frac{a}{C}\right)_P \right] (u_P - u_s) - \frac{1}{2} \left[\bar{H}_s + \bar{H}_P \right] \Delta t \tag{63}$$

The finite-difference equations must now be applied to the various boundary conditions that are encountered. At the ends of the pipe, one of the compatibility relations cannot be used. Therefore, the type of boundary condition supplies the additional information as its influence on the flow.

At the upstream boundary, if the head is known the velocity can be determined from Equations (54) and (59) to give

$$u_P = u_s + \left(\frac{\bar{C}}{a}\right)_s (H_P - H_s + \bar{H}_s \Delta t) \tag{64}$$

$$u_P = u_s + 2\left[\left(\frac{a}{\bar{C}}\right)_s + \left(\frac{a}{\bar{C}}\right)_P\right]^{-1}\left[H_p - H_s + \frac{1}{2}(\bar{H}_s + \bar{H}_P)\Delta t\right] \tag{65}$$

If the velocity is known, Equations (54) and (59) can be solved for the head to obtain

$$H_P = H_s + \left(\frac{a}{\bar{C}}\right)_s (u_P - u_s) - \bar{H}_s \Delta t \tag{66}$$

$$H_P = H_s + \frac{1}{2}\left[\left(\frac{a}{\bar{C}}\right)_s + \left(\frac{a}{\bar{C}}\right)_P\right](u_P - u_s) - \frac{1}{2}\left[\bar{H}_s + \bar{H}_P\right]\Delta t \tag{67}$$

At the downstream boundary, if the head is known the velocity can be determined from Equations (53) and (58) to be

$$u_P = u_r + \left(\frac{\bar{C}}{a}\right)_r \left[H_r - H_P - \bar{G}_r \Delta t\right] \tag{68}$$

$$u_P = u_r + 2\left[\left(\frac{a}{\bar{C}}\right)_r + \left(\frac{a}{\bar{C}}\right)_P\right]^{-1}\left[-H_P + H_r - \frac{1}{2}(\bar{G}_r + \bar{G}_P)\Delta t\right] \tag{69}$$

If the velocity is known then Equations (53) and (58) can be solved for

the head to obtain

$$H_P = H_r - \left(\frac{a}{C}\right)_r (u_P - u_r) - \bar{G}_r \Delta t \tag{70}$$

$$H_P = H_r - \frac{1}{2}\left[\left(\frac{a}{C}\right)_r + \left(\frac{a}{C}\right)_P\right](u_P - u_r) - \frac{1}{2}\left[\bar{G}_r + \bar{G}_P\right]\Delta t \tag{71}$$

3.3 Integration of the Pathline Characteristic

Attention is now focused upon the integration of the pathline characteristic Equation (46), which relates the dependence of the void fraction to the head. Making the assumptions $K_\ell >> K_g$ and $\rho_\ell(1-\alpha) >> \rho_g \alpha$, the coefficient terms $\bar{E}$ and $\bar{F}$ can be approximated as

$$\bar{E} \cong \frac{K_g}{\alpha \rho_g g} \tag{72}$$

$$\bar{F} \cong \frac{\Gamma K_g}{\alpha \rho_g \rho_\ell g} - u \sin\theta \tag{73}$$

Substituting Equations (72) and (73) into Equation (46) yields

$$\frac{K_g}{\alpha}\frac{d\alpha}{dt} + \rho_\ell g \frac{dH}{dt} = \frac{K_g \Gamma}{\rho_g \alpha} - u \rho_\ell g \sin\theta \tag{74}$$

Differentiating Equation (25) with respect to time;

$$\frac{dH}{dt} = \frac{1}{\rho_\ell g}\frac{dp}{dt} - u \sin\theta \tag{75}$$

and substituting into Equation (74) gives

$$\frac{K_g}{\alpha}\frac{d\alpha}{dt} + \frac{dp}{dt} = \frac{K_g \Gamma}{\rho_g \alpha} \tag{76}$$

Furthermore, using the polytropic gas relation the compressibility of a gas can be shown to be

$$K_g = n'p \tag{77}$$

where n' is the polytropic gas constant. In addition, the ideal gas law can be written as

$$\rho_g = p/kT \tag{78}$$

where k is the universal gas constant and T is the absolute temperature. Using Equations (77) and (78), Equation (76) becomes

$$\frac{d\alpha}{\alpha} + \frac{1}{n'} \frac{dp}{p} = \frac{kT\ \Gamma\ dt}{p\alpha} \tag{79}$$

For a polytropic process it can be shown [18] that

$$T = \left(\frac{p}{p_o} \right)^{1-1/n'} T_o \tag{80}$$

where p_o and T_o are a known pressure and temperature at some time. Substituting Equation (80) into (79) yields

$$\frac{d\alpha}{\alpha} + \frac{1}{n'} \frac{dp}{p} = \frac{p^{-1/n'}}{\alpha} \left(\frac{k\ T_o}{p_o^{1-1/n'}} \right) \Gamma\ dt \tag{81}$$

Multiplying by $\alpha p^{1/n'}$ results in

$$p^{1/n'} d\alpha + \frac{\alpha}{n'} p^{1/n'-1}\ dp = \left(\frac{k\ T_o}{p_o^{1-1/n'}} \right) \Gamma\ dt \tag{82}$$

Equation (82) is equivalent to

$$d(\alpha p^{1/n'}) = \left(\frac{k\ T_o}{p_o^{1-1/n'}} \right) \Gamma\ dt \tag{83}$$

Equation (83) is valid only along dx/dt = u. As previously mentioned, since this slope is very large with respect to the absolute magnitude

of the C^+ and C^- characteristics, it is assumed as an approximation, that the equation is also valid along a time line. Integrating Equation (83) from point C to point P of Figure 6 yields

$$\alpha_P \, p_P^{1/n'} - \alpha_C \, p_C^{1/n'} = (k \, T_o \, p_o^{(1/n'-1)}) \int_C^P \Gamma \, dt \tag{84}$$

The last term on the right-hand side of Equation (84) can be approximated as

$$\int_C^P \Gamma \, dt = \frac{1}{2} \Delta t \, (\Gamma_C + \Gamma_P) \tag{85}$$

Substituting Equation (85) into (84) and rearranging yields

$$\alpha_P = \left(\frac{p_C}{p_P} \right)^{1/n'} \left[\alpha_C + \frac{k \, T_o}{p_C} \left(\frac{p_C}{p_o} \right)^{1-1/n'} \frac{\Delta t}{2} (\Gamma_C + \Gamma_P) \right] \tag{86}$$

Equation (86) can be used to obtain values for the void fraction at a new time. Together with the first-order Equations (60) and (61) and second-order Equations (62) and (63), the three unknown variables can be solved at any interior point provided that the variables are known at the previous time.

3.4 Interpolation Scheme

If the wave speed is constant, the method of specified distance and time increments can produce an accurate solution without interpolation damping [19]. With reference to Figure 7, if a constant wave speed is present throughout the pipe, the grid could be arranged such that points r and s coincide with points L and M. Since the unknowns have been solved at points L and M at the previous time step, the characteristics transmit exact information from points L and M to

point P. However, if points r and s do not coincide with L and M, information from r and s must be transmitted to node P. An approximation to the unknowns at r and s can be found by interpolating between points L, C, and M. This information is then used to obtain unknown values at P. This interpolation leads to numerical damping and dissipation of the wave front [19].

In a pipe where the wave speed is changing, it is impossible to avoid interpolations when using a fixed grid. As the celerity changes, the location of r and s will change. In the conventional interpolations scheme with changing wave speed, the grid is arranged such that points r and s are within the points L, C and C, M. In this manner the Courant condition is always satisfied, since

$$\frac{a\ \Delta\ t}{\Delta x} \leq 1 \tag{87}$$

The linear interpolation equations as outlined by Lister [12] for the above case are

$$\phi_r = \phi_C - \zeta'(\phi_C - \phi_L) \tag{88}$$

$$\phi_s = \phi_C - \zeta'(\phi_C - \phi_M) \tag{89}$$

where ϕ is the variable being interpolated such as velocity, void fraction, or pressure head and where

$$\zeta' = \frac{a\ \Delta\ t}{\Delta x}\ ;\ 0 \leq \zeta' \leq 1 \tag{90}$$

The term ζ' indicates the position of r and s. As ζ' approaches zero the interpolation points approach C and as ζ' approaches one, r and s approach L and M. A value of $\zeta' = 1$ represents no interpolations since the characteristics then coincide with points L and M.

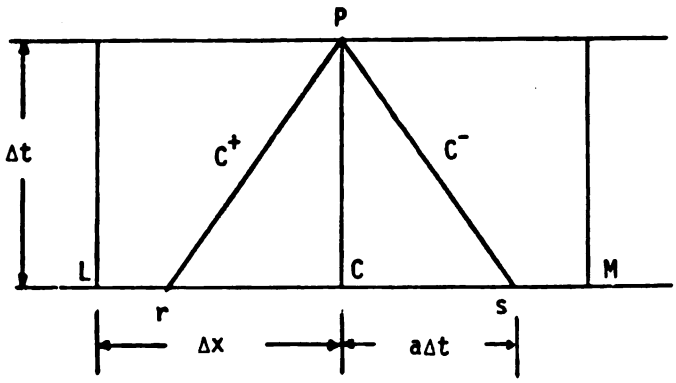

Figure 7. Definition Sketch Illustrating Interpolations taken within One Distance Increment.

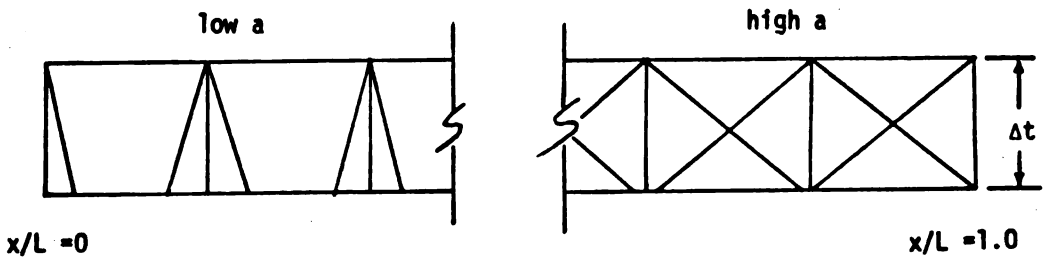

Figure 8. Definition Sketch Showing Possible Interpolations within One Distance Increment Associated with Variable Wave Speed.

With this scheme the maximum wave speed that is to be attained controls the grid size. This usually requires a very small grid size and fixed $\Delta t/\Delta x$ ratio. Figure 8 depicts this situation. It characterizes a pipe which at one end exhibits a low wavespeed while the wave speed at the other end is near its maximum value. This condition may exist due to gas release in liquids at regions of low pressure. It is apparent that severe interpolations will occur in the low wave speed regions. In these regions a larger time step is desirable but is prohibited due to the limiting condition of Equation (87).

However, as suggested by Vardy [23], it is not necessary to stay within one distance increment. It is possible to increase the time step such that points r and s lie outside the nodes adjacent to node P. Referring to Figure 9, interpolations for points r and s may now be taken between L and C', and between C" and M.

We can now define n as the number of distance increments to point L or M:

$$n = \text{IFIX}\ (a\Delta t/\Delta x) + 1 \tag{91}$$

where IFIX $(a\Delta t/\Delta x)$ is the integer equivalent of $a\Delta t/\Delta x$.

Again defining ζ to be the relative position between the nodes L and C' or C" and M:

$$\zeta = a\,\frac{\Delta t}{\Delta x} - n + 1 \tag{92}$$

The interpolation equations are

$$\phi_r = \phi_{C'} - \zeta(\phi_{C'} - \phi_L) \tag{93}$$

$$\phi_s = \phi_{C''} - \zeta(\phi_{C''} - \phi_M) \tag{94}$$

Notice that when n = 1, equations (92), (93) and (94) reduce to the

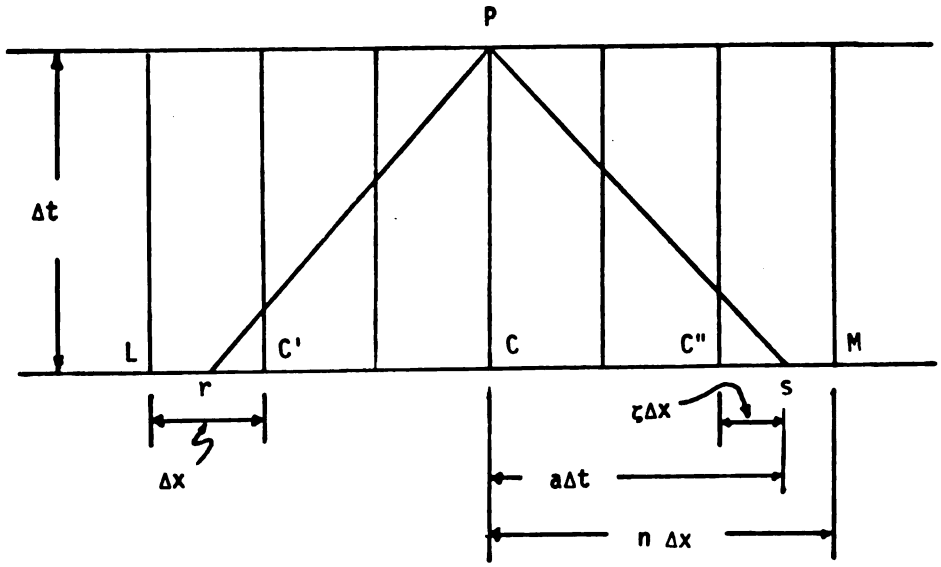

Figure 9. Definition Sketch Illustrating Interpolations taken Beyond One Distance Increment.

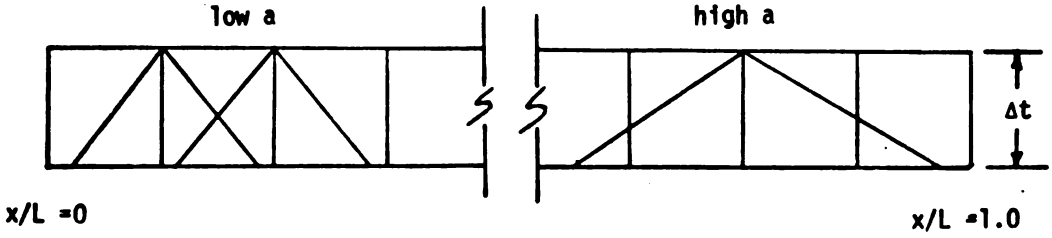

Figure 10. Definition Sketch Showing Possible Interpolations Associated with Increased $\Delta t/\Delta x$ ratio for a Variable Wave Speed Situation.

conventional interpolation Equations (88), (89) and (90). Application of an increased time step to a system which experiences regions of low and high wave speed is shown in Figure 10.

The grid is now closer to the preferred $\Delta t/\Delta x$ ratio in the low wave speed region. In the high wave speed region the characteristics span over several distance increments; however, interpolations can still be made between the nodes closest to r and s.

In light of the above discussion, perhaps by increasing the time step and allowing interpolations to take place outside of the first distance increment, reduced interpolation damping may occur. To investigate this, the following numerical experiments are provided.

A pressure transient is simulated in a 400 foot horizontal frictionless line by the instantaneous closure of a valve. A constant head reservoir is situated at the other boundary. The initial velocity is 2.0 fps and the reservoir elevation is 500 feet of head. In the analysis a constant wave speed is used. The fixed grid is adjusted such that the conditions described in Table 1 are simulated.

Table 1. Important Variables Used in Numerical Experiment Comparing Increased $\Delta t/\Delta x$ Ratio with Conventional Ratio

Figure	Number of sections	n	ζ	Computing time (sec)
11	10	1	0.25,0.50,0.75,1.0	21.7
11	10	2	"	8.5
12	20	1	"	83.6
12	20	2	"	27.1
13	40	1	"	325.4
13	40	2	"	99.3

In summary, interpolation damping was directly compared for interpolations taken within the first distance increment (n=1) and interpolations taken within the second distance increment (n=2). The simulation was run for three different number of sections of pipe with four ζ values. Figure 11 represents the total length of pipe divided into 10 distance increments; Figure 12 represent 20 sections; and Figure 13 is the 40 section case. The dimensionless head at the valve is plotted against the dimensionless time. The exact solution in each figure is the n=1 and ζ = 1.0 situation, since this represents no interpolation. The amount of damping that occurs for each case can be visually determined by comparison with the ζ = 1.0 case.

In observing the n = 1 cases only, it is evident that the amount of interpolation damping decreases as ζ approaches one and as the number of sections of the pipe increases. The damping is very severe in the ten section simulations and is also undesirable in the 40 section runs.

In viewing the n = 2 cases, an improvement is seen. In every instance, the n = 2 interpolations produced much less numerical damping as compared to the n = 1 case. As can be witnessed in Figure 13, the damping associated with 40 sections is acceptable. Also, it seems that the degree of interpolation plays a small role on the damping as the graphs for the different ζ values nearly coincide.

The results are clear. By increasing the time step and interpolating outside of the nodes adjacent to the node being solved, a reduction of the numerical damping associated with interpolations results when compared to the conventional grid. This also has an added benefit of reduced computing cost associated with the larger time step as can be seen from the computing times tabulated in Table 1.

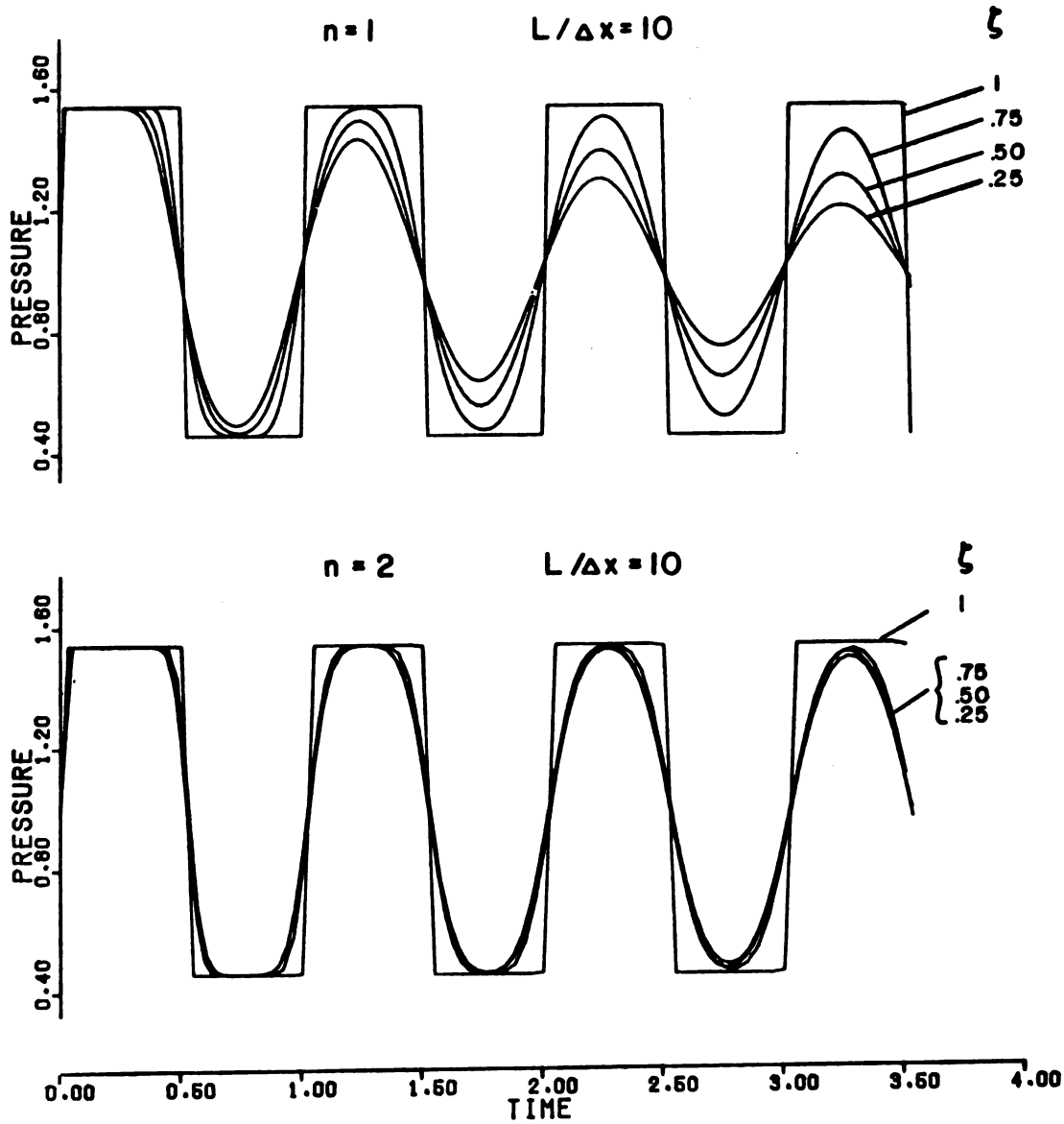

Figure 11. Comparison of Pressure Response at the Valve for n=1 and n=2 with the Pipe Divided into 10 Computing Sections.

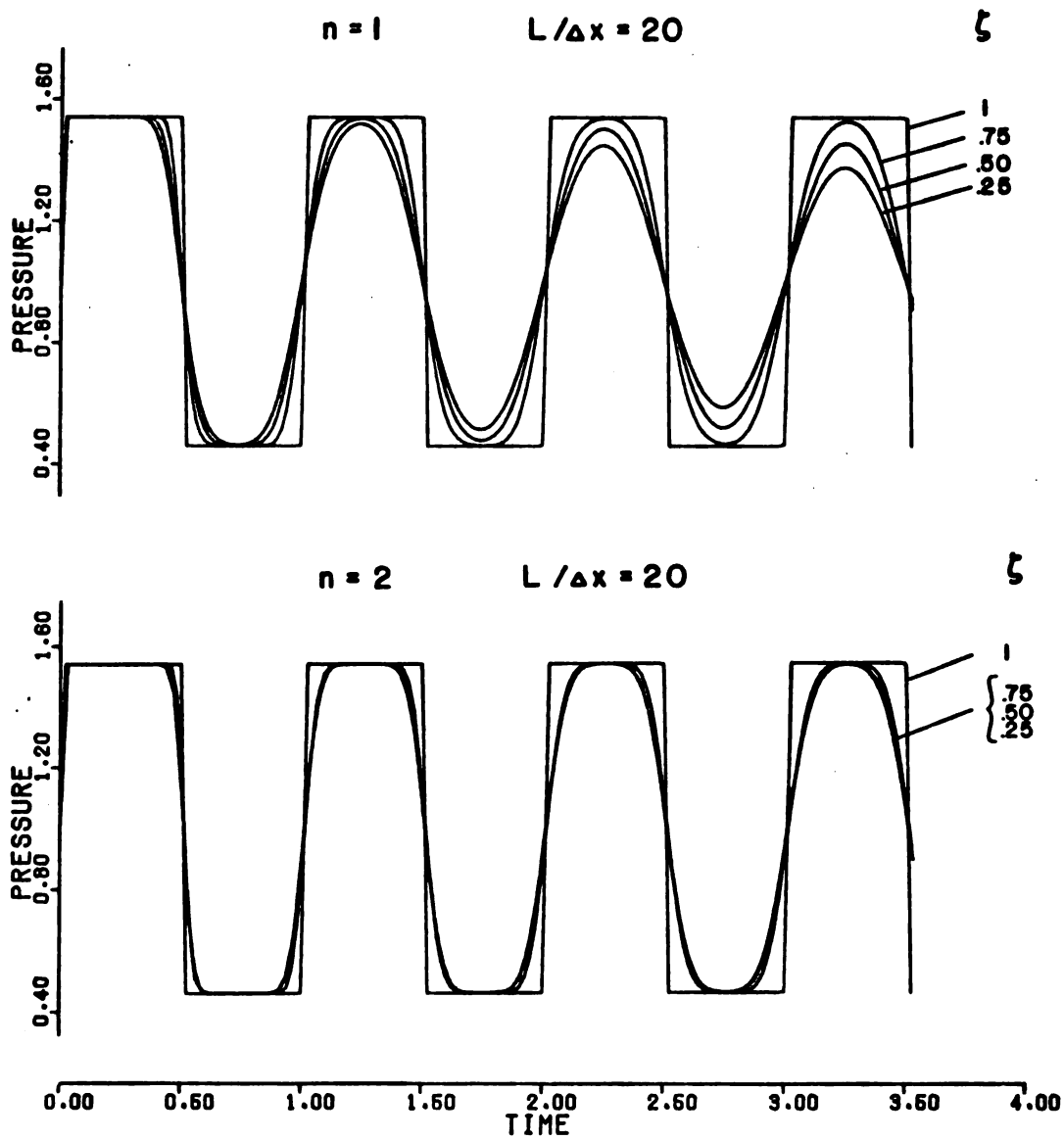

Figure 12. Comparison of Pressure Response at the Valve for n=1 and n=2 with the Pipe Divided into 20 Computing Sections.

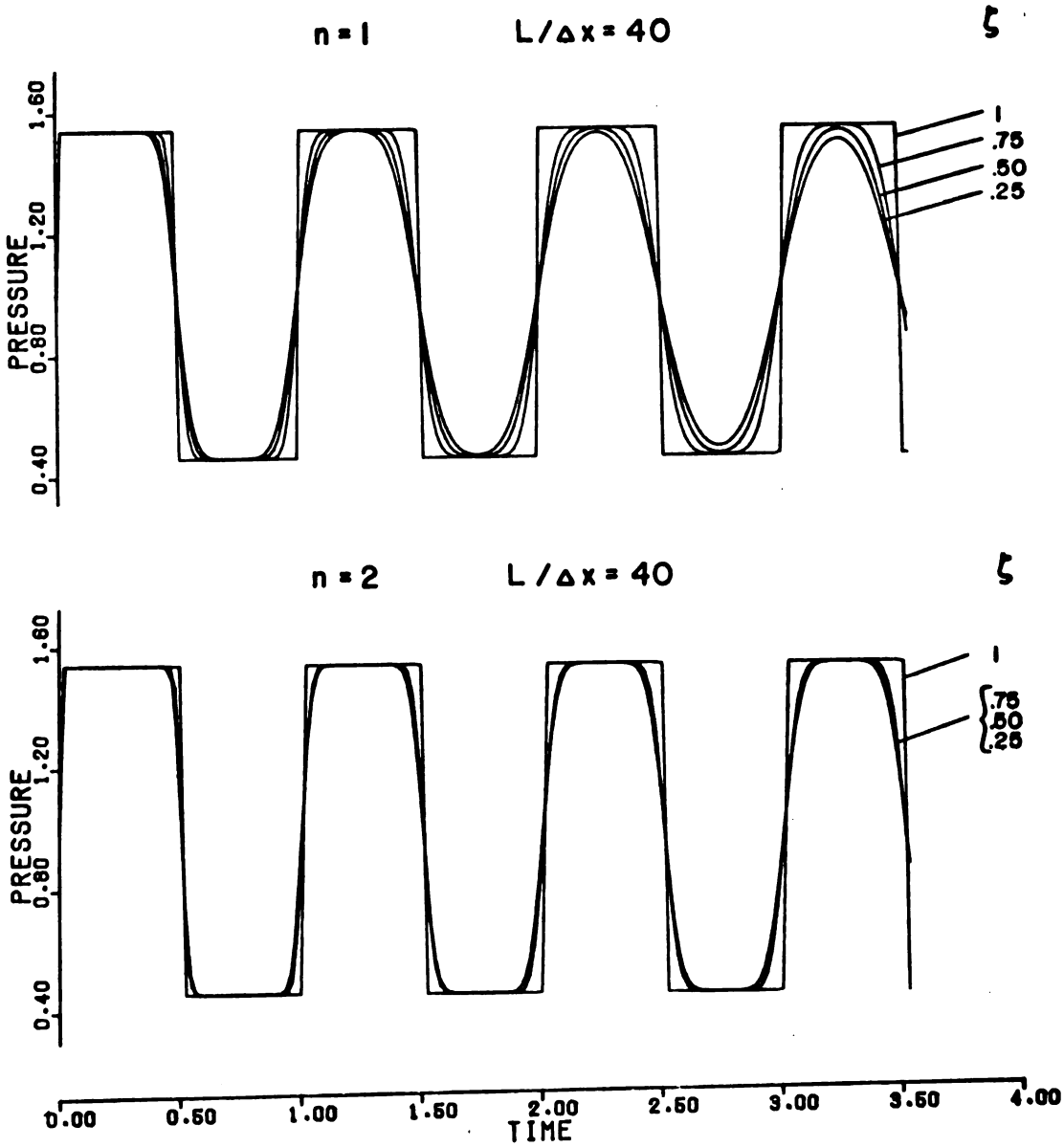

Figure 13. Comparison of Pressure Response at the Valve for n=1 and n=2 with the Pipe Divided into 40 Computing Sections.

A numerical experiment was also conducted for a variable wave speed situation. In this experiment, a pressure transient was simulated in a 400 foot horizontal lucite pipe of one-inch diameter by an instantaneous valve closure. The flow regime was a bubbly, two-phase, air-water mixture with a void fraction of 0.0354 as referenced to atmospheric pressure. Adibatic expansion and compression of the air was assumed. The initial velocity was 5.0 fps and the upstream reservoir pressure was 55 psia. A friction factor of .022 was used. Based on the maximum wave speed attained during the transient, the time step was adjusted such that the $n = 1$ and $n \leq 2$ interpolations schemes were simulated. The wave speed varied in the simulation from about 440 fps to 1050 fps. Therefore, interpolations ranged from $\zeta = 0.42$ to 1.0 for the $n = 1$ case and for the increased time-step situation ranged from $\zeta = 0.84$, $n = 1$ to $\zeta = 1.0$, $n = 2$. In addition, the Lax-Wendroff two-step scheme was used to model the identical transient [13]. In each case, 40 computing sections were used. Figures 14 and 15 are the plotted results of the pressure at the valve and midpoint of the pipe for the three runs.

In comparing the results for the pressure at the valve, the $n = 1$ and the Lax-Wendroff results show a nearly identical pressure trace while the $n = 2$ case exhibits a slightly sharper response with less smoothing. In viewing the midpoint pressures, the Lax-Wendroff scheme produced slightly more smoothing than the n=1 case, with n=2 displaying the least amount of smoothing.

From this experiment it is evident that the $n \leq 2$ case produced less numerical damping of the pressure computations than either $n = 1$ or the Lax-Wendroff scheme. If one were to perform a formal error analysis similar to that used by Liggett and Cunge [11], less damping of higher frequency components would be seen with $n \leq 2$. It seems

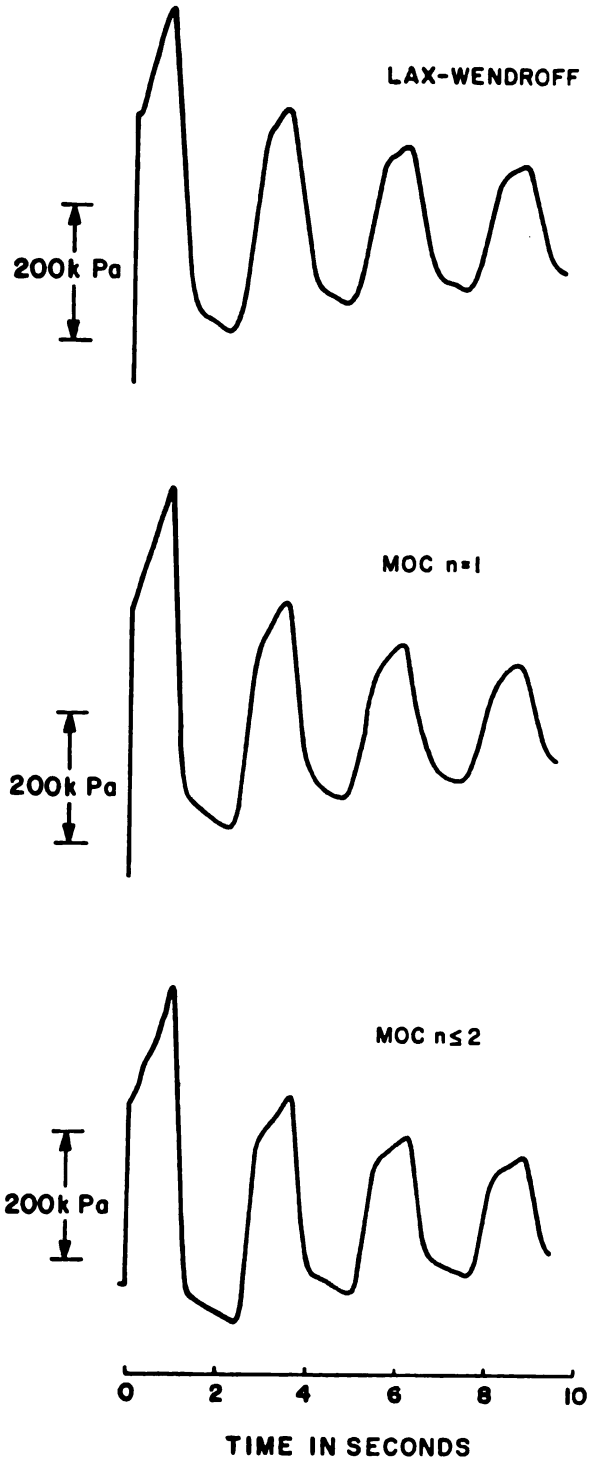

Figure 14. Comparison of Pressure Response at the Valve for Two-Phase Flow with the Lax-Wendroff Two-Step Scheme and the Method of Characteristics with n=1 and n≤2.

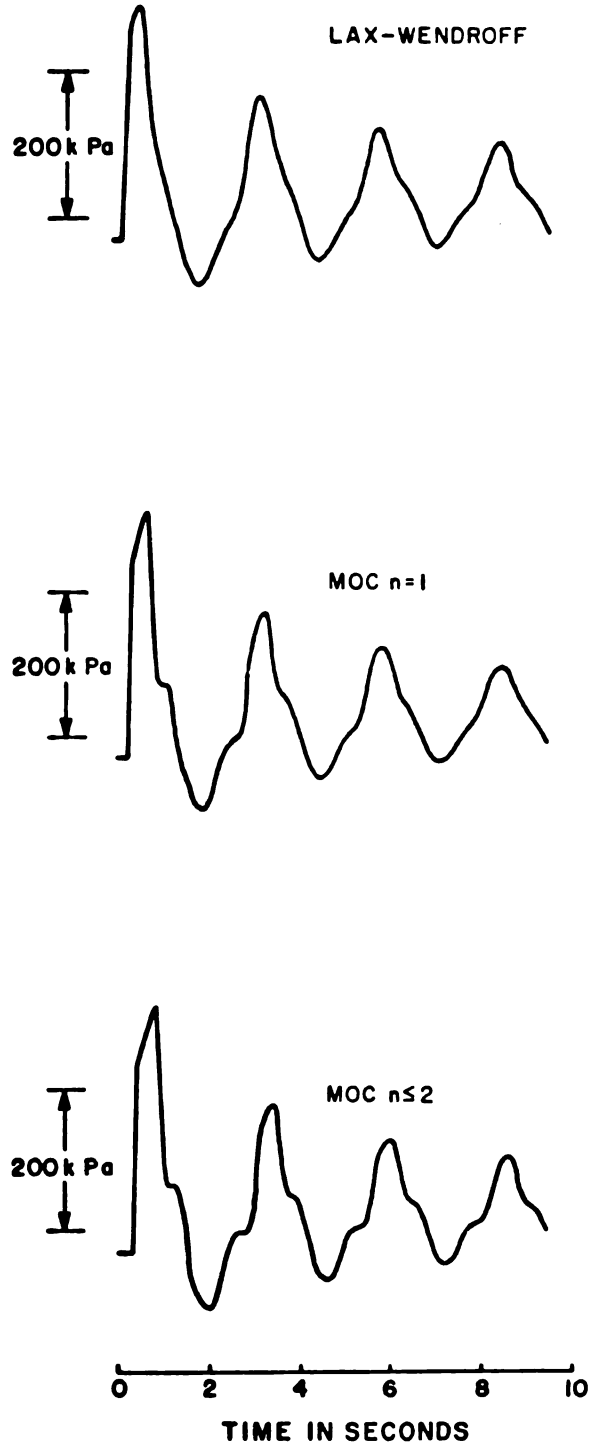

Figure 15. Comparison of Pressure Response at the Midpoint of the Pipe for Two-Phase Flow with the Lax-Wendroff Two-Step Scheme and the Method of Characteristics with n=1 and n≤2.

reasonable to conclude that in a changing wave speed situation the numerical damping can be reduced by taking $\Delta t/\Delta x$ ratios which are larger than that dictated by Equation (87), thereby producing a more accurate solution. Since Martin et al [14] and Kranenburg [9] found the numerical damping associated with the Lax-Wendroff scheme to be acceptable when comparing computed results to experimental data, it would seem that the method of characteristics as applied to the fixed grid with increased $\Delta t/\Delta x$ ratios would be a competitive scheme for dealing with changing wave speed situations. In addition, this scheme could be modified to accomodate a changing time step which would minimize the amount of interpolation error that occurs over that time step.

Vardy [23] also showed the advantages of an increased $\Delta t/\Delta x$ ratio in a numerical experiment in which an air duct is connected to two reservoirs. The pressure was reduced in one reservoir and the duct midpoint pressure-time history was observed. Using the convential grid he found an accurate solution with an acceptable amount of interpolation error was simulated at a $\Delta x = 0.4$ meters. He then increased Δx to 1.6 meters and by using a $\Delta t/\Delta x$ ratio greater than that permitted by Equation (87) obtained a result that was indistinguishable from the $\Delta x = 0.4$ meter case, thereby greatly reducing the computing cost.

When interpolating with increased $\Delta t/\Delta x$ ratios, attention must be paid to points which are near the boundary. Figure 16 shows the characteristic as it intercepts the boundary. Values at point Y are needed to solve for values at point P. Interpolating between points Z and X can be done to accomplish this. The interpolation equation for this case would be

$$\phi_Y = \phi_Z - \frac{n''\Delta x}{\Delta t\, a} (\phi_Z - \phi_X) \tag{95}$$

where n" is the number of distance increments to the boundary.

A more accurate approach could be taken as follows. Interpolations between points C" and X could be made to attain values for s. Values for Y could then be solved by writing the compatibility relations between s and Y.

3.5 Modeling Aspects

A specific numerical technique has been described which will simulate two-phase hydraulic transients including gas release by using the method of characteristics. An algorithm has been devised and by the use of a high speed digital computer, values for the velocity, pressure and void fraction along the pipe can be calculated. The purpose of this section is to point out some important aspects of the numerical model.

To minimize numerical errors, the equations of second-order accuracy will be employed. This entails solving the first-order equations to find initial values of head, velocity and void fraction. These values are then used in the second-order equations to obtain more refined answers. Also, to reduce interpolation errors, an increased time step will be used as proposed in the previous section. It is believed that by taking these measures the numerical damping is reduced to an acceptable level.

The gas release aspect will be handled in the following manner. Whenever the pressure at a node is below the gas saturation pressure, some mass of gas is allowed to evolve out of solution in a distributed manner throughout that computing section. This is accomplished through the gas generation term Γ, which is present in the compatibility relations. Γ is defined as the time rate of change of mass of gas per unit volume of mixture. It is a function which recognizes the time dependent

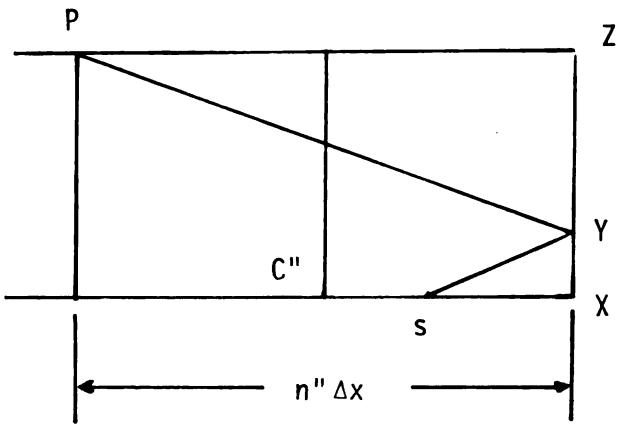

Figure 16. Interpolations taken at Boundary with Increased $\Delta t/\Delta x$ Ratio.

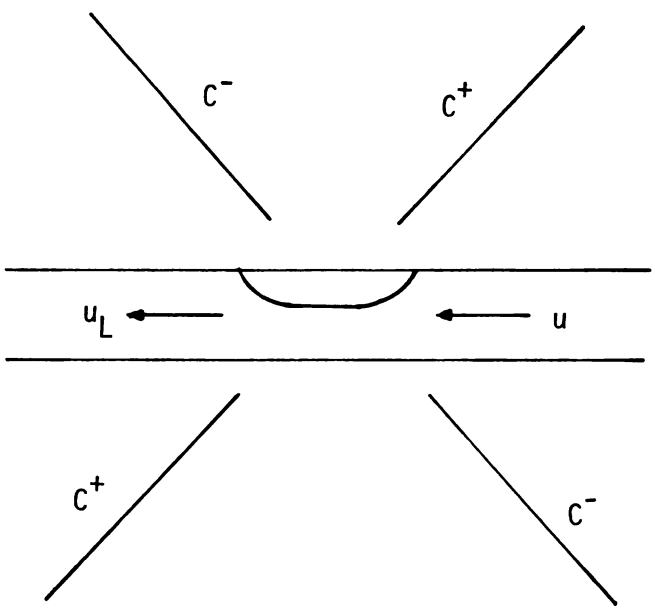

Figure 17. Definition Sketch of Vapor Void Occurring at a Computing Node.

nature of gas release. However, the rate of gas release is not well documented in the literature. In Chapter V the results of a laboratory experiment will be presented in which the rates of gas release in supersaturated solutions are determined. These results are used to approximate the time dependent nature of gas release occurring in the pipe through the selection of a suitable gas release function.

In modeling column separation phenomenon, which occurs when the pressure is calculated to be below the vapor pressure, the pressure at that node is set to vapor pressure. By bringing the C^- and C^+ characteristics up to this point, the only unknown in their respective compatibility equations is the velocity. Therefore, a velocity can be calculated for each side of the node as represented in Figure 17. With these two velocities, a vapor void can be accounted for by a simple continuity balance of the flow leaving the node.

Using the first-order finite difference Equations (53) and (54) the velocities on each side of the cavity are

$$u_L = \left(\frac{\bar{C}}{a}\right)_r \left[H_r - H_P\right] - \left(\frac{\bar{C}}{a}\right)_r \bar{G}_r \Delta t + u_r \tag{96}$$

$$u = \left(\frac{\bar{C}}{a}\right)_s \left[H_P - H_s\right] + \left(\frac{\bar{C}}{a}\right)_s \bar{H}_s \Delta t + u_s \tag{97}$$

Using the second-order finite difference Equations (58) and (59) the velocities on each side of the cavity are

$$u_L = 2\left[\left(\frac{a}{\bar{C}}\right)_r + \left(\frac{a}{\bar{C}}\right)_P\right]^{-1}\left[-H_P + H_r - \frac{1}{2}\left(\bar{G}_r + \bar{G}_P\right)\Delta t\right] + u_r \tag{98}$$

$$u = 2\left[\left(\frac{a}{\bar{C}}\right)_s + \left(\frac{a}{\bar{C}}\right)_P\right]^{-1}\left[H_P - H_s + \frac{1}{2}\left(\bar{H}_s + \bar{H}_P\right)\Delta t\right] + u_s \tag{99}$$

Since velocities are known from the previous time step, a second-order approximation to the cavity volume can be made:

$$(\text{Cavity Volume})_{t+\Delta t} = (\text{Cavity Volume})_t + \frac{1}{2} A\Delta t \left[(u-u_L)_{t+\Delta t} + (u-u_L)_t\right] \tag{100}$$

Using Equation (100) the size of the vapor void can be monitored. The pressure is kept at vapor pressure until the cavity closes.

When a cavity exists at a node, the question arises as to what velocity should be transmitted along the characteristics to the next time step. In this study, the averaged value of u and u_L is sent along the C^- and C^+ characteristics [16]. An alternate approach would be to transfer u_L along the C^- characterisitic and u along the C^+ characteristic. However, the former method seems to admit the presence of some momentum transfer across the void and does not produce the instabilities that are sometimes associated with transmitting two velocities from the same node.

CHAPTER IV

LABORATORY APPARATUS AND INSTRUMENTATION

The observation of gas release occurring under controlled conditions and the gathering of transient pipe data which exhibits gas release are essential to this study. The following is a detailed description of the experimental apparatus and procedures used to obtain the required data.

4.1 Gas Release Experiment

As previously cited, the time rates of gas release occurring in a supersaturated liquid has not been extensively researched. Schweitzer and Szebehely [17] conducted detailed experiments to determine the amount of air evolved from water in a closed container with a constant air-liquid volume ratio. Their measurement technique was to monitor the increasing air pressure above the free surface and relate that information to the amount of evolved air. They found that the air release rate decayed exponentially with time for a step decrease in pressure and was dependent upon an experimentally determined half-life of evolution. They also found that this half-life was dependent upon the air-liquid volume ratio in the container. In a developing two-phase pipe situation, there is essentially no initial air volume except for the presence of nuclei. Indeed, as gas is released, the air-liquid volume ratio would change with time. Therefore, there is some question as to the direct use of Schweitzer and Szebehely's findings in the present study. Alternately, the equations describing the mass transfer of gas into a single

bubble as developed by Parkin and Kermeen [15] or Van Wijngaarden [22] could be used. However, several additional unknown constants, such as the number of nuclei present and their radii, would be introduced.

To obtain a more realistic picture of the manner in which gas is released in a filled, closed container under turbulent conditions, a bench-top experiment was conducted. From this, gas release rates were obtained that gave an order of magnitude approximation to the gas generation term appearing in the compatibility relations.

4.1.1 Description of Apparatus and Instrumentation

A schematic of the experimental set-up is shown in Figure 18. The test section is composed of a lucite cylinder of 7.5 inch diameter and height of 14 inches. Extending vertically into the cylinder is an MTS-actuated rod to which has been attached a series of three, 1/4 inch square mesh grids spaced at 4-inch intervals from one another. The grid system, in which one grid is shown in Figure 19, can be oscillated sinusoidally over a range of frequencies and amplitudes to produce a desired fluid agitation, or grid turbulence.

Attached to the test section by means of 0.25 inch copper tubing is a reservoir in which water can be saturated with CO_2 or air at elevated pressures. Also attached to the test cylinder is a series of three vertical lucite tubes of 1.0, 1.5 and 2.0 inch I.D. The test section can be directly connected to any one of these tubes by a quick-opening valve. With the test cylinder filled with water saturated with gas at some elevated pressure and isolated from the reservoir, quickly opening a valve to one of the lucite tubes would cause a step decrease in pressure to atmospheric in the test section initiating gas release. As bubbles start to form they will displace the fluid volume which will be

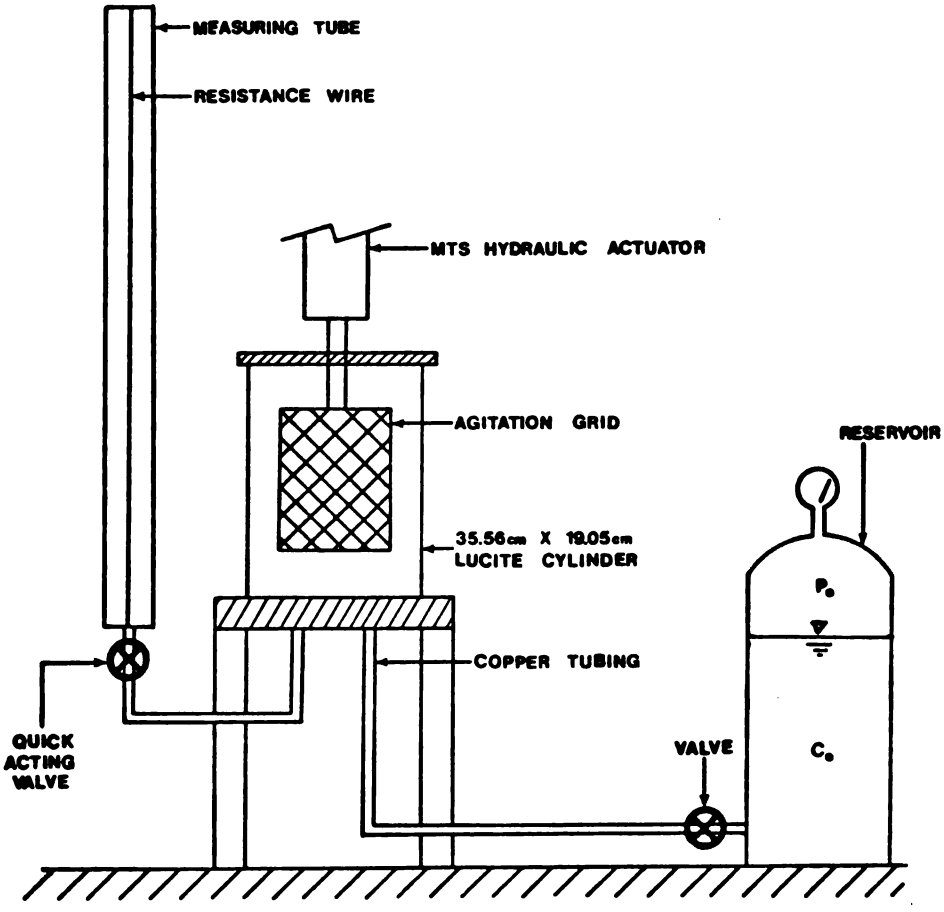

Figure 18. Detailed Schematic of Gas Release Experiment.

reflected in the water surface rise within the measuring tubes. By monitoring this water surface rise, a gas release-time history can be obtained. Figure 20 shows an overview of the entire set-up while under test conditions. The reservoir can be seen in the lower right. Figure 21 is a close-up of the test cylinder under test conditions.

The measurement devise to record the water surface level in the lucite measuring tube consisted of a 0.001 inch diameter tungsen resistance wire looped through the interior of the tube. This wire then served as one leg of a Wheatstone bridge. As water ascended in the tube, the resistance associated with this leg of the bridge changed, thereby creating a voltage potential across the bridge which could then be recorded. The bridge was activated by a Sanborn carrier-preamplifier, which also amplified the response and recorded the signal on a strip-chart recorder.

A Van Slyke apparatus, shown in Figure 22 and schematized in Figure 23 was used to monitor the dissolved gas content of the water. The apparatus was modified such that dissolved gas contents up to 200% by volume could be measured. To check the accuracy of this device, the results of several tests in which CO_2 was bubbled through the water until equilibrium conditions existed were checked against Henry's equilibrium law. Figure 24 shows this comparison and exhibits the close agreement between the measured and theoretical value.

4.1.2 Experimental Procedure

The actual gas release experiments could only be conducted after the accuracy and stability of the wire gage was assured. Since the resistance characteristics of the gage varied from day to day, the gage was physically calibrated before and after each series of tests to determine if

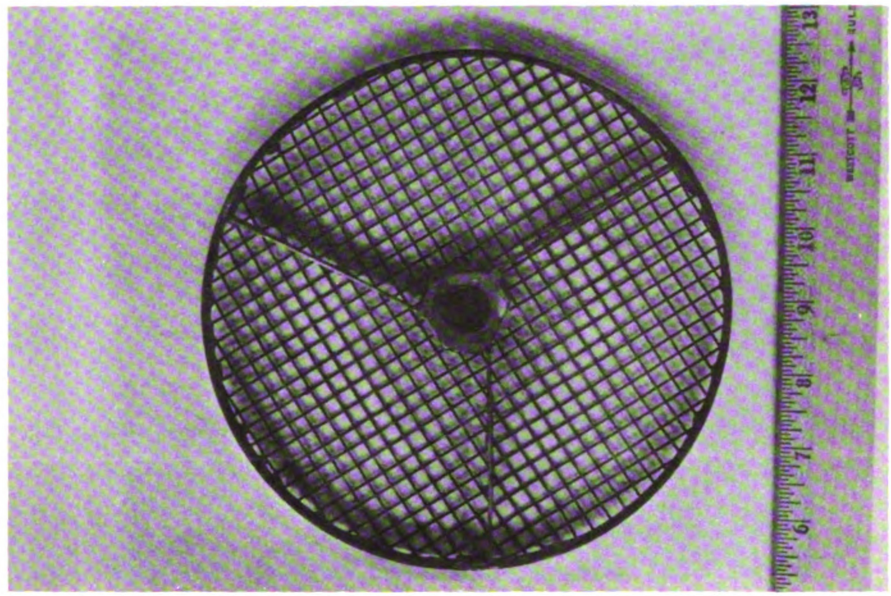

Figure 19. Close-up View of an Agitation Grid.

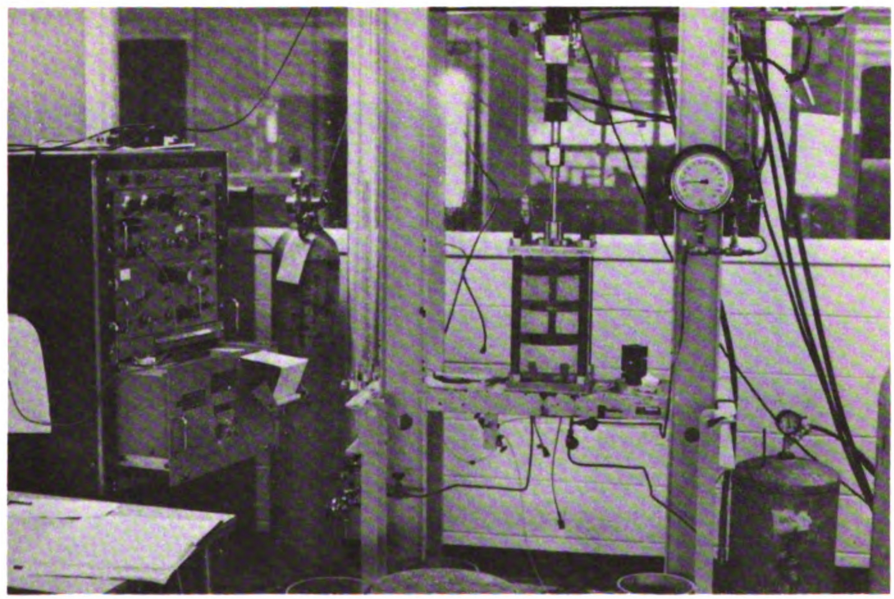

Figure 20. View of Gas Release Experiment under Test Conditions.

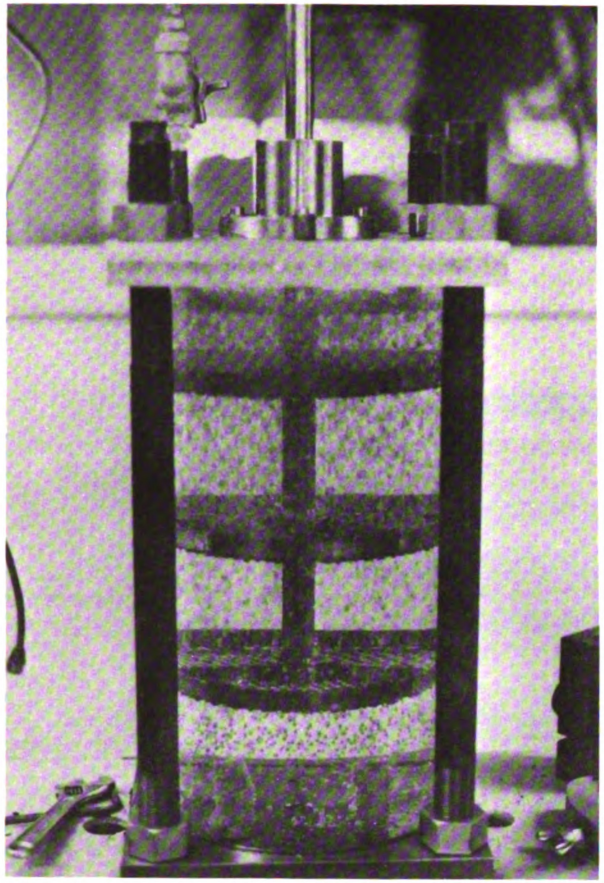

Figure 21. Close-up View of Lucite Test Cylinder During Actual Testing.

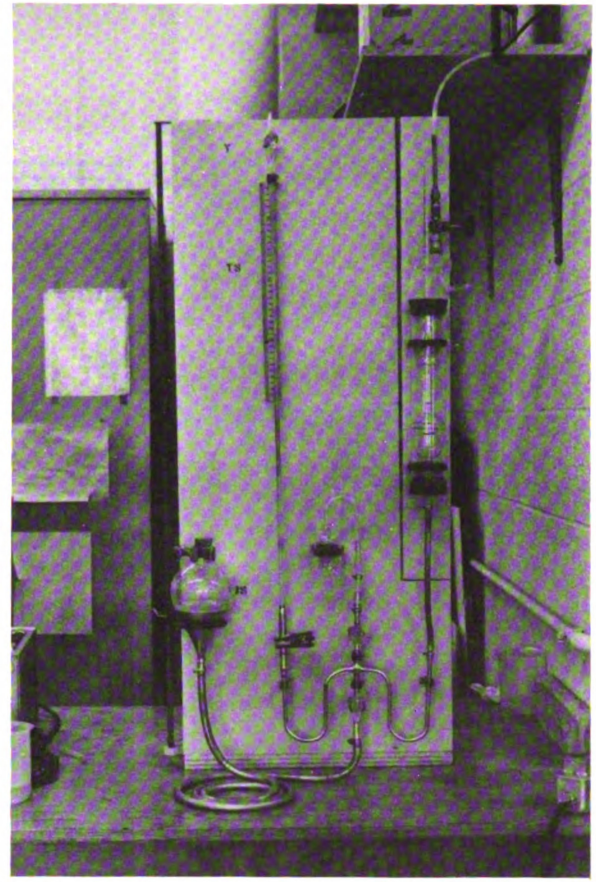

Figure 22. View of Van Slyke Dissolved Gas Measuring Apparatus.

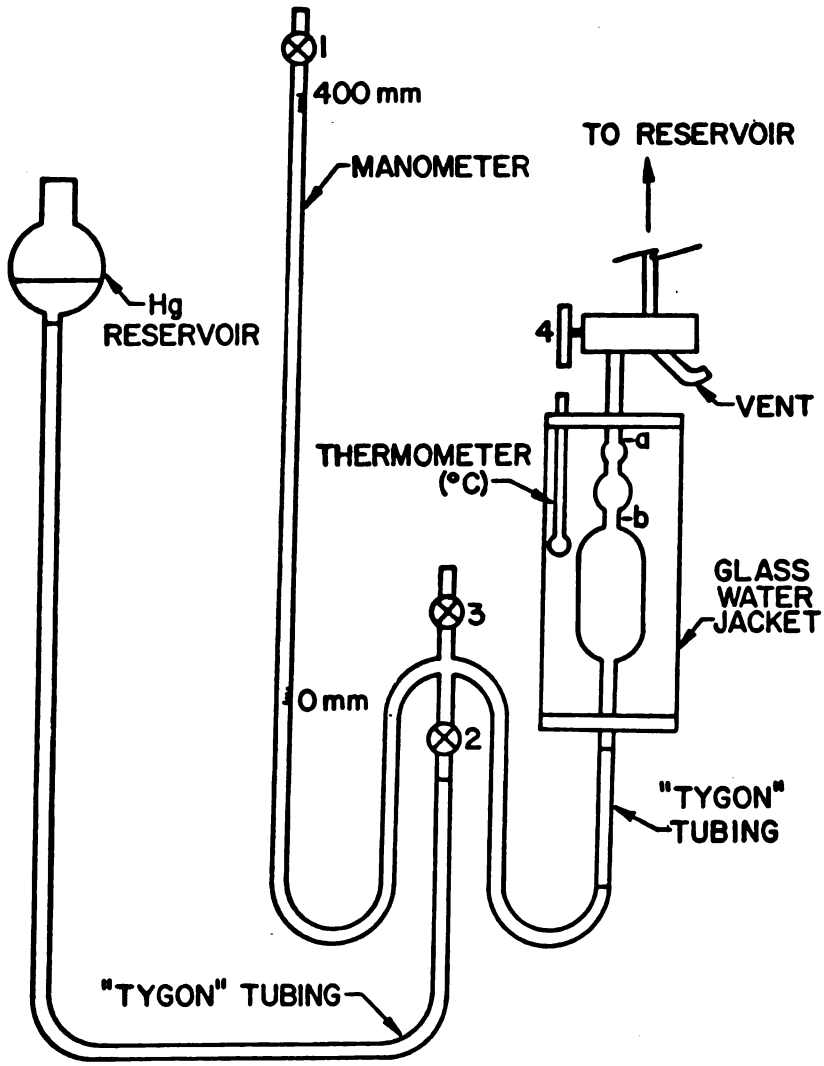

Figure 23. Van Slyke Apparatus Schematic.

any variance occurred. Small changes did occur; however, compensation for these changes were considered in the plotting of the data. A typical calibration curve is shown in Figure 25. As can be seen, the calibration is nonlinear.

A typical run consisted of the following procedure. The water in the reservoir was saturated with CO_2 by bubbling the gas through the water for a 40-minute to one-hour period at an elevated pressure accomplished by the adjustment of a needle valve. A sample was then introduced directly into the Van Slyke apparatus and the gas content tested to insure that the water was saturated at that pressure. The valve between the test cylinder and reservoir was then opened and water was introduced into the test-section. During this time, both the test cylinder and reservoir pressures were above the gas-saturation pressure, preventing any release of gas during the transfer. The gas in the test cylinder was bled out through a needle valve in the top of the cylinder during the filling. Once filled, it was then isolated from the reservoir.

The grid system was then oscillated at a given frequency and amplitude. Next, the quick acting valve connecting the test cylinder to a measuring tube was opened, resulting in a step decrease in pressure to atmospheric. The water was then in a supersaturated condition and gas evolution began which displaced the fluid volume resulting in the rise of the water surface in the measuring tube. During this time the wire gage was monitoring the water surface elevation. Figure 26 displays an actual experimental record.

4.2 Hydraulic Transient Experiment

4.2.1 Description of Apparatus and Instrumentation

A pipeline has been assembled which consists of 400 feet of coiled,

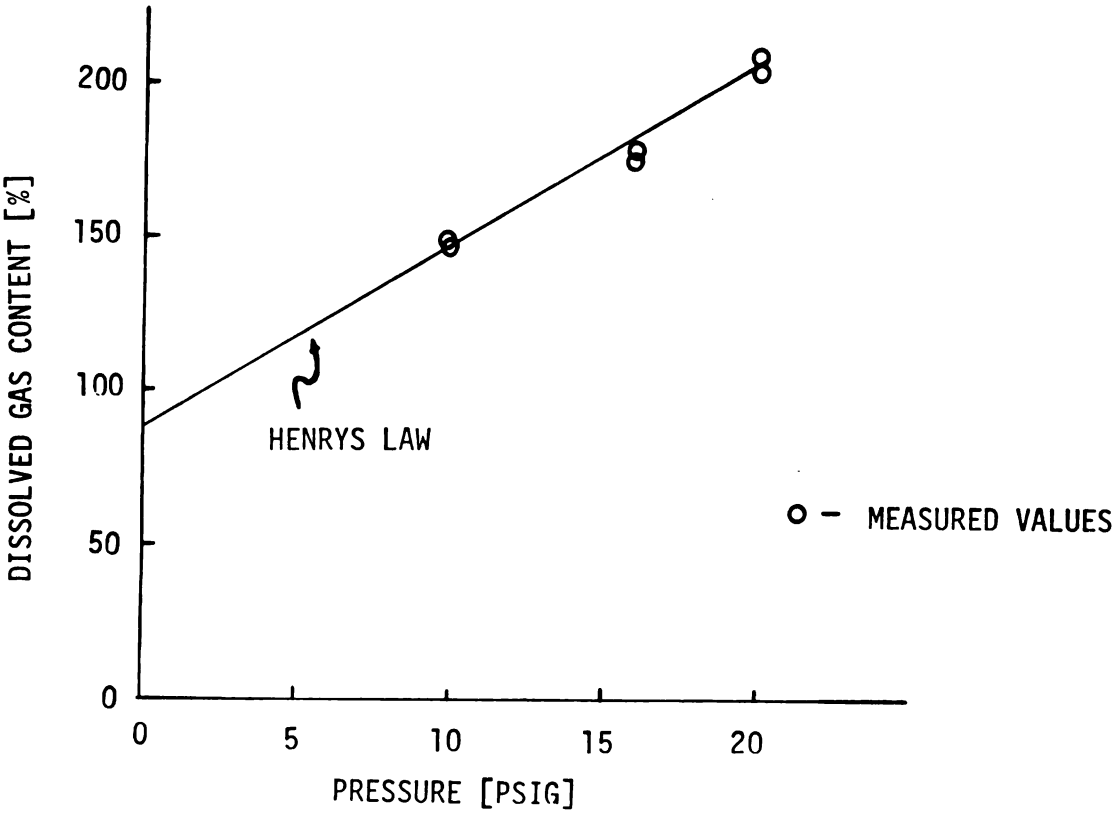

Figure 24. Comparison of Van Slyke Measurements versus Henrys Law.

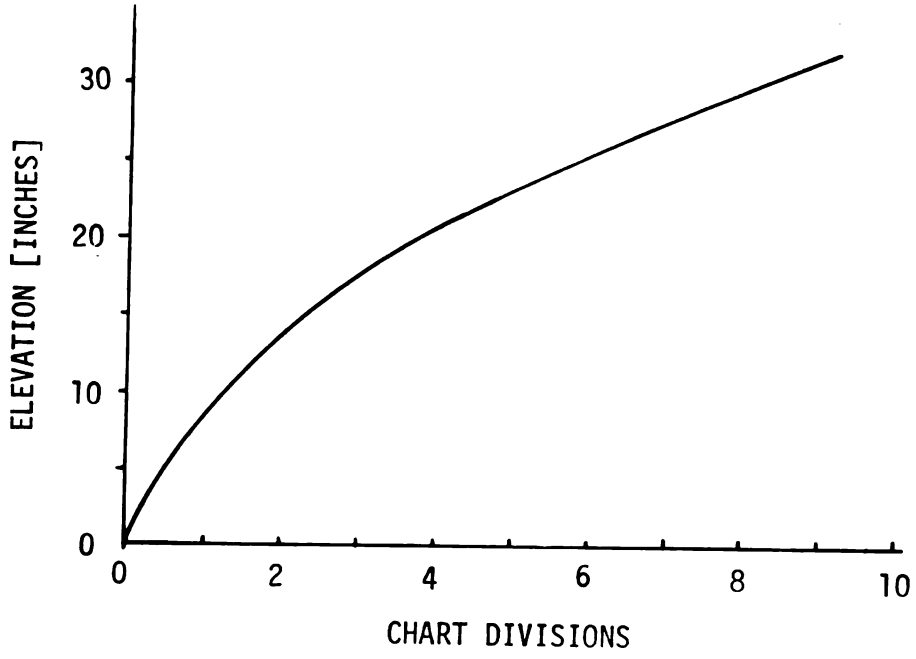

Figure 25. Typical Wire Gage Calibration Curve.

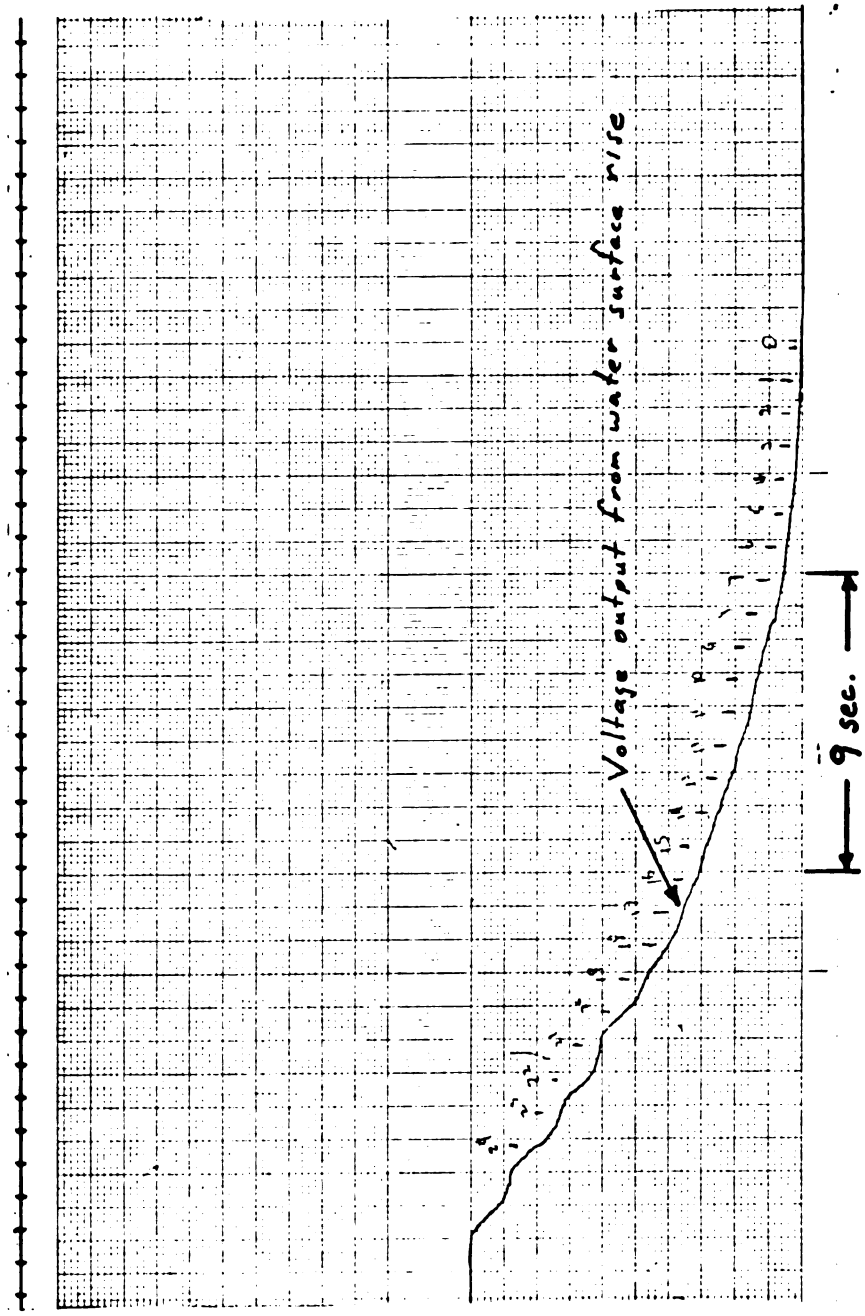

Figure 26. Typical Data Trace Showing Water Elevation Rise in Measuring Tube During a Gas Release Experiment.

one-inch I.D. copper pipe. At each end of the coil has been connected 12.2 foot sections of one-inch I.D. lucite pipe for visualization purposes. Reservoirs located at the upstream and downstream ends of the loop, having the capacity to be pressurized, complete the system. Figure 27 is a schematic of the apparatus and Figure 28 shows the coil and lucite sections. The upstream reservoir has been constructed such that the water can be saturated with CO_2 or air. The Van Slyke apparatus was used to determine dissolved gas contents. A quick-acting solenoid-activated valve which can be located in either an upstream or downstream location was used to initiate the transients. Measurements of the closing action of the valve showed a closure time of 20 to 30 milliseconds.

Velocity measurements were made by the use of an elbow meter attached to an inverted air-water manometer. The elbow meter was calibrated volumetrically. Figure 29 shows the elbow meter leading to the manometer and the valve in the upstream position. The calibration curve for the meter in the upstream position is shown in Figure 30.

To determine the frictional characteristics of the pipeline, piezometer taps were installed at the ends of the copper coil and lucite sections. Steady state losses associated with a range of flows were found using manometers. Figure 31 shows the measured friction factors versus Reynolds number for the copper and lucite pipes.

Five transducer mountings were placed within the system to accept the placement of flush-mounted, miniature Sensotec strain-gage pressure transducers. The transducers were activated by a four channel Sensotec U-4 amplifier. The tranducers were statically calibrated within the system. They were also temperature compensated by the application of a thin layer of silicone rubber over the diaphragm. Figure 32 shows

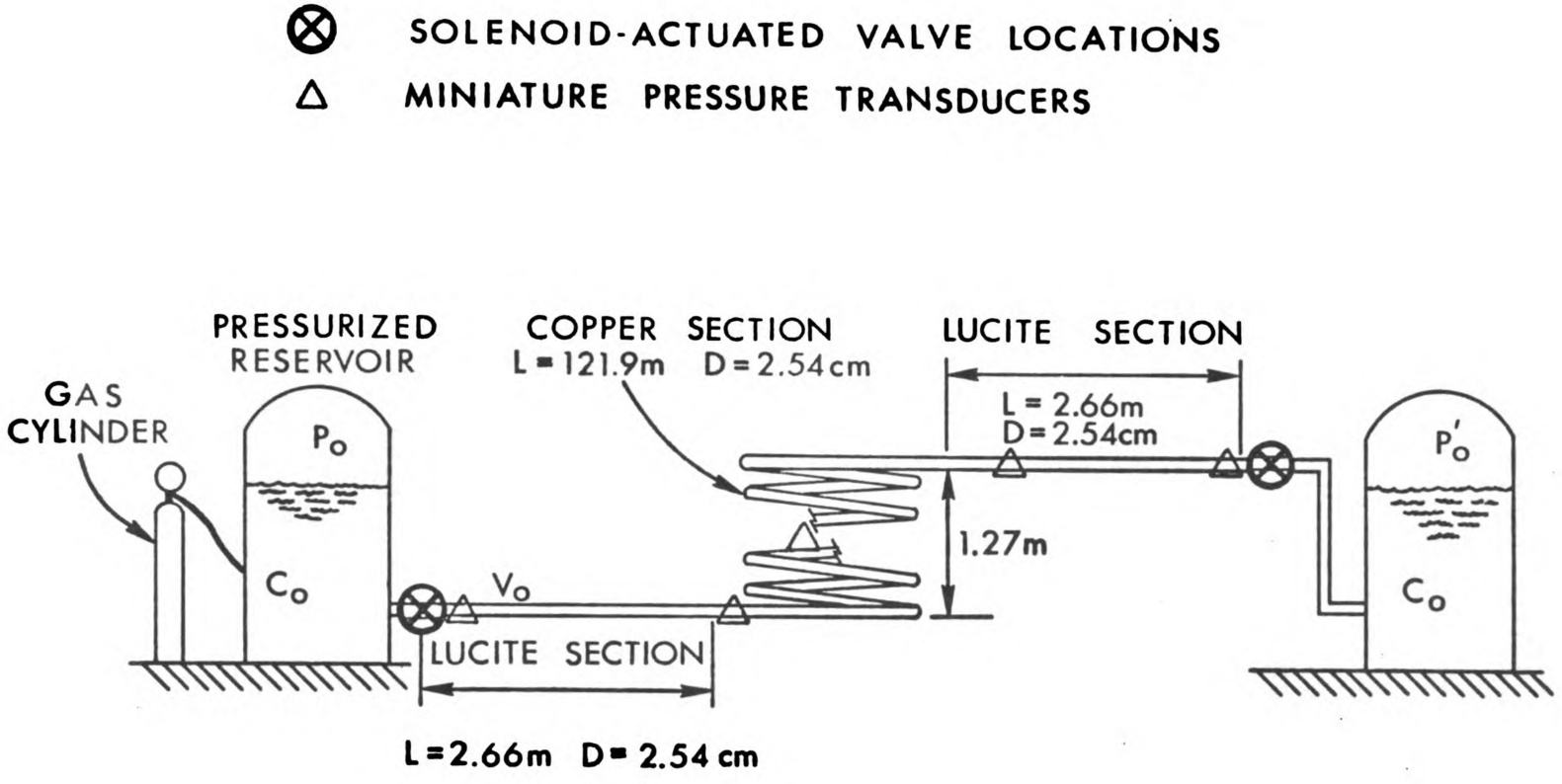

Figure 27. Detailed Schematic of Experimental Transient Pipeline.

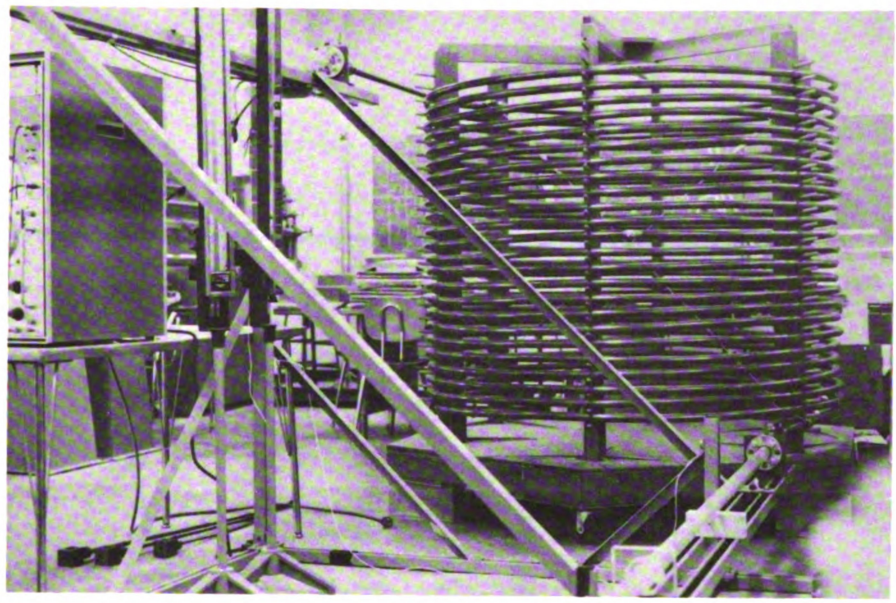

Figure 28. View of Copper Coil and Lucite Pipes.

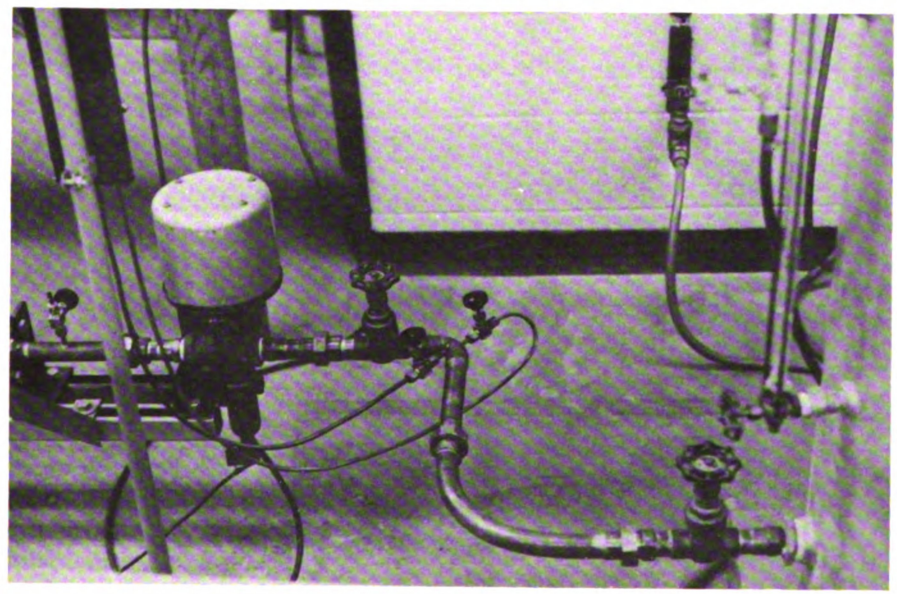

Figure 29. Close-up View of Elbow Meter and Solenoid-Actuated Valve in the Upstream Location.

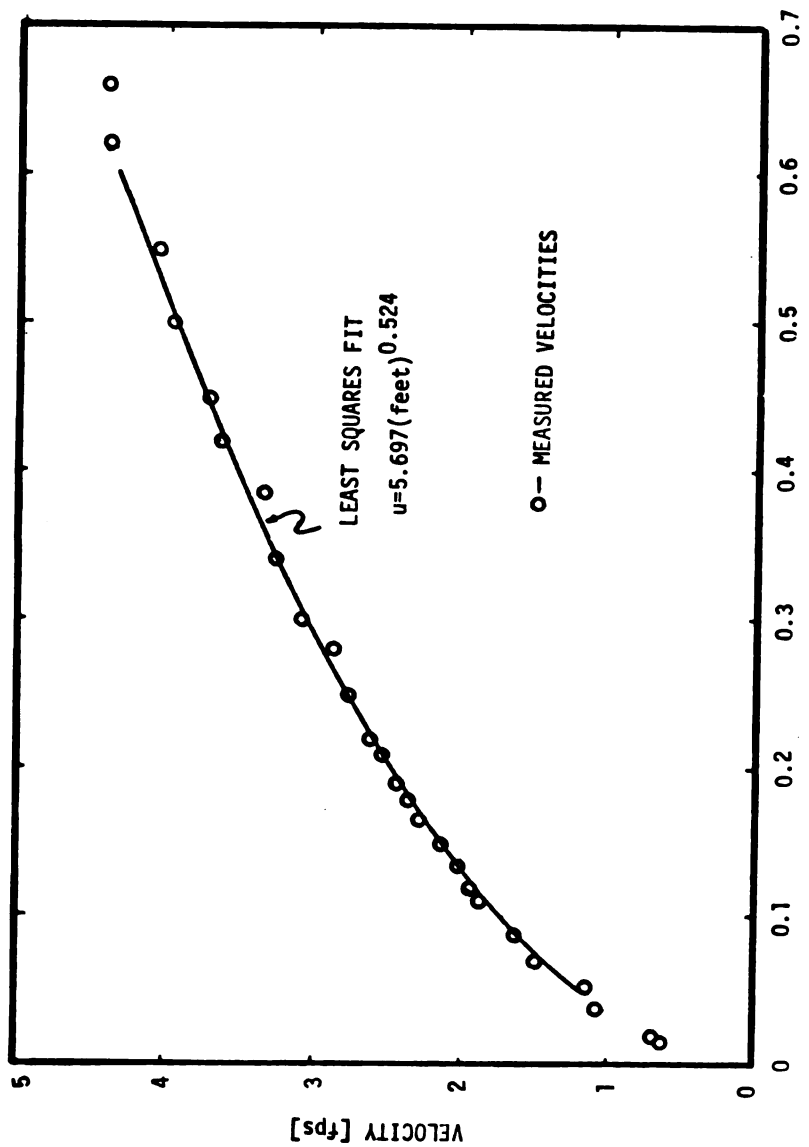

Figure 30. Elbow Meter Calibration Curve.

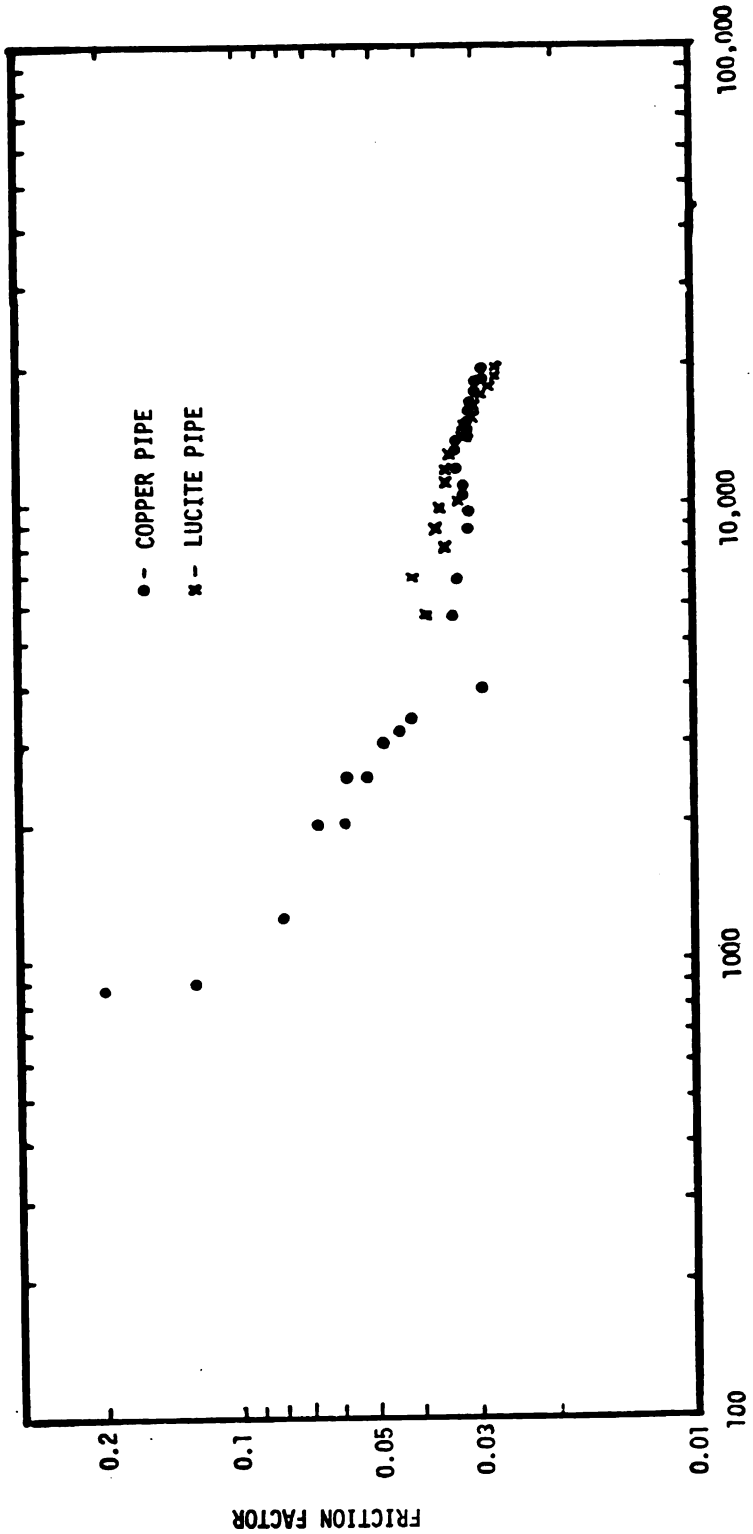

Figure 31. Flow Resistance Curve for Copper and Lucite Pipes.

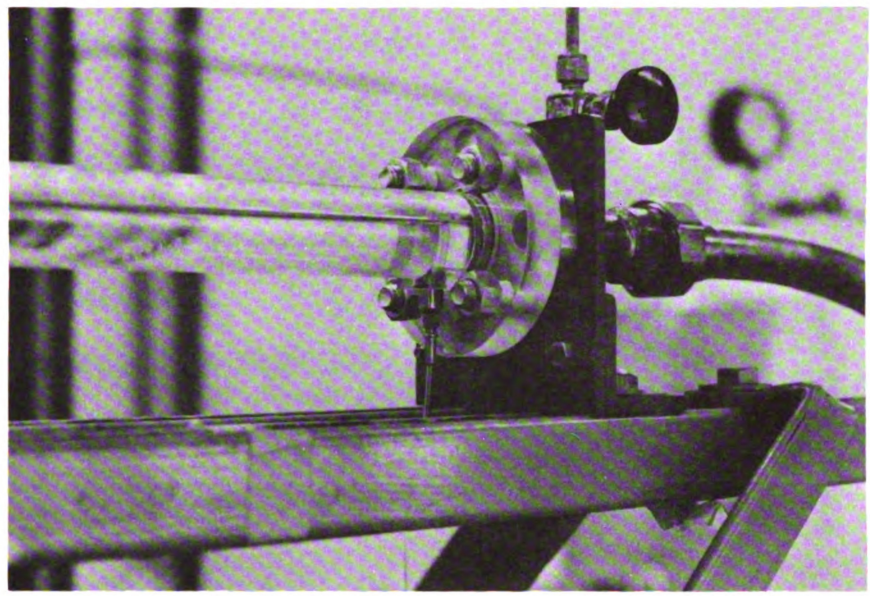

Figure 32. Close-up View of Miniature Strain Gage Transducer Mounted in the Lucite Pipe.

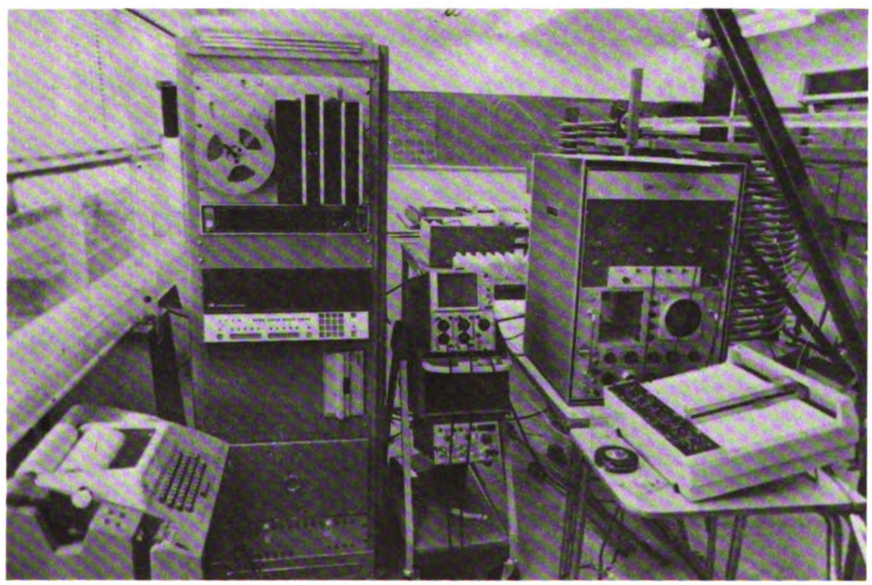

Figure 33. Photograph of Electronic Data Gathering System which includes Amplifier, Storage Oscilloscope, Mini-Computer, D/A Converter and X-Y Plotter.

a transducer mounted in the lucite pipe.

A Computer Automation mini-computer was programmed to sample the amplifier output voltages every 10 milliseconds and store these values on a floppy disc. Upon command, these voltage values were then sent to a Hewlett-Packard X-Y recorder to obtain a permanent, visual record of the experimental run. The transducer signals were also sent to a Tektronix storage oscilloscope for quick visualization purposes. Figure 34 is a schematic of the electronic set-up and Figure 33 shows the amplifier, oscilloscope, mini-computer and X-Y recorder.

4.2.2 Experimental Procedure

Carbon dioxide gas was bubbled through the upstream reservoir with the reservoir pressure adjusted by the throttling of a needle valve. Water samples were directly introduced into the Van Slyke apparatus to determine the dissolved gas content. When the desired degree of saturation was obtained, the reservoir was kept at a constant pressure by a pressure regulator connected to the building air system. Records of the room and water temperature along with the atmospheric pressure were also maintained.

Transducers were installed at the valve and the midpoint locations of the pipe. The calibration of the transducers was checked periodically throughout the testing and were found to remain stable with very little drift.

Steady-state flow was then established in the system. The desired velocity was attained through the adjustment of a throttle valve. Steady-state pressures throughout the pipe were always above the gas saturation pressure of the water; therefore, the initial flow was essentially one-phase. Considerable care was taken to insure that all gas bubbles were

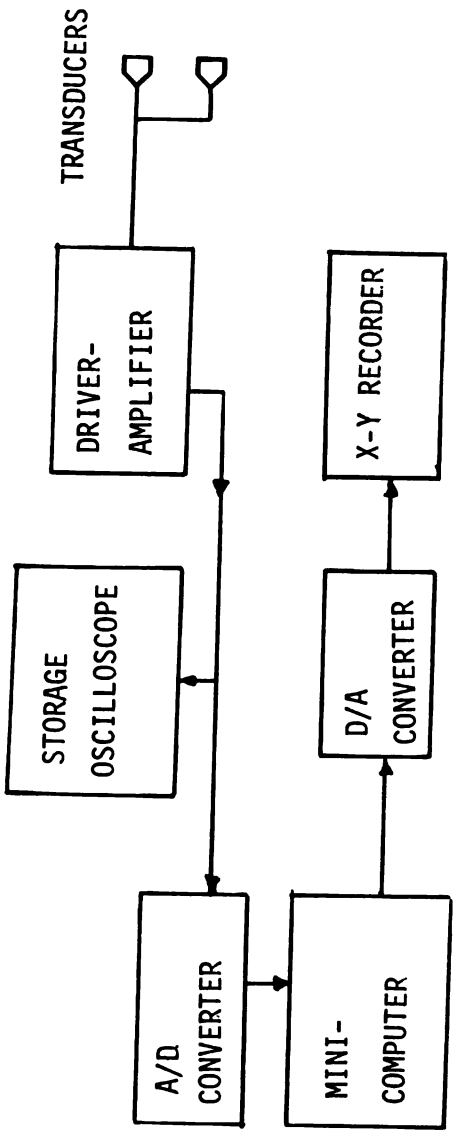

Figure 34. Schematic of Electronic Data Gathering System.

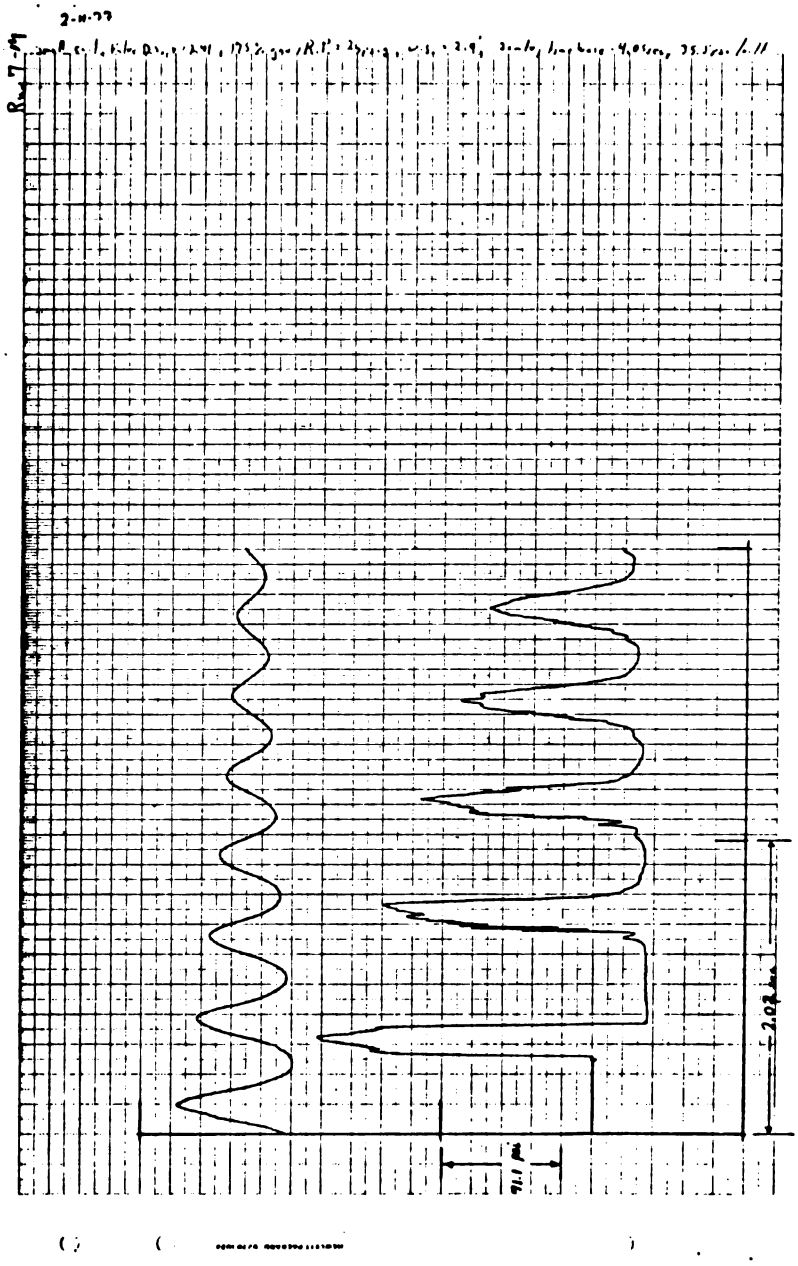

Figure 35. Actual Data Trace of Transient Pressures at Valve as Recorded on the X-Y Plotter.

bled out of the system before an experimental run was conducted.

The mini-computer was then activated to start sampling moments before the valve switch was thrown. The mini-computer next sampled the voltage output from the transducers for 8.05 seconds. The stored data could then be transferred to the X-Y plotter. This data-gathering system and procedure produced accurate results and provided large plots with good resolution of the transducer output. Figure 35 shows an actual data trace from the X-Y recorder. In the figure, the first 4.025 seconds of the transient are plotted below the second half of the trace.

CHAPTER V

COMPARISON AND DISCUSSION OF EXPERIMENTAL AND THEORETICAL RESULTS

The culmination of the present study on column separation and gas release in highly saturated fluids takes place in this chapter. The first section deals with the results of the gas release experiment and the influence of these results on the modeling of the gas release phenomenon. Next, the observed experimental results obtained from the hydraulic transient study along with the associated computer-simulated, theoretical comparisons are presented. A discussion of these comparisons and the effects of gas release is included.

5.1 Gas Release Experiment

As discussed earlier, the purpose of these experiments were to obtain, in a preliminary way, an order of magnitude approximation to the gas production rate to be used in the pipe transient modeling. These experiments did provide insight into the gas production rates and the time-dependent nature of gas release occurring in a closed container with grid turbulence present. However, one should be cautious in directly applying these results to an actual pipeline situation due to differing turbulence conditions and possible scaling differences. In this light, the gas release rates used in the model are recognized not as a precise description of the gas release phenomena in turbulent pipe flow, but rather as a more refined approximation than what is presently available in the literature.

5.1.1 Conditions Investigated

To gain an understanding of some of the important variables which may influence gas release it is of benefit to review some present theory. In an attempt to improve on an initial study by Parkin and Kermeen [15], Van Wijngaarden [22] investigated convective diffusion of gas into small bubbles attached to a submerged body. As reviewed in Chapter One, assuming slow growth and neglecting viscous forces, Van Wijngaarden describes the time rate of volume change for a single bubble to be

$$\frac{dV_b}{dt} = \frac{kT}{p_f - p_v + \frac{4}{3}(\sigma/R)} \frac{dN}{dt} \tag{101}$$

The term dN/dt is the molar flux of gas into the bubble. The concentration gradient of the gas in the fluid provides the driving potential for diffusion. This gradient is caused by the difference in concentration far away from the bubble c'_∞ and the equilibrium concentration c'_o at the bubble surface. The mass flux is related to the component $\partial c'/\partial n$ of this gradient normal to the bubble surface by

$$\frac{dN}{dt} = \int D' \frac{\partial c'}{\partial n} ds \tag{102}$$

where D' is the diffusion coefficient and ds is a surface element.

Attention is now given to the calculation of dN/dt. The concentration distribution in the field can be described by the diffusion equation. For the bubble size and growth rates studied by Van Wijngaarden, the diffusion process was approximately steady; therefore, the governing

equation would be

$$v \nabla c' = D' \nabla^2 c' \tag{103}$$

where v is the velocity vector in the region around the bubble. For the solution of Equation (103) with the boundary conditions $c' = c'_\infty$ at infinity and $c' = c'_o$ at the bubble surface, the velocity distribution around the bubble must be known. This presents a very complicated problem in which some approximations must be made. One particular model proposed to represent this mass transfer into the bubble is described by Levich [10]. In summary, Levich argues that there is no velocity boundary layer on the bubble in the usual sense. Therefore, assuming inviscid flow, the velocity distribution around the bubble can be calculated. Also, he observed that the diffusion takes place in a narrow region around the bubble as compared to the bubble radius; thereby simplifying Equation (103). Utilizing this observation and using the inviscid flow assumption to calculate a velocity distribution from the oncoming velocity u'; Equation (102) can be integrated to yield

$$\frac{dN}{dt} = 4(c'_\infty - c'_o)(2\pi R^3 u' D')^{\frac{1}{2}} \tag{104}$$

Using Henry's Law, the concentration difference $c'_\infty - c'_o$ can be related to the difference in the saturation pressure of the fluid and the instantaneous pressure. Letting Δp be equal to this pressure difference, Equation (104) becomes

$$\frac{dN}{dt} = 4\beta\Delta p(2\pi R^3 u' D')^{\frac{1}{2}} \tag{105}$$

where β is the Henry's Law proportionality constant. Equation (105) was also used by Kranenburg [9] in modeling gas release during hydraulic transients.

Equation (105) describes the mass influx into a single bubble. It states that the bubble growth rate is directly proportional to Δp, $R^{3/2}$, $(U')^{\frac{1}{2}}$ and $(D')^{\frac{1}{2}}$. Applying Equation (105) locally to every bubble within a specific volume of fluid could be used to estimate Γ; the total gas production rate per unit volume of mixture. Therefore, the Γ term would also be expected to be proportional to the above variables. In this study, no attempts were made to correlate the observed gas release data with Equation (105).

In the laboratory, the parameters that were varied were Δp and the turbulence level. The turbulence level was varied by the adjustment of the frequency of grid oscillation, thereby changing the convective transport around the bubble which was related to changing the slip velocity u'.

A series of tests were then conducted as described by Table 2 with ω being the frequency of oscillation of the grid system. Water was saturated with CO_2 gas at pressures of 10 psig, 20 psig, 30 psig and 40 psig. In the test cylinder, the pressure was then dropped to atmospheric conditions. At each Δp value, five experimental runs were made at different frequencies of grid system oscillation. In each case, the full amplitude was maintained at a constant 0.5 inches; thus, turbulence levels were solely dependent on the frequency.

The data was then hand-smoothed such that the numerical

Table 2. Summary of Gas Release Experiment.

Run No.	Δp (psi)	ω (Hz)	Full Amplitude (in.)	Water Temp. (^{o}C)	Atmos. Pressure (in. Hg)
1	10	0	0.5	18.5	29.25
2	10	1	0.5	18.5	29.25
3	10	3	0.5	18.5	29.25
4	10	5	0.5	18.5	29.25
5	10	7	0.5	18.5	29.25
6	20	0	0.5	18.0	29.25
7	20	1	0.5	18.0	29.25
8	20	3	0.5	18.0	29.25
9	20	5	0.5	19.0	29.48
10	20	7	0.5	19.0	29.48
11	30	0	0.5	19.0	29.48
12	30	1	0.5	19.0	29.48
13	30	3	0.5	19.0	29.48
14	30	5	0.5	19.0	29.48
15	30	7	0.5	19.0	29.48
16	40	0	0.5	20.0	29.32
17	40	1	0.5	20.0	29.32
18	40	3	0.5	20.0	29.32
19	40	5	0.5	20.0	29.32
20	40	7	0.5	20.0	29.32

differentiation of the data to determine actual Γ values would also produce a somewhat smooth curve. This numerical differentiation was done by computer using a simple weighted differencing technique between data points. Figure 36 shows the experimentally measured void fraction and the associated time rates for Δp = 10 psi. Figures 37, 38, and 39 are the results for Δp = 20, 30, and 40 psi, respectively.

5.1.2 Discussion of Results and Modeling Implications

Before discussing the analysis of the gas-release data, possible experimental and measurement errors that may have occurred are examined. These errors were primarily due to the design of the particular apparatus and measurement technique. Some possible sources of error are:

1. Upon the quick-opening of the valve to depressurize the test cylinder, an initial surge occurred in the measuring tube due to the compressibility of a small amount of entrapped air remaining at the top of the test cylinder which could not be bled out. This initial surge complicated the obtaining of accurate measurements within the first two seconds.
2. The nonlinearity of the resistance wire gage exhibited a more sensitive calibration at higher water surface levels than lower levels, thus further complicating early-time measurements.
3. At the larger Δp values, the pressure in the test cylinder may not have remained constant at atmospheric. A rise in pressure may have occurred due to the resistance associated with the small ¼" copper line connecting the test cylinder to the measuring tube.

4. When running the Δp = 40 psi tests, there was considerable gas release occurring in the water entering the measuring tube causing slug flow to evolve therein.

Some observations of the actual testing are important to note. Upon the initial depressurization of the test cylinder, small bubbles could be seen to form on the walls of the cylinder and on the grid system. These bubbles would then grow, break loose and rise to the top of the cylinder. After a short time, extensive bubble growth could be observed throughout the cylinder. The pretest condition of the test cylinder also had a large bearing upon the experiment. It was observed during the preliminary testing that much more gas release occurred during a test when the test cylinder and agitation grid system were completely dry before the test was conducted, as opposed to the prior wetting of these components. This seems to indicate that there were more nucleation sites available for gas diffusion when the components were originally dry. In the experiments described in Table 2, these components were thoroughly wetted before testing. Due to constraints on the profitable use of time, a check on the repeatability of these tests was not conducted. However, preliminary testing with water saturated with air showed that repeatable results were not usually obtained.

In examining Figures 36 through 39 certain consistancies are noticable. For each Δp value examined, more gas release occurred at increasing frequencies of agitation. It is apparent that the translational fluid motion around the bubbles increased with higher frequencies, thus enhancing the evolution of gas. Also, another expected result was for a given frequency, the amount of gas released increased with increasing

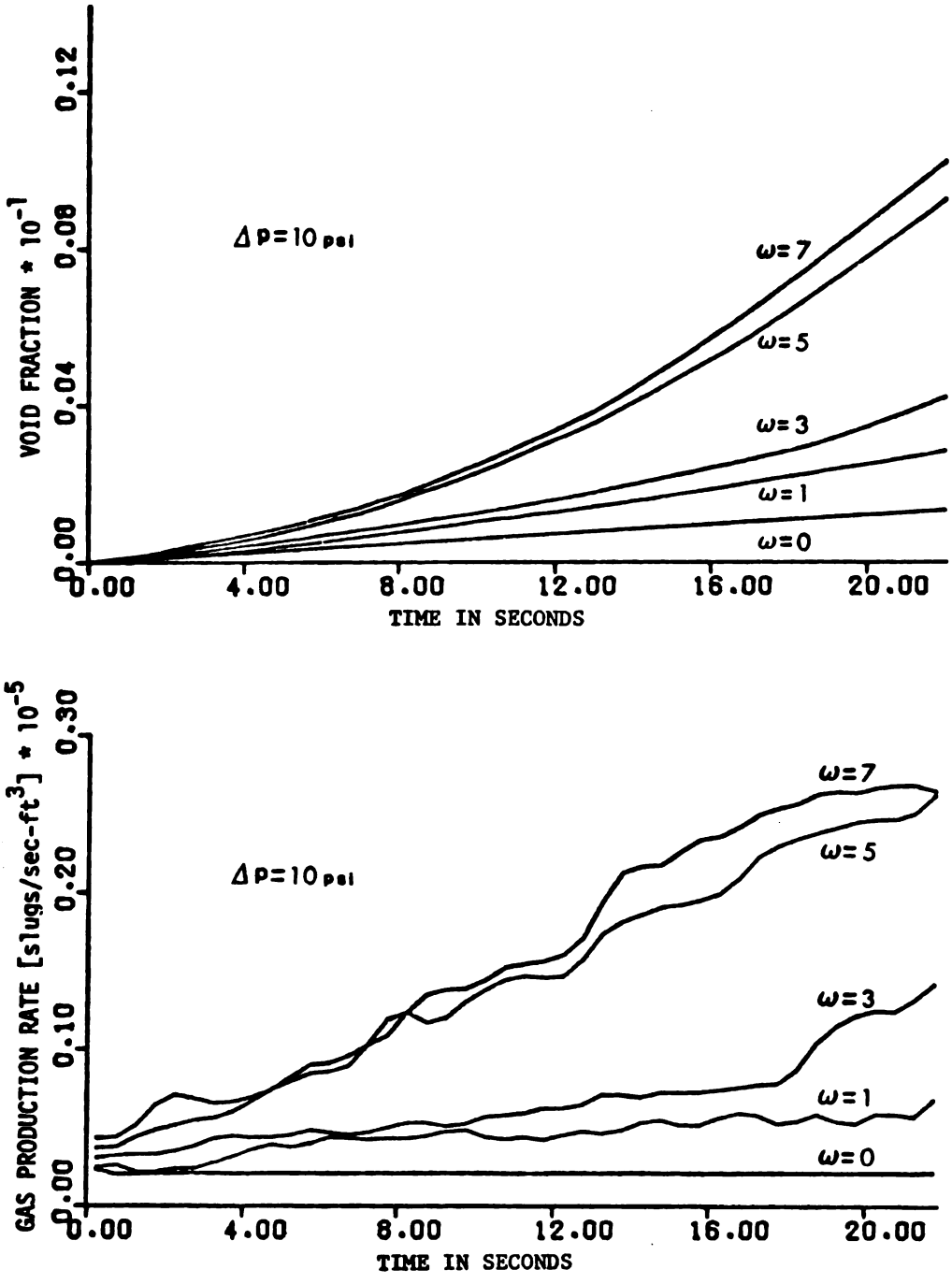

Figure 36. Results of Gas Release Experiment for Δp=10 psi.

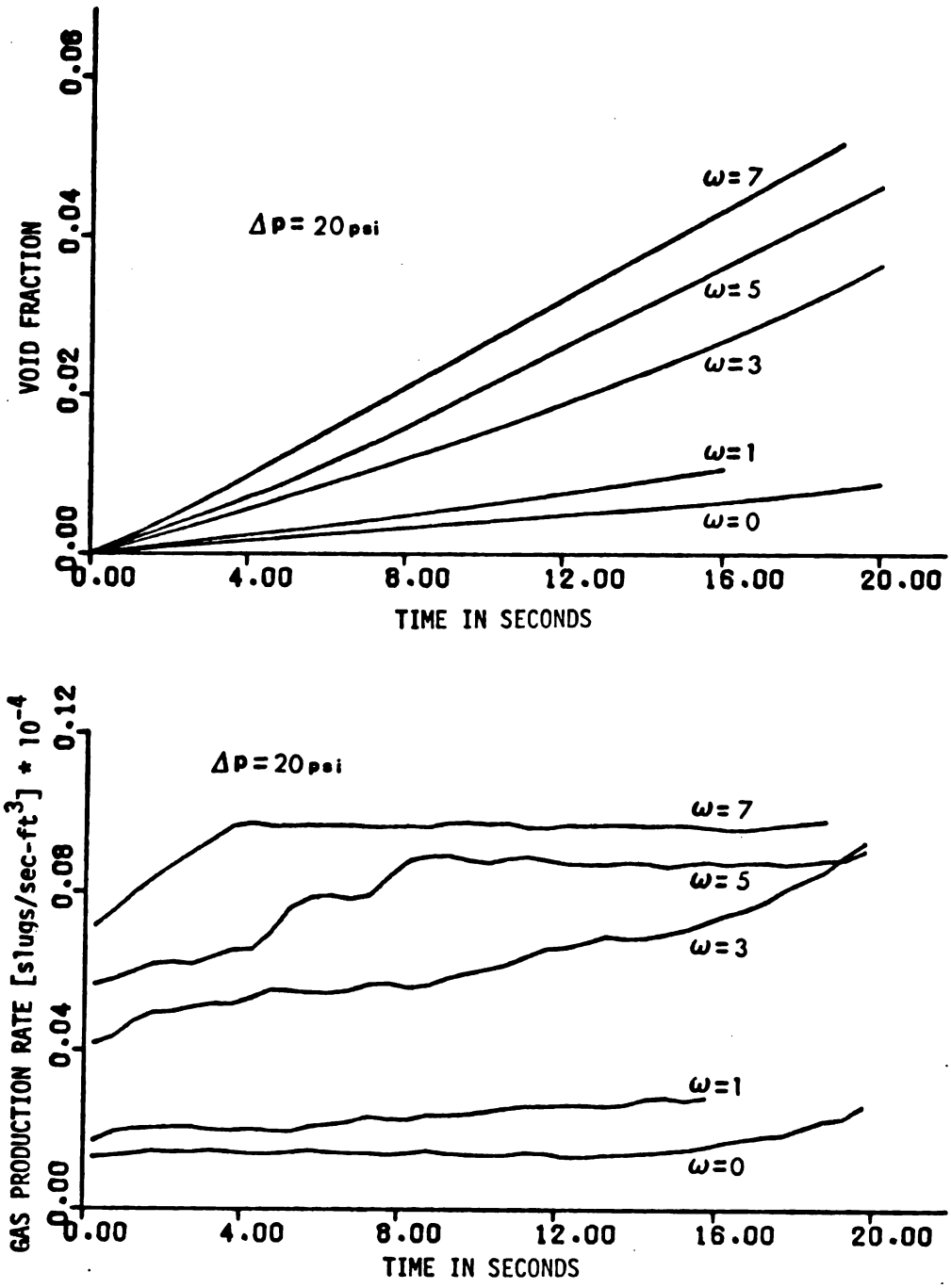

Figure 37. Results of Gas Release Experiment for Δp=20 psi.

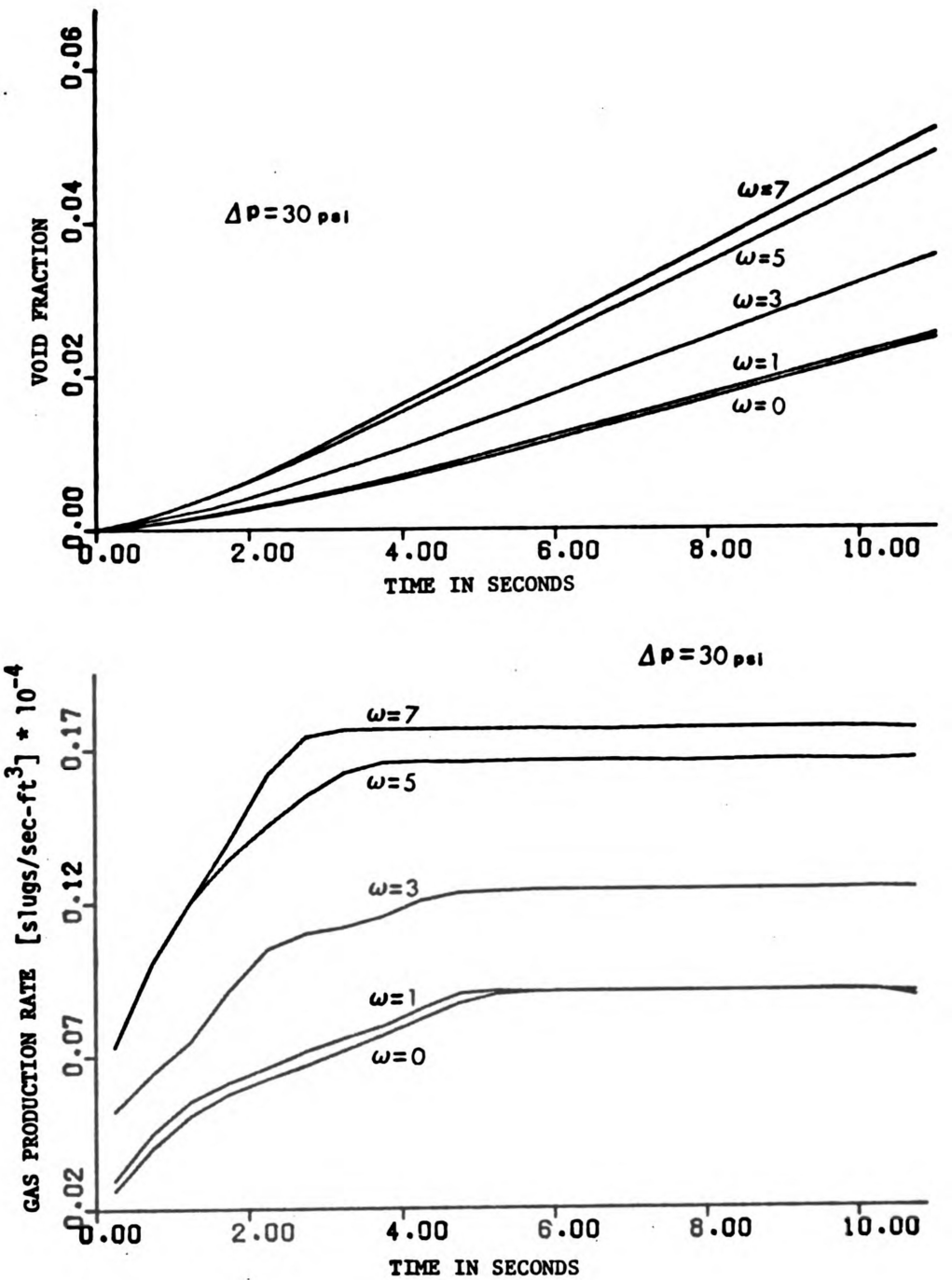

Figure 38. Results of Gas Release Experiment for Δp=30 psi.

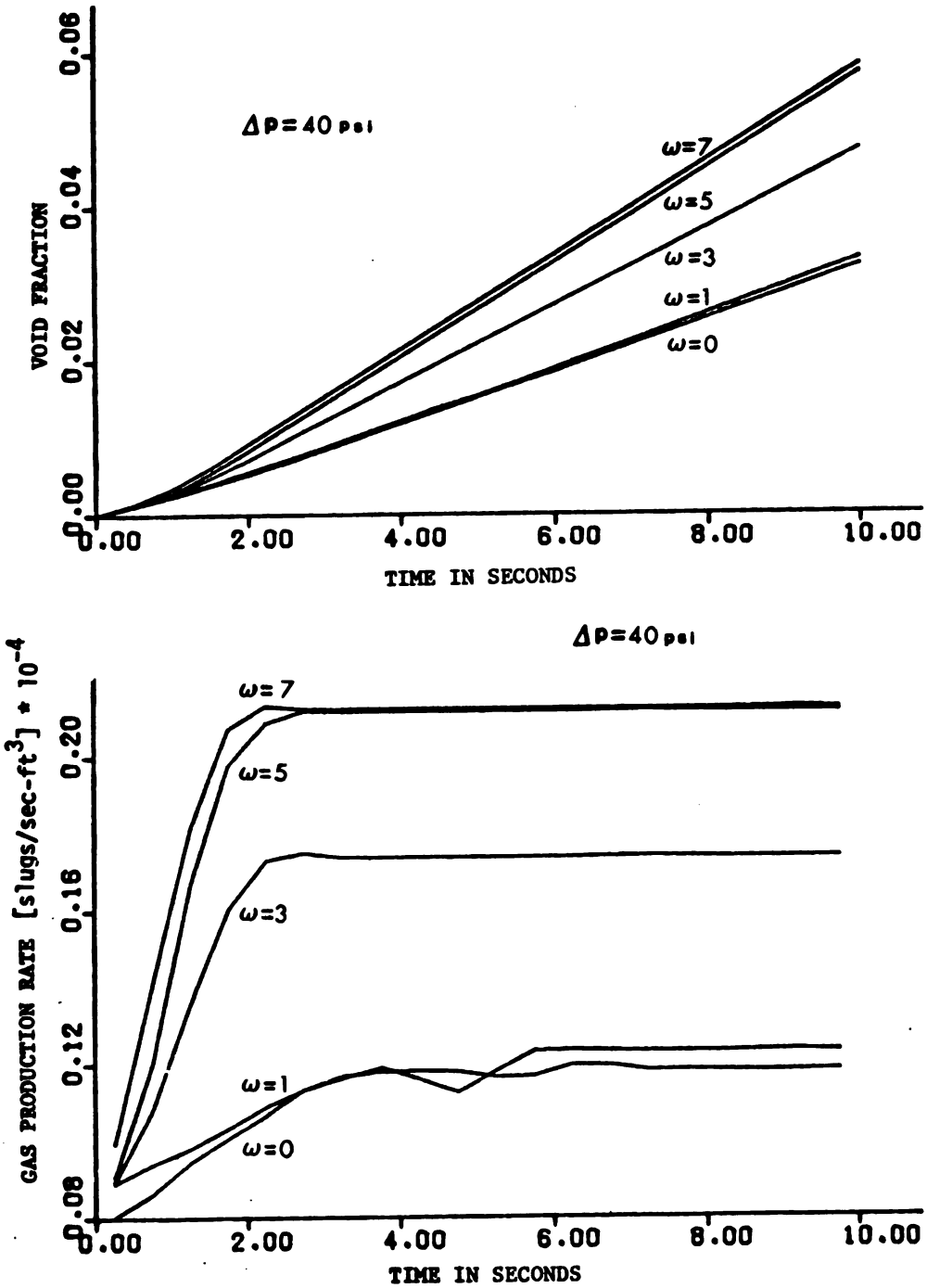

Figure 39. Results of Gas Release Experiment for Δp=40 psi.

Δp values. A third important trend can be noted in observing the actual Γ values. The gas production rate initially increased with time with the Δp = 30 psi and 40 psi cases reaching a constant limiting value. In reference to Equation (105), this initial increase would be an expected result. Since the gas production rate is proportional to the diameter of the bubbles, a smaller rate would be expected at the beginning of the experiment when only very small diameter bubbles exist. The reason for the limiting rates in the Δp = 30 psi and 40 psi runs is uncertain. It may have been due to a pressure rise in the test cylinder due to the extensive gas release associated with these runs or perhaps a steady state situation may have been achieved since the bubble size was restricted in a sense that the bubbles could only become so large before they would ascend and collect at the top of the cylinder.

In light of the above findings, it was decided to numerically model gas release with the curve described by Figure 40, in which Γ was normalized by Δp. Normalizing the actual data curves did produce an order of magnitude range of values that were used to describe this curve. In the figure, GAM1 is the normalized ordinate at time equal zero and GAM2 is the normalized ordinate at time equal to TS. These three variables were entered into the computer program to determine the slope of the gas production rate, the limiting value and the time at which it was reached. The procedure used in the algorithm was as follows. If the pressure at a node was calculated to be below the gas saturation pressure of the fluid, a $\Gamma/\Delta p$ value was calculated according to the total amount of time a supersaturated condition existed at that node since the beginning of the transient. Multiplying by the instantaneous Δp resulted in a Γ for that node and time. If the pressure was calculated to exist

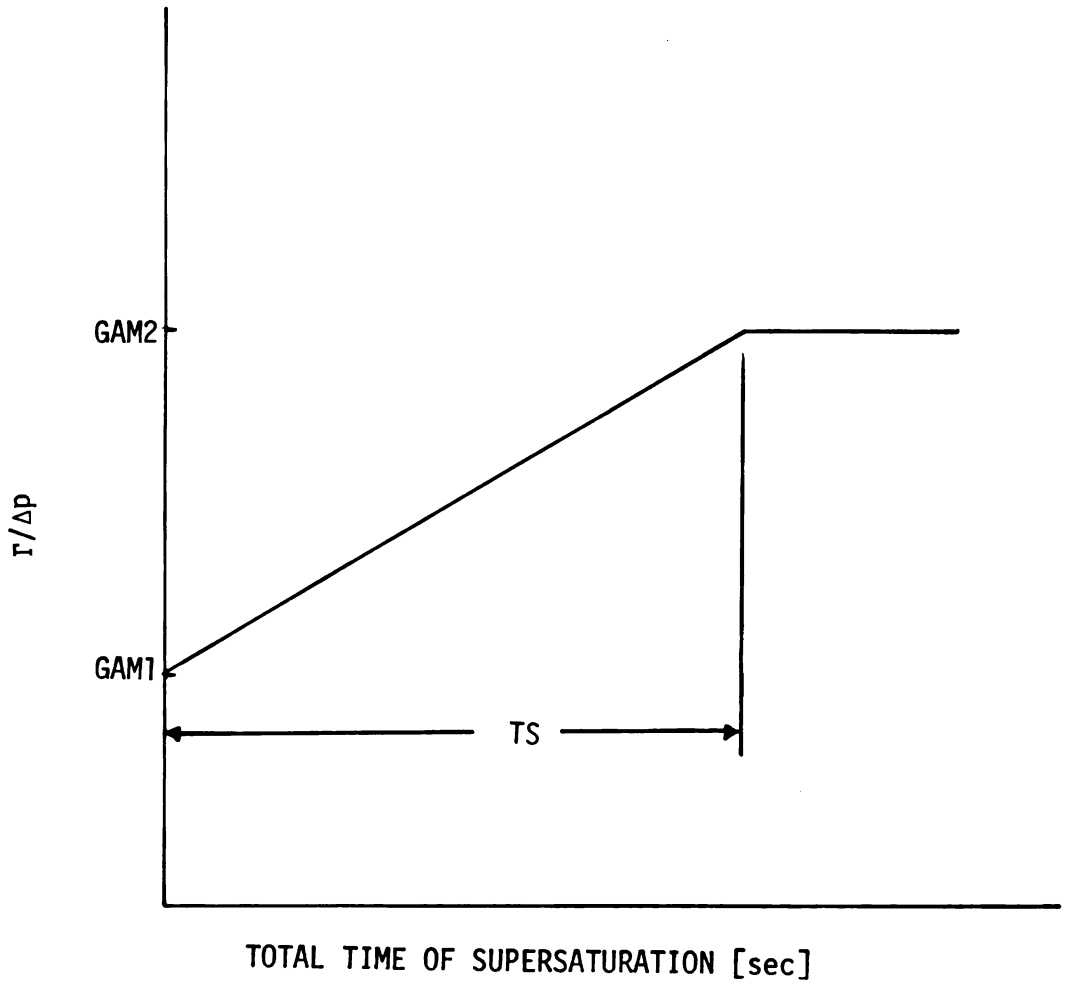

Figure 40. Gas Production Rate Curve used in Numerical Model.

above the gas saturation pressure, no resolution of the gas was assumed and Γ was set to zero. Upon returning to a supersaturated condition, ordinate values were again calculated using the total amount of time that node had experienced supersaturation, which implies starting from the point on the time axis where ordinate values were last calculated. When the time TS was reached, the limiting value of GAM2 was used. However, in the simulations conducted in this study, in which a TS value of four seconds was used, values from the sloped portion of the curve were always used since a supersaturated condition never existed for that length of time.

It is often difficult to obtain repeatable results during hydraulic transient testing. Several factors may cause this including differences in the number and sizes of available nuclei between experimental runs. In this study, the amount of gas release occurring during the transient was also affected by these variables which could not be controlled. The actual GAM1 and GAM2 values used in the modeling were in the range of 1.0E-8 to 1.5E-7. These were the approximate normalized values for the $\omega = 1$ and $\omega = 3$ data runs. Values were selected from this range with regard to the apparent gas release characteristics of a particular experimental run.

5.2 Pipeline Transients

5.2.1 Conditions Investigated

The capability to place the solenoid-actuated valve at either an upstream or downstream location combined with the ability to control important variables created a combination of possible laboratory conditions that could have been investigated. To systematically compare laboratory results, the three variables that were manipulated were the

dissolved gas content, reservoir pressure and valve position.

Transient data was gathered from both upstream and downstream valve closures. With the valve located in the downstream position, the steady-state velocity was maintained at 2.41 fps for all data runs. The upstream reservoir was varied between three pressure levels, approximately 10 psig, 25 psig and 40 psig. The dissolved gas content of the water ranged from approximately 2% by volume, which was water which had not been saturated with CO_2 and contained mostly dissolved air, to 175% which was almost totally dissolved CO_2 gas.

When upstream valve closures were conducted, a steady-state velocity of 2.50 fps was used. The downstream reservoir pressure was varied between approximately atmospheric pressure to 10 psig and 20 psig with the dissolved gas content ranging from approximately 2% to 145% by volume. Table 3 describes the experimental runs conducted.

5.2.2 Comparison of Results

Figures 41 through 44 show the comparisons of the experimental data and the theoretical results for Experimental Runs 1, 4, 5 and 8, which were downstream valve closures. Comparisons for the upstream valve closures are exhibited in Figures 45 through 48; which correspond to Experimental Runs 9, 15, 16 and 14. Although numerical comparisons were conducted for all the experimental runs, these were judged as representative examples of the predictions. Shown in the figures is the pressure at the valve and midpoint of the pipe. Table 4 shows the GAM1, GAM2 and TS values used in the numerical predictions. A polytopic constant of one was used for all predictions which implies isothermal compression and expansion of the gas.

Before discussing the predictions, examining only the experimental

Table 3. Summary of Transient Pipeline Experiments.

Run Number	Date 1977	Valve Location	Velocity (fps)	Gas Content (pereent)	Reservoir Pressure (psig)	Water Temperature (°C)	Atmospheric Pressure (in. Hg)
1	2-11	Downstream	2.41	2	11.79	16	29.18
2	2-11	"	2.41	2	26.41	16	29.18
3	2-11	"	2.41	2	41.61	16	29.18
4	2-11	"	2.41	95	11.58	16	29.18
5	2-11	"	2.41	95	26.99	16	29.18
6	2-11	"	2.41	95	41.90	16	29.18
7	2-11	"	2.41	175	26.04	16	29.18
8	2-11	"	2.41	175	42.91	16	29.18
9	2-12	Upstream	2.50	2	0.69	13	29.06
10	2-12	"	2.50	2	11.78	13	29.06
11	2-12	"	2.50	2	21.91	13	29.06
12	2-12	"	2.50	95	5.82	13	29.06
13	2-12	"	2.50	95	10.00	13	29.06
14	2-12	"	2.50	95	21.33	13	29.06
15	2-13	"	2.50	50	3.19	15	28.66
16	2-13	"	2.50	50	11.20	15	28.66
17	2-13	"	2.50	50	21.21	15	28.66
18	2-13	"	2.50	145	10.91	15	28.66
19	2-13	"	2.50	145	20.33	15	28.66

Table 4. Gas Release Variables Used in Numerical Model.

Experimental Run	GAM1 (Slugs/sec-ft^4)	GAM2 (Slugs/sec-ft^4)	TS (sec)
1	0.0	0.0	-
4	2.0E-8	5.0E-8	4.0
5	5.0E-8	1.2E-7	4.0
8	7.0E-8	1.5E-7	4.0
9	0.0	0.0	-
15	1.0E-8	6.0E-8	4.0
16	3.5E-8	1.0E-7	4.0
14	7.0E-8	1.5E-7	4.0

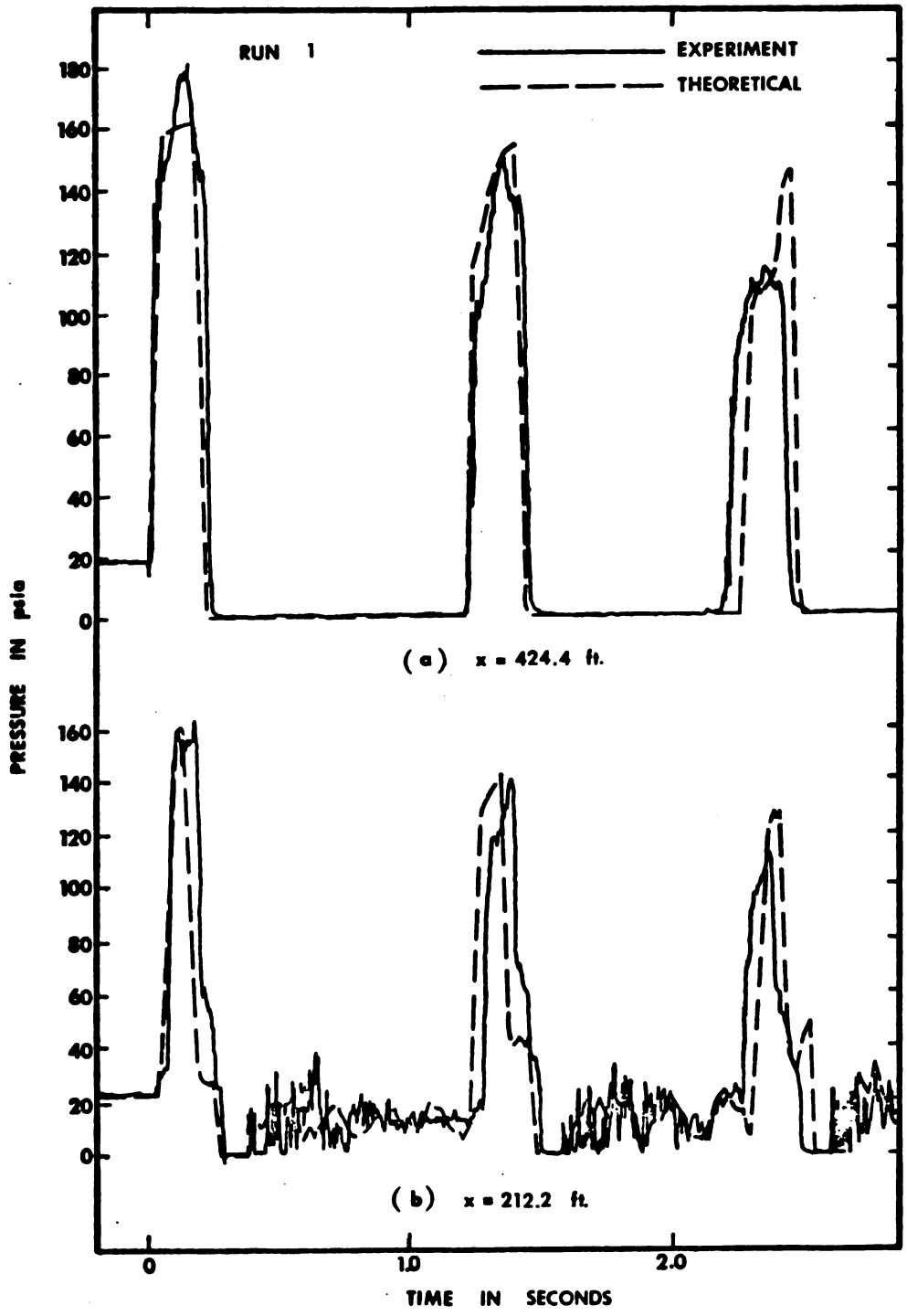

Figure 41. Comparison of Measured Transient Pressures with Theoretical Results for Experimental Run 1.

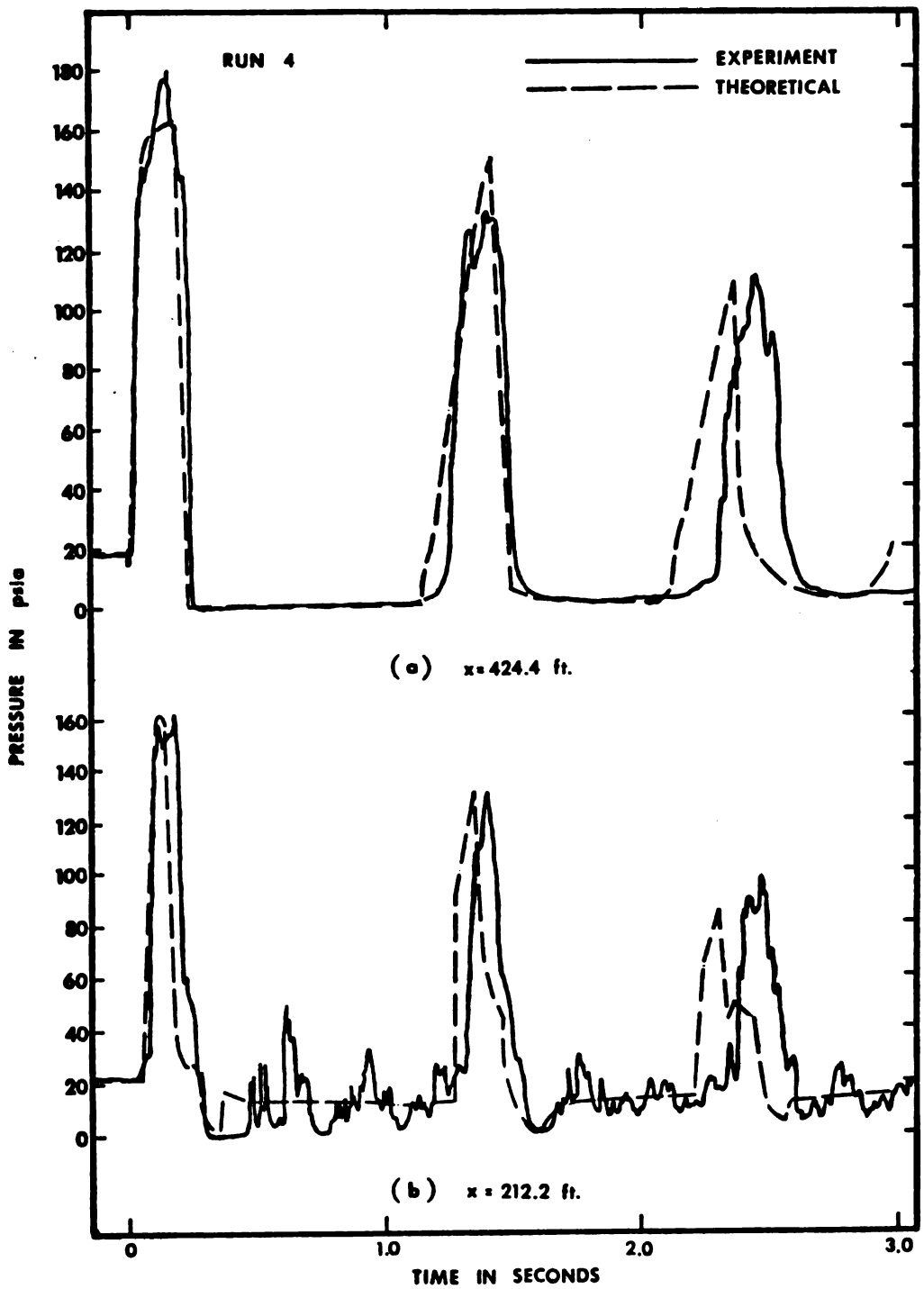

Figure 42. Comparison of Measured Transient Pressures with Theoretical Results for Experimental Run 4.

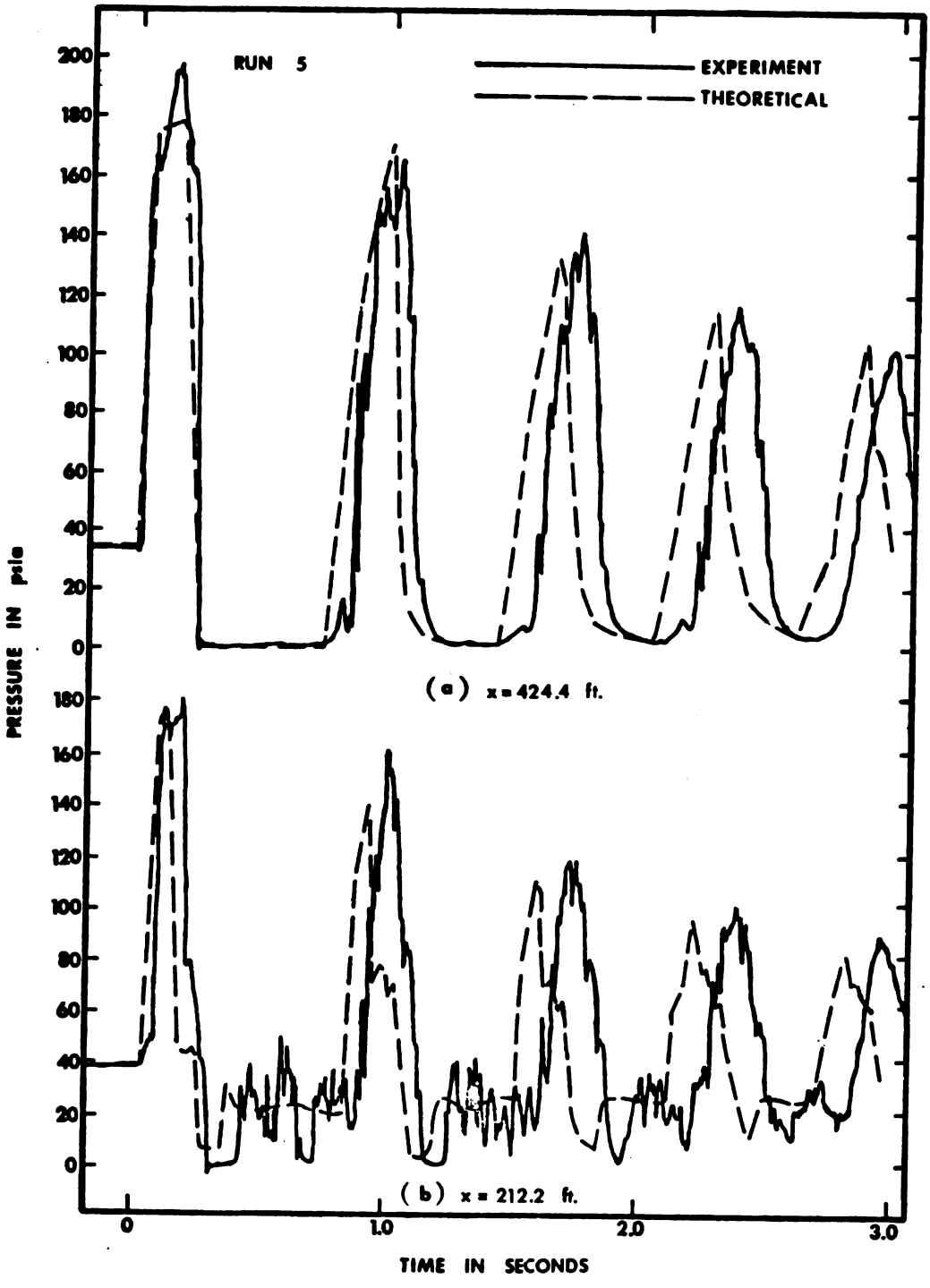

Figure 43. Comparison of Measured Transient Pressures with Theoretical Results for Experimental Run 5.

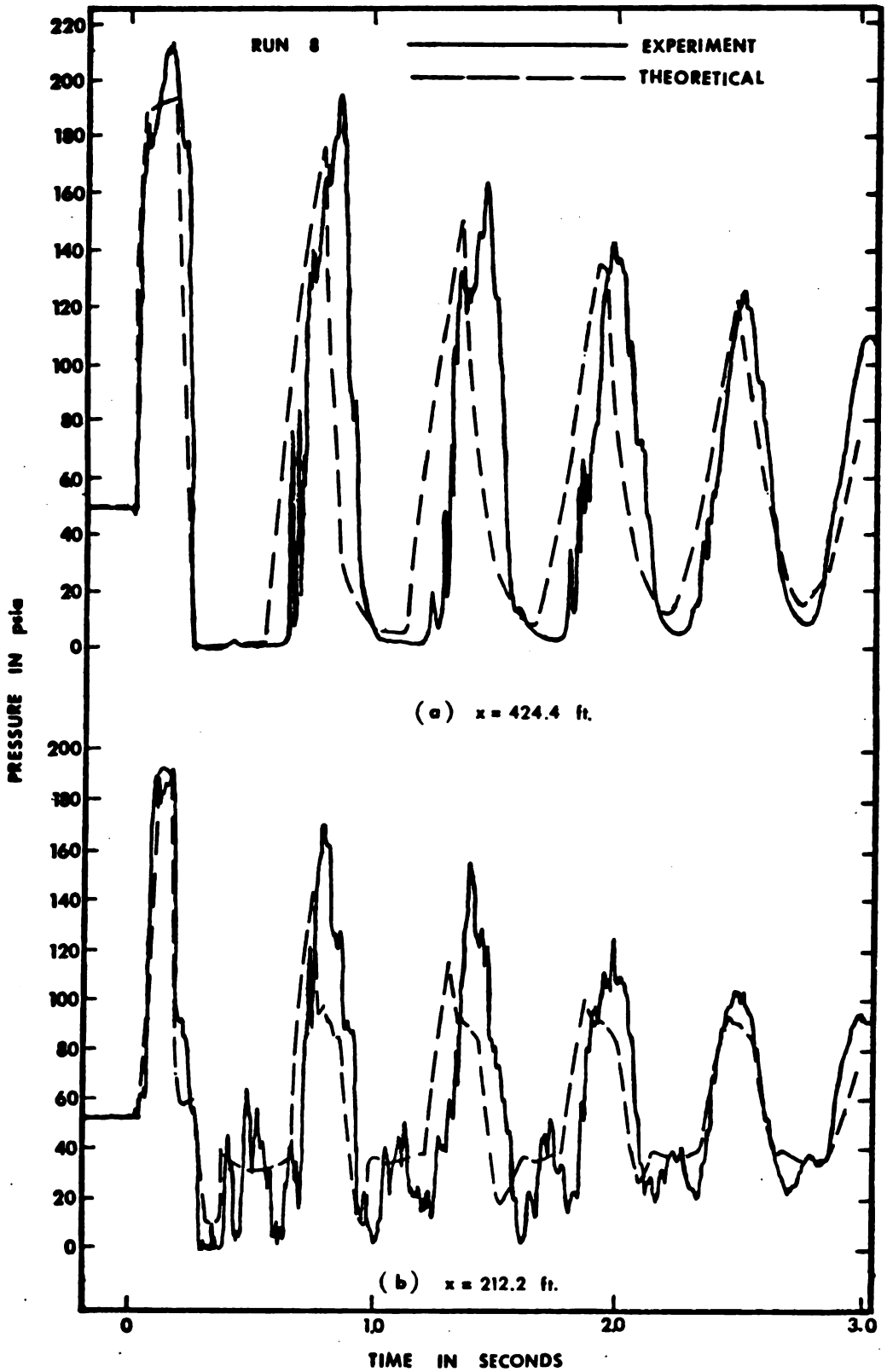

Figure 44. Comparison of Measured Transient Pressures with Theoretical Results for Experimental Run 8.

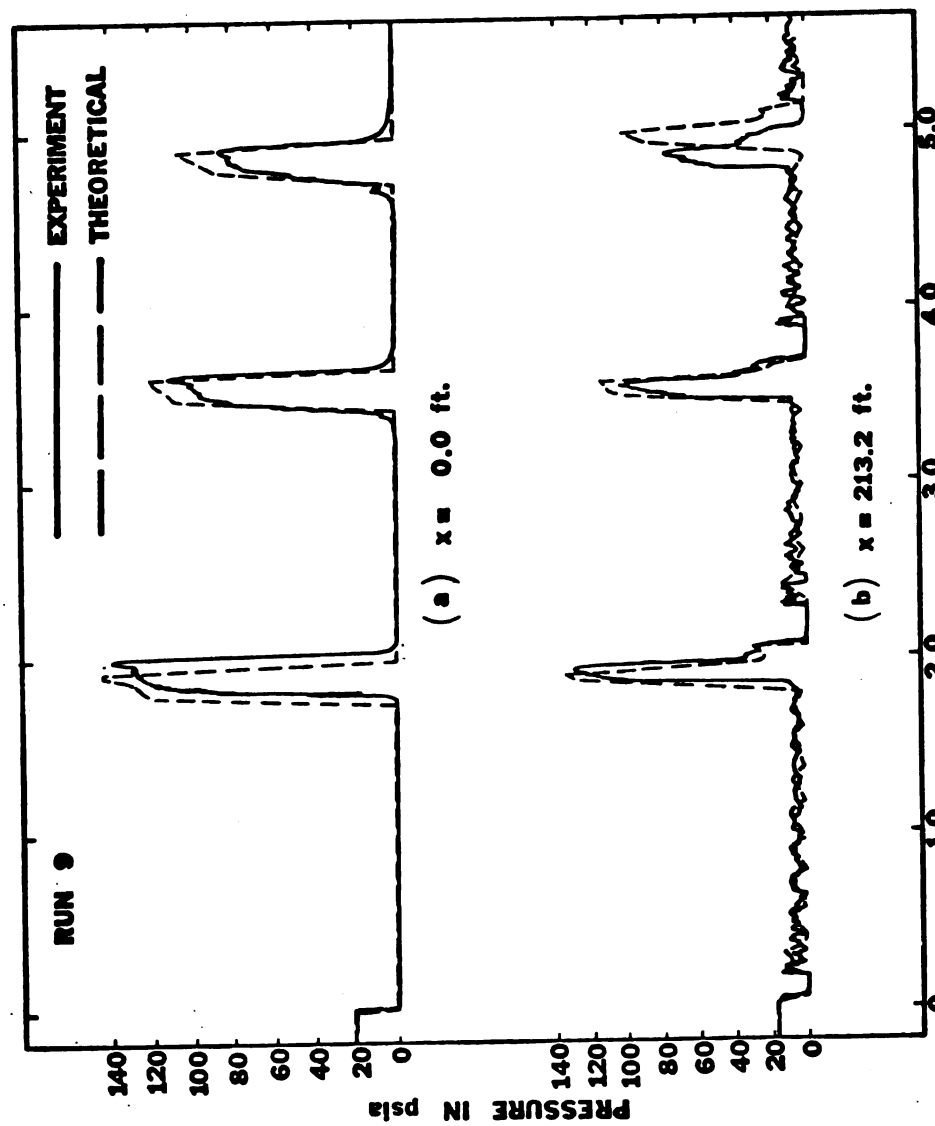

Figure 45. Comparison of Measured Transient Pressures with Theoretical Results for Experimental Run 9.

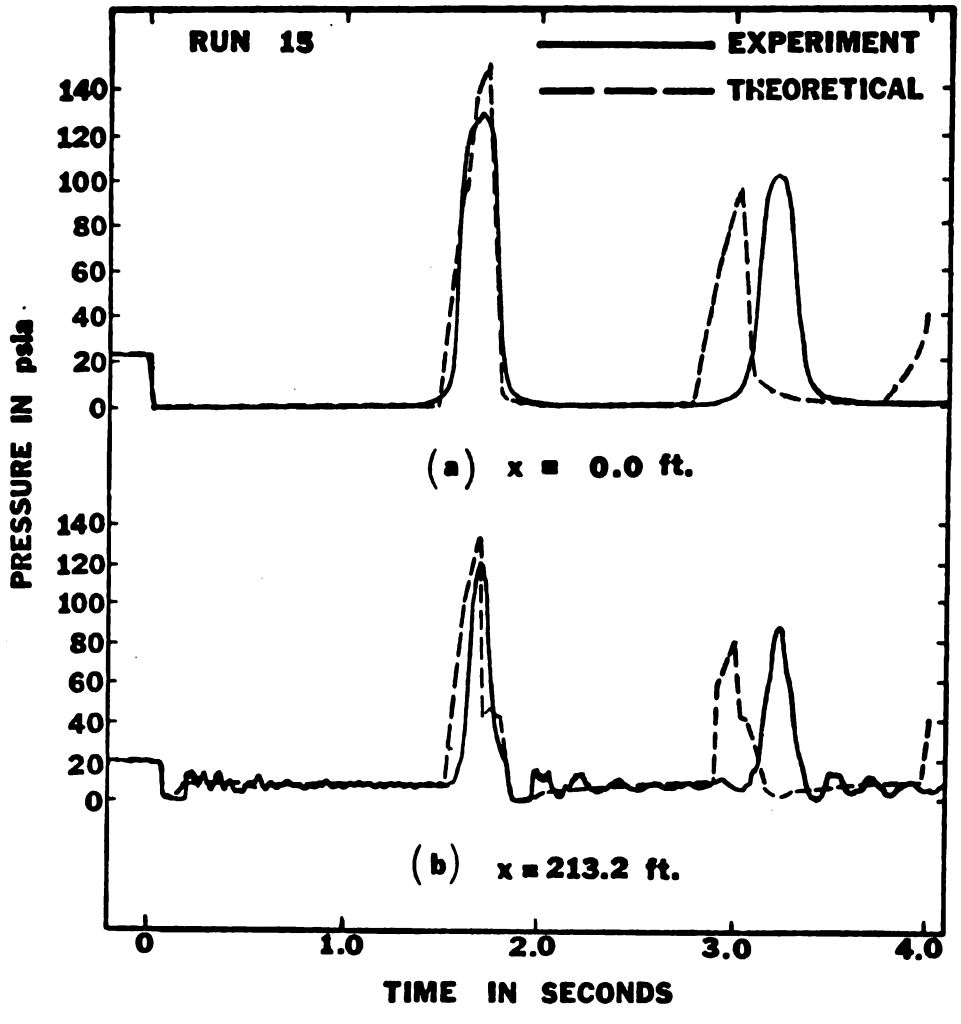

Figure 46. Comparison of Measured Transient Pressures with Theortical Results for Experimental Run 15.

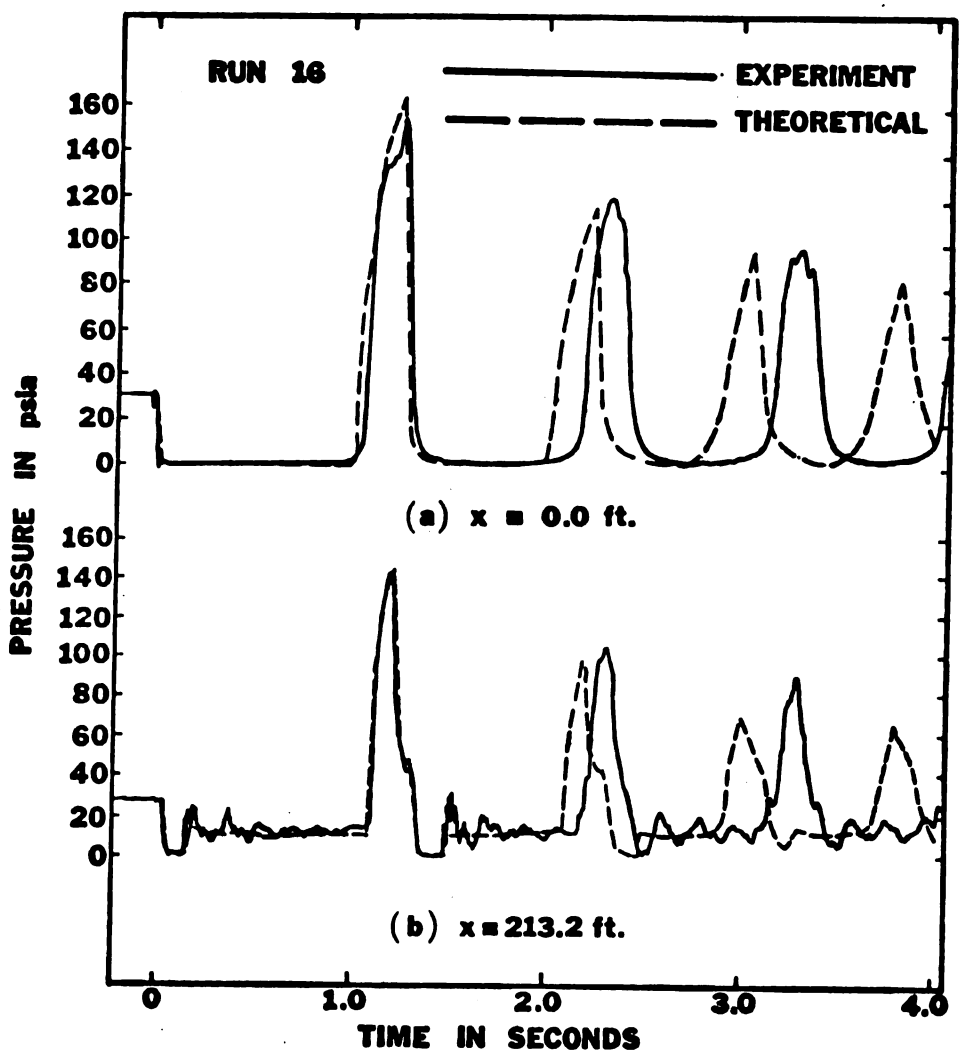

Figure 47. Comparison of Measured Transient Pressures with Theoretical Results for Experimental Run 16.

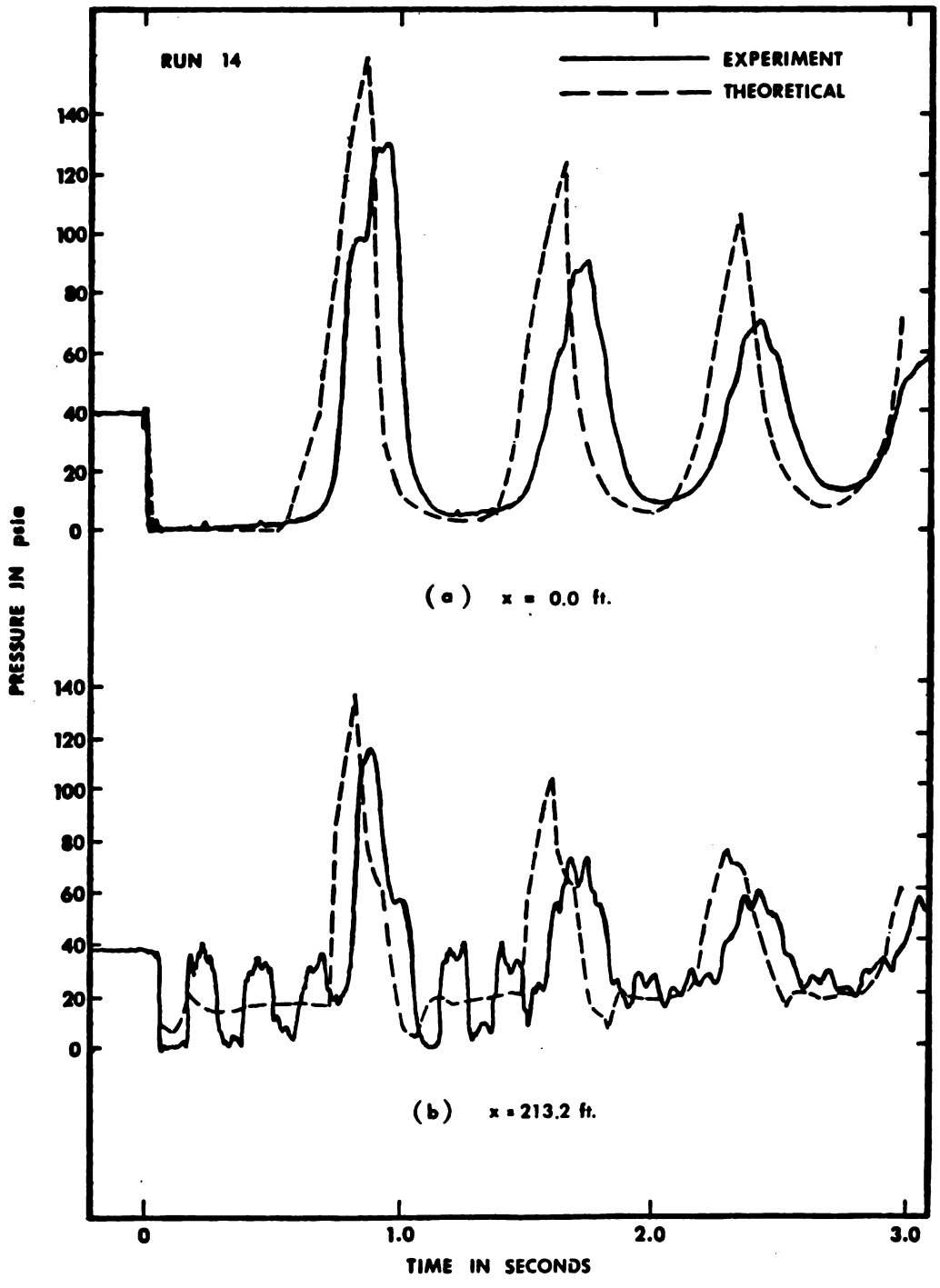

Figure 48. Comparison of Measured Transient Pressures with Theoretical Results for Experimental Run 14.

data does provide insight into the effects of gas release on the transient. Figures 41 and 45 show experimental runs in which the water was not saturated with CO_2. These runs where characterized by sharp pressure changes and vapor pressure conditions being reached at the valve several times. In these runs, it is doubtful if any significant gas release occurred. In examining the runs in which the water was saturated to some degree with CO_2 gas, the effects of released gas become apparent. Some of the characteristics of these runs are a much smoother pressure trace and during the initial column separation at the valve, a slightly rising pressure until the return of high pressure conditions. Also common to these runs, apparently due to significant gas release during the first low-pressure cycle, is the reaching of vapor pressure at the valve only during the first low-pressure cycle.

Visual observations of the transient flow in the lucite pipe revealed the presence of tiny cavitation bubbles that immediately formed throughout the pipe during the initial column separation period. These bubbles would disappear upon the return of high pressure and would again become visible during periods of low pressure. In the low gas content runs (2% by volume), when the transient had been completely damped, a few very small bubbles were seen to remain in the pipe suggesting the release of gas during the transient. In the higher gas content runs, the size and number of these bubbles were considerably larger. Motion pictures were then taken of the transient flow in the lucite pipe. From these pictures it was seen that in the higher gas content runs the bubbles did not completely collapse upon the return of the first high-pressure conditions, whereas, within the resolution of the camera, the bubbles were seen to completely disappear in the low-gas content runs when high-pressure conditions existed.

In examining the predicted results for Runs 1 and 9, good agreement was obtained for the pressure at both the valve and midpoint. These runs were associated with low-gas content water. In the modeling of these runs, no gas release was allowed, and the compatibility equations reduced to the usual one-phase waterhammer equations. This suggests that good results can be obtained from the simpler one-phase model in cases were insignificant gas release occurs.

The prediction of the downstream valve closures, Runs 4, 5, and 8 also showed good agreement in the peak pressures and phasing at both the valve and midpoint locations. However, the theoretical results did not reproduce the higher frequency pressure oscillations that were present between peak pressures which were observable at the midpoint of the pipe.

In examining the upstream valve closures with gas release, varied success was achieved. Runs 15 and 16 showed a fair agreement while Run 14 exhibits larger predicted pressures than actually occurred. Again, the higher order pressure fluctuations at the midpoint were not predicted.

It is apparent that closer agreement was obtained with the valve located downstream. Since the valve required a finite time to close, vapor pressure may have occurred behind the valve before it completely closed complicating the transient. Indeed, in the numerical model, vapor pressure was calculated at the valve before complete closure occurred. Since this caused difficulties in the model, all upstream valve closures were modeled as instantaneous. This inconsistency between the modeling and reality may have been a factor complicating the attaining of better comparisons of the upstream valve closures.

As previously mentioned, the experimental results showed the passage of small pressure fluctuations along the pipe during periods of reduced pressure which the theoretical results failed to reproduce. The reason for this is not clear. It is possible that the oscillations were smoothed out due to numerical damping primarily caused by interpolations. However, to suppress these oscillations a considerable amount of damping would be needed. Since much of the detail and phasing of the primary pressure peaks were predicted, it seems reasonable to conclude that the numerical damping that did occur was not significantly large enough to smooth these pressure fluctuations.

A more plausible explanation would seem to lie in the modeling of the gas release phenomena. The numerical model simulating gas release was based upon the results of the gas release experiment. The actual gas release occurring in the pipeline may have taken a different form due to several factors. In the gas release experiment a grid turbulence was generated throughout the duration of the test. Obviously, turbulence conditions experienced in the transient pipeline would be different and could be described as a decaying turbulence with the turbulence level dependent on the oscillating velocity field; this would imply a different type of gas release. Also, the gas release characteristics of water when vapor conditions are reached are not known. Perhaps the opening of vapor voids increases the gas release occurring at that point due to the increased gas-liquid interface.

In addition, the numerical model did not account for the evolution of gas into the vapor pockets. In the model it was assumed that the gas was released in a distributed manner throughout the pipe with vapor cavities forming at computing nodes. Perhaps the inclusion of gas evolution

into the vapor voids would more closely model the actual situation, thus resulting in better agreement.

CHAPTER VI

SUMMARY AND CONCLUSIONS

The primary objective of this study was to provide a better understanding of the effects of gas release on hydraulic transients and to develop a mathematical model to quantitatively predict transient pipe flow which experiences gas release. Along with modeling the distributed release of gas throughout the pipe, the phenomenon of column separation was also taken into account. The theoretical findings were then compared with experimentally obtained pressure data.

The results and conclusions of this study are:

(a) The differential equations which characterize two-phase hydraulic transients including gas release are recognized to be a set of three, nonlinear, hyperbolic equations which are amenable to solution by the method of characteristics.

(b) A sophisticated mathematical model can be developed using the method of characteristics with specified distance and time intervals. Evidence is presented which shows that reduced interpolation errors occur by the application of $\Delta t/\Delta x$ ratios larger than those conventionally used. Due to the reduced numerical damping, this method appears to be competitive with other finite-difference schemes such as the Lax-Wendroff two-step scheme in dealing with variable wavespeed situations. Another advantage of this

method is the capability to integrate the pathline characteristic along a time line.

(c) The gas release experiment provides insight into the evaluation of gas in a closed container. By controlling Δp and the grid turbulence, certain gas release trends are observed. It is recognized that the evolution of gas under turbulent pipe conditions is a complicated process and that the results of this experiment are not a precise description of gas release occurring during transient pipeflow; however, it does provide a basis from which a gas release model is developed along with supplying an order of magnitude range for the gas release variables that are used in the model.

(d) Experimental data obtained from the transient pipeline apparatus provides insight into the effects of gas release when water is saturated to some degree with carbon dioxide gas. Systematically changing the gas content and reservoir pressure reveals that in cases of higher dissolved gas content pressure peaks are slightly attenuated, a smoother response is obtained and the timing of the peaks are delayed.

(e) The comparisons of the experimental data and theoretical results obtained from the mathematical model show good agreement in the predictions of the timing and magnitude of the maximum pressure peaks when using a gas release model based upon results of the gas release

experiment. However, higher frequency pressure oscillations traveling along the pipe during periods of reduced pressure are not simulated. This discrepancy is attributed to inconsistancies between the actual gas release that occurred in the pipe and that described by the model. In addition, it was found that in cases where insignificant gas release occurs, the standard one-phase waterhammer approach which accounts for the formation of vapor voids at computing nodes utilizing a simple continuity balance adequately predicts transient pressures.

It is recommended that future studies of the effect of released gas on hydraulic transients be concerned with acquiring a better understanding of the nature of gas release during turbulent pipe flow conditions. Further gas release testing should probably be done on a prototype scale and also be concerned with the number and size of available nuclei. In addition, incorporating the thermodynamic aspects of the vaporization process would be desirable since heat conduction, condensation and other thermodynamic considerations may be significant factors in describing and predicting the occurance of column separation and cavitation bubbles. It is also recommended that future laboratory studies utilize a longer pipe. This would increase the wave travel time resulting in longer durations of supersaturated conditions, thus permitting the evolution of other more insoluble gas, such as air, to be studied.

LIST OF REFERENCES

LIST OF REFERENCES

1. Ames, W. F., Nonlinear Partial Differential Equations in Engineering, Academic Press, New York, 1965.

2. Baltzer, R. A., "A Study of Column Separation Accompanying Transient Flow of Liquids in Pipes," Ph.D. Dissertation, University of Michigan, February 1967.

3. Driels, M. R., "An Investigation of Pressure Transient in a System Containing a Liquid Capable of Air Absorption," ASME Paper No. 73-FE-28.

4. Epstein, P. S., and Plesset, M. S., "On the Stability of Gas Bubbles in Liquid-Gas Solutions," Journal of Chemical Physics, Vol. 18, No. 11, Nov. 1950, pp. 1505-1509.

5. Forsythe, G. E. and Wasow, W. R., Finite-Difference Methods for Partial Differential Equations, John Wiley and Sons, Inc., New York, 1960.

6. Holl, J. W., "Nuclei and Cavitation," Journal of Basic Engineering, ASME, December 1970, pp. 681-688.

7. Kalkwijk, J. P., and Kranenburg, C., "Cavitation in Horizontal Pipelines due to Water Hammer," Journal of the Hydraulics Division, ASCE, 97, HY10, October 1971.

8. Kranenburg, C., "The Effect of Free Gas on Cavitation in Pipelines Induced by Water Hammer," Proceedings First International Conference on Pressure Surges, BHRA Fluid Engineering, Cranfield, Bedford, England, 1972.

9. Kranenburg, C., "Gas Release during Transient Caviation in Pipes," Journal of the Hydraulics Division, ASCE, 100, HY10, October 1974.

10. Levich, V. G., Physicochemical Hydrodynamics, Prentice-Hall, New Jersey, 1962.

11. Liggett, J. A., and Cunge, J. A., "Numerical Methods of Solutions of the Unsteady Flow Equations," in Mahmood, K., and Yevjevich, V., eds., Unsteady Flow in Open Channels, Vol. 1, Water Resources Publications, Fort Collins, Colorado, 1975, pp. 89-182.

12. Lister, M., "The Numerical Solution of Hyperbolic Partial Differential Equations by the Method of Characteristics," in Ralston, A., and Wilf, H. S., eds., Mathematical Methods for Digital Computers, John Wiley and Sons, Inc., New York, 1960, pp. 165-179.

13. Martin, C. S., and Padmanabhan, M., "The Effects of Free Gas on Pressure Transients," Final Report, Research Grant GK-38570, National Science Foundation, June, 1976.

14. Martin, C. S., Padmanabhan, K., and Wiggert, D. C., " Pressure Wave Propagation in Two-Phase Bubbly Air-Water Mixtures," Proceedings Second International Conference on Pressure Surges, BHRA Fluid Engineering, Cranfield, Bedford, England, 1976.

15. Parkin, B. R., and Kermeen, R. W., "The Role of Convective Air Diffusion and Liquid Tensile Stresses During Cavitation Inception," Proceedings IAHR Symposium on Cavitation and Hydraulic Machinery, Dendai, Japan, 1962.

16. Safwat, H. H., and de Kluyer, J. P., "Digital Computations for Water Hammer-Column Separation," Proceedings First International Conference on Pressure Surges, BHRA Fluid Engineering, Cranfield, Bedford, England, 1972.

17. Schweitzer, P. H., and Szebehely, V. G., "Gas Evolution in Liquids and Cavitation," Journal of Applied Physics, Vol. 21, December 1950, pp. 1218-1224.

18. Streeter, V. L., Fluid Mechanics, 5th ed., McGraw-Hill Book Company, New York, 1971.

19. Streeter, V. L., and Wylie, E. B., Hydraulic Transients, McGraw-Hill Book Company, New York, 1967.

20. Swaffield, J. A., "A Study of the Influence of Air Release on Column Separation in an Aviation Kerosene Pipeline," The Institution of Mechanical Engineers, Proceedings 1972, Vol. 186 56/72. pp. 693-703.

21. Tullis, J. P., Streeter, V. L., and Wylie, E. B., "Waterhammer Analysis with Air Release," Proceedings Second International Conference on Pressure Surges, BHRA Fluid Engineering, Cranfield, Bedford, England, 1976.

22. Van Wijngaarden, L., "On the Growth of Small Cavitation Bubbles by Convective Diffusion," International Journal of Heat and Mass Transfer, Vol. 10, No. 2, February 1967, pp. 127-134.

23. Vardy, A. E., "On the Use of the Method of Characteristics for the Solution of Unsteady Flows in Networks," Proceedings Second International Conference on Pressure Surges, BHRA Fluid Engineering, Cranfield, Bedford, England, 1976.

24. Yadigaroglu, G., and Lahey, R. T. Jr., "On the Various Forms of the Conservation Equations in Two-Phase Flow," International Journal of Multiphase Flow, Vol. 2, 1976, pp. 477-494.

APPENDICES

APPENDIX A

DETERMINATION OF CHARACTERISTIC EQUATIONS

APPENDIX A

DETERMINATION OF CHARACTERISTIC EQUATIONS [5]

The system of Equations (42) are of the form

$$[B]\{w\}_t + [A]\{w\}_x + \{d\} = 0 \tag{A.1}$$

where $\{w\}$ is a column vector of unknowns with the subscripts x and t referring to the partial derivatives with respect to distance and time and where $[B]$, $[A]$ and $\{d\}$ may be functions of x, t, and w. Equation (A.1) is subjected to a linear transformation with a nonvanishing determinant so that a new system of similar form is obtained which is equivalent to the original one. The coefficients of the transformation may depend on x, t, and w. If $[T]$ is such a transformation, multiplying Equation (A.1) by $[T]$ results in

$$[T][B]\{w\}_t + [T][A]\{w\}_x + [T]\{d\} = 0 \tag{A.2}$$

A convenient form of the transformation is one in which

$$[T][A] = [C][T][B] \tag{A.3}$$

where $[C]$ is a diagonal matrix. If we set $[T][B] = [A^*]$ and $[T]\{d\} = \{d^*\}$ then Equation (A.2) becomes

$$[A^*]\{w\}_t + [C][A^*]\{w\}_x + \{d^*\} = 0 \tag{A.4}$$

Equation (A.4) indicates that every equation in the system now contains

differentiation in one direction only, that is, dx/dt = [C]. By the transformation we have eliminated one of the differential operators and reduced the system of equations (A.1) to a simpler system of ordinary differential equations. To calculate [C], the condition of equality of indiviual rows in Equation (A.3) represents a system of homogeneous linear algebraic equations with the unknowns [T]. For a non-trivial solution to exist, it is necessary that

$$\det ([A] - [C]\,[B]) = 0 \tag{A.5}$$

Letting [C] = λ[I], where [I] is the identity matrix, allows Equation (A.5) to be written as

$$\det ([A] - \lambda[I]\,[B]) = 0 \tag{A.6}$$

The λ values are termed the characteristic roots or the eigenvalues. If λ are all real and distinct roots, the system of equations (A.1) is hyperbolic. Once [C] is determined by the solution of Equation (A.6), then [T] can be found by substitution of [C] into Equation (A.3). Using the transformation matrix, the system of ordinary differential equations can be found by the substitution of [T] into Equation (A.4).

The following is the application of this procedure to the system of Equations (42).

Step A: Determination of eigenvalues [C].

Applying Equation (A.6) to the system of Equations (42) yields

$$\det ([A] - \lambda[I]\,[B]) = \begin{vmatrix} u - \lambda & -\overline{A} & 0 \\ 0 & u - \lambda & \overline{C} \\ \overline{E}(u-\lambda) & 0 & u - \lambda \end{vmatrix} = 0 \tag{A.7}$$

Expanding Equation (A.7) results in

$$(u - \lambda)[(u - \lambda)^2 - \bar{A}\,\bar{C}\,\bar{E}] = 0 \tag{A.8}$$

in which the eigenvalues are found to be

$$\begin{aligned} \lambda_1 &= u + (\bar{A}\,\bar{C}\,\bar{E})^{\frac{1}{2}} \\ \lambda_2 &= u \\ \lambda_3 &= u - (\bar{A}\,\bar{C}\,\bar{E})^{\frac{1}{2}} \end{aligned} \tag{A.9}$$

Step B: Determination of transformation matrix [T].

From Equation (A.3) it is known that

$$\begin{bmatrix} t_{11} & t_{12} & t_{13} \\ t_{21} & t_{22} & t_{23} \\ t_{31} & t_{32} & t_{33} \end{bmatrix} \begin{bmatrix} u & -\bar{A} & 0 \\ 0 & u & \bar{C} \\ u\bar{E} & 0 & u \end{bmatrix} - \begin{bmatrix} u + (\bar{A}\,\bar{C}\,\bar{E})^{\frac{1}{2}} & 0 & 0 \\ 0 & u & 0 \\ 0 & 0 & u - (\bar{A}\,\bar{C}\,\bar{E})^{\frac{1}{2}} \end{bmatrix}$$

$$\begin{bmatrix} t_{11} & t_{12} & t_{13} \\ t_{21} & t_{22} & t_{23} \\ t_{31} & t_{32} & t_{33} \end{bmatrix} \begin{bmatrix} 1 & 0 & 0 \\ 0 & 1 & 0 \\ \bar{E} & 0 & 1 \end{bmatrix} = 0 \tag{A.10}$$

Expanding Equation (A.10) yields

$$\begin{bmatrix} -(\bar{A}\,\bar{C}\,\bar{E})^{\frac{1}{2}}(t_{11} + \bar{E}\,t_{13}) & -\bar{A}\,t_{11} - (\bar{A}\,\bar{C}\,\bar{E})^{\frac{1}{2}}t_{12} & \bar{C}\,t_{12} - (\bar{A}\,\bar{C}\,\bar{E})^{\frac{1}{2}}t_{13} \\ 0 & -\bar{A}\,t_{21} & \bar{C}\,t_{22} \\ (\bar{A}\,\bar{C}\,\bar{E})^{\frac{1}{2}}(t_{31} + \bar{E}t_{33}) & -\bar{A}\,t_{31} + (\bar{A}\,\bar{C}\,\bar{E})^{\frac{1}{2}}t_{32} & \bar{C}\,t_{32} - (\bar{A}\,\bar{C}\,\bar{E})^{\frac{1}{2}}t_{33} \end{bmatrix} = 0$$

(A.11)

Equation (A.11) can be rearranged into the following form:

$$\left[\begin{array}{ccc:ccc:ccc}
-(\bar{A}\,\bar{C}\,\bar{E})^{\frac{1}{2}} & 0 & -E(\bar{A}\,\bar{C}\,\bar{E})^{\frac{1}{2}} & & & & & & \\
-A & -(\bar{A}\,\bar{C}\,\bar{E})^{\frac{1}{2}} & 0 & & & & & & \\
0 & 0 & -(\bar{A}\,\bar{C}\,\bar{E})^{\frac{1}{2}} & & & & & & \\
\hdashline
 & & & 0 & 0 & 0 & & & \\
 & & & -\bar{A} & 0 & 0 & & & \\
 & & & 0 & \bar{C} & 0 & & & \\
\hdashline
 & & & & & & (\bar{A}\,\bar{C}\,\bar{E})^{\frac{1}{2}} & \bar{E}(\bar{A}\,\bar{C}\,\bar{E})^{\frac{1}{2}} & \\
 & & & & & & -\bar{A} & (\bar{A}\,\bar{C}\,\bar{E})^{\frac{1}{2}} & 0 \\
 & & & & & & 0 & \bar{C} & (\bar{A}\,\bar{C}\,\bar{E})^{\frac{1}{2}}
\end{array}\right]
\left\{\begin{array}{c} t_{11} \\ t_{12} \\ t_{13} \\ t_{21} \\ t_{22} \\ t_{23} \\ t_{31} \\ t_{32} \\ t_{33} \end{array}\right\} = 0 \qquad (A.12)$$

The components of the transformation can now be determined. Examination of Equation (A.12) results in

$$\begin{array}{lll}
t_{11}=1 & t_{12}= -(\bar{A} \,/\, \bar{C}\,\bar{E})^{\frac{1}{2}} & t_{13}= -\bar{E}^{-1} \\
t_{21}=0 & t_{22} = 0 & t_{23} = 1 \\
t_{31}=1 & t_{32} = (\bar{A} \,/\, \bar{C}\,\bar{E})^{\frac{1}{2}} & t_{33} = -\bar{E}^{-1}
\end{array}$$

or written in matrix form:

$$[T] = \begin{bmatrix} 1 & -(\bar{A} \,/\, \bar{C}\,\bar{E})^{\frac{1}{2}} & -\bar{E}^{-1} \\ 0 & 0 & 1 \\ 1 & (\bar{A} \,/\, \bar{C}\,\bar{E})^{\frac{1}{2}} & -\bar{E}^{-1} \end{bmatrix} \qquad (A.13)$$

Step C: Determination of transformed equations.

Using the transformation matrix [T], $[A^*]$ and $\{d^*\}$ are computed to be

$$[A^*] = \begin{bmatrix} 0 & -(\bar{A} / \bar{C}\,\bar{E})^{\frac{1}{2}} & -\bar{E}^{-1} \\ E & 0 & 1 \\ 0 & (\bar{A} / \bar{C}\,\bar{E})^{\frac{1}{2}} & -\bar{E}^{-1} \end{bmatrix} \tag{A.14}$$

$$\{d^*\} = \begin{Bmatrix} \bar{B} - (\bar{A} / \bar{C}\,\bar{E})^{\frac{1}{2}}\,\bar{D} - \bar{F} / \bar{E} \\ \bar{F} \\ \bar{B} + (\bar{A} / \bar{C}\,\bar{E})^{\frac{1}{2}}\,\bar{D} - \bar{F} / \bar{E} \end{Bmatrix} \tag{A.15}$$

The transformed system of equations can now be written as

$$[A^*] \frac{d}{dt} \begin{Bmatrix} \alpha \\ u \\ H \end{Bmatrix} = \{d^*\} \tag{A.16}$$

or writing each equation separately and letting $a = (\bar{A}\,\bar{C}\,\bar{E})^{\frac{1}{2}}$ results in

$$\frac{a}{\bar{C}} \frac{du}{dt} + \frac{dH}{dt} + \bar{E}\,\bar{B} - \bar{F} - \frac{a}{\bar{C}}\bar{D} = 0, \quad \frac{dx}{dt} = \lambda_1 = u + a \tag{A.17}$$

$$\bar{E} \frac{d\alpha}{dt} + \frac{dH}{dt} - \bar{F} = 0, \quad \frac{dx}{dt} = \lambda_2 = u \tag{A.18}$$

$$-\frac{a}{\bar{C}} \frac{du}{dt} + \frac{dH}{dt} + \bar{E}\,\bar{B} - \bar{F} + \frac{a}{\bar{C}}\bar{D} = 0, \quad \frac{dx}{dt} = \lambda_3 = u - a \tag{A.19}$$

APPENDIX B

COMPUTER PROGRAM AND SAMPLE OUTPUT

APPENDIX B

COMPUTER PROGRAM AND SAMPLE OUTPUT

The following is a listing of the FORTRAN language computer program developed to numerically simulate hydraulic transients in a bubbly, two-phase gas-liquid mixture including gas release. The program is divided into major sections with comment cards describing the purpose of that section. Also included is some sample output for the numerical simulation of Experimental Run 16.

```
      PROGRAM TWOPH(INPUT,OUTPUT)                                       1
C     THIS PROGRAM SIMULATES TWO-PHASE TRANSIENT PIPE FLOW INCLUDING
C     GAS RELEASE IN A SERIES OF THREE PIPES OF SAME DIAMETER.  MATERIAL
C     PROPERTIES OF THE BEGINNING AND END PIPES ARE THE SAME.  COLUMN
C     SEPARATION CAVITIES ARE CALCULATED AT NODES WHEN VAPOR PRESSURE
C     IS REACHED.  THE METHOD OF CHARACTERISTICS WITH SPECIFIED TIME
C     AND DISTANCE INCREMENTS IS UTILIZED.  INCREASED TIME-DISTANC RATIOS
C     MAY BE USED. THE VALVE CAN BE LOCATED AT EITHER AN UPSTREAM OR
C     DOWNSTREAM LOCATION.  EQUATIONS OF FIRST OR SECOND ORDER ACCURACY
C     MAY BE USED.  IN THE VARIABLE DESCRIPTION BELOW IT IS ASSUMED THAT
C     THE INTERIOR PIPE IS COPPER WITH THE EXTERIOR PIPES BEING LUCITE.
C
C       INPUT VARIABLES AND UNITS
C       L - FT    COPPER PIPE LENGTH
C       D - FT    PIPE DIAMETER
C       TH - FT   PIPE WALL THICKNESS
C       EP - LB/SQ. FT    PIPE MODULUS
C       C1          PIPE CONSTRAINT PARAMETER
C       F           PIPE FRICTION COEFFICIENT
C       KL - LB/SQ FT   FLUID MODULUS OF ELASTICITY
C       RL - SLUGS/FT**3    FLUID DENSITY
C       KS-         POLYTROPIC GAS CONSTANT
C       P0 - HYDRAULIC GRADE LINE IN FEET OF WATER ABSOLUTE AT UPSTREAM
C            RESERVOIR
C       V0 - FT/SEC    REFERENCE VELOCITY
C       B0 - INITIAL VOID FRACTION REFERENCED TO ATMOSPHERE PRESSURE
C       DT - SEC    TIME INCREMENT
C       TMAX - SEC    MAXIMUM TIME
C       N           NUMBER OF COPPER REACHES
C       K      PRINTING AND PLOTTING INCREMENT
C       IFLAG - 0=FIRST ORDER ONLY    1=SECOND ORDER  PROCESS
C       IT      NUMBER OF ITERATIONS IN 2ND ORDER PROCESS(MUST EQUAL ZERO
C            FOR 1ST ORDER)
C       TC - SEC    TIME OF CLOSURE
C       G - FT/SQ.SEC    GRAVITY
C       PATM - FT. OF WATER ABS.       ATMOSPHERE PRESSURE
C       EL - FT       ELEVATIONS
C       HV - FT ABSOLUTE      VAPOR PRESSURE
C       THETA - RADIANS     PIPE ANGLE
C       CONST         GAS DENSITY CONSTANT
C       TML - FT      LUCITE WALL THICKNESS
C       EPL - LB/SQ.FT.    LUCITE PIPE MODULUS
C       C2 - LUCITE CONSTRAINT PARAMETER
C       LL - FT     LENGTH OF LUCITE PIPE
C       FL       LUCITE FRICTION FACTOR
C       NL      NUMBER OF REACHES PER LUCITE PIPE
C       IVALVE          1=VALVE DOWNSTREAM  0=VALVE UPSTREAM
C       R - GAS CONSTANT
C       TEMP - TEMPERATURE IN DEGREES RANKINE
C       IPRINT      1=SUSPEND PRINTOUT  0=PRINT AT K INCREMENTS
C       TS - SEC     TIME OF BREAK IN GAMMA CURVE
C       PS - FT. ABS.      SATURATION PRESSURE
C       GAM1  INITIAL POINT ON GAMMA CURVE
C       GAM2 - POINT ON GAMMA CURVE AT TS
C       IQU=     PLOTTING QUEUE
C       MPLOT       1=PLOT VARIABLES DESCRIBED BELOW    0=NO PLOTS
C                 PLOTPM=1   PLOT PRESSURE AT MIDPOINT
C                 PLOTPV=1   PLOT PRESSURE AT VALVE
C                 PLOTAM=1   PLOT VOID FRACTION AT MIDPOINT
C                 PLOTAV=1   PLOT VOID FRACTION AT VALVE
C                 IF =0   NO PLOT OF THAT VARIABLE

      DIMENSION U(45),UP(45),P(45),PP(45),B(45),BP(45),A(45),PR(45),EL(4
     15),ICAV(45),VCAV(45),UL(45),ULP(45),UT(45),IBUF(257),PLOTPV(250),P
     1LOTPM(250),PLOTAV(250),PLOTAM(250),TT(250),GAMMAP(45),GAMMA(45),PI
     1(45),ICAVP(45),VCAVP(45)
      COMMON/A/FL,KS,RL,CC,G,CCL,NN,NL/B/TS,PS,GAM2,SLOPE,DT,TX(45),GAM1
     1,GFACTOR,HV,DSLVE/C/DD,DDL,R,TEMP,THETA
      REAL L,KL,KS,LL
  100 FORMAT (7E10.4/7E10.4/3I10,3E10.4,I10/7E10.4/2E10.4,5I10/2I10,6E10
     1.4)
  101 FORMAT(*0COPPER LENGTH=*T40*L=*T50,E10.4/* PIPE DIAMETER=*T40*D=*T50,
     1E10.4/* COPPER WALL THICKNESS=*T40*TH=*T50,E10.4/* PIPE MODULUS=*
     2T40*EP=*T50,E10.4/* PIPE CONSTRAINT PARAMETER=*T40*C1=*T50,E10.4/
     3* COPPER FRICTION COEFF     =*T40*F=*T50,E10.4/* FLUID MODULUS OF ELA
```

```
     4STICITY=*T40*KL=*T50,E10.4/* FLUID DENSITY=*T40*RL=*T50,E10.4/      2
     5* POLYTROPIC GAS CONSTANT=   T40*KS=*T50,E10.4/* REFERENCE PRESSURE=*
     6T40*P0=*T50,E10.4/* REFERENCE VELOCITY=*T40*U0=*T50,E10.4/* REFERENCE
     7 VOID FRACTION=*T40*B0=*T50,E10.4/* TIME INCREMENT=*T40*DT=*T50,E10.4/
     8* MAXIMUM TIME=*T40*TMAX=*T50,E10.4/* REACHES OF COPPER=*T40*N=*T50,
     913/* NO. OF TIME INCREMENTS PER PRINTOUT=*T40*K=*T50,13/* NO. OF ITE
     1RATIONS IN 2ND ORDER PROCESS=*T40*IT=*T50,I3/* TIME OF CLOSURE=*T40=T
     5C=*T50,E10.3/* GRAVITY=*T40*G=*T50,E10.3/* ATMOSPHERE PRESSURE=*T40=PA
     3TM=*T50,E10.3/* VAPOR PRESSURE=*T40=HV=*T50,E10.3/* PIPE ANGLE=*T40=TH
     1ETA=*T50,E10.3/* TEMPERATURE          =*T40=TEMP =*T50,E10.3/* LUCITE
     1WALL THICKNESS=*T40=THL=*T50,E10.3/* LUCITE PIPE MODULUS=*T40=EPL=*T50
     1,E10.3/* LUCITE CONSTRAINT PARAMETER=*T40=C2=*T50,E10.3/* LENGTH OF
     1LUCITE=*T40=LL=*T50,E10.3/* LUCITE FRICTION FACTOR=*T40=FL=*T50,E10.3/
     1* NUMBER OF LUCITE REACHES=*T40=NL=*T50,I10/* GAS CONSTANT=*T40=R=*T50
     1,E10.3)
  114 FORMAT(* GAMMA TIME PARAMETER=*T40=TS=*T50,E10.3/* SATURATION PRESSU
     1RE=*T40=PS=*T50,E10.4/* INITIAL GAMMA=*T40=GAM1=*T50,E10.4/* GAMMA AT
     1TS=*T40=GAM2=*T50,E10.4/* GAMMA FACTOR=*T40=GFACTOR=*T50,E10.4/* SOLUT
     110N FACTOR=*T40=DSLVE=*T50,E10.4/)
  102 FORMAT(* T=*E10.4/* P=*7E10.4/* U=*7E10.4/* B=*7E10.4/* A=*7E10.4/
     6)
  103 FORMAT(*0COMPUTED VALUES OF PRESSURE, VELOCITY, VOID FRACTION AND
     1WAVE SPEED*//* UNITS - PRESSURE  LB/SQ.IN. ABSOLUTE*/*          - VEL
     2OCITY   FT/SEC*/*          -WAVE SPEED   FT/SEC*)
  104 FORMAT (16F5.2/16F5.2/16F5.2)
  105 FORMAT (*0ELEVATIONS ALONG PIPE*/10F10.2/10F10.2/10F10.2/10F10.2/1
     10F10.2//*0X/L=      0.0       0.167       0.333       0.500       0.667
     20.833       1.00 *//)
  106 FORMAT (*0FIRST ORDER ACCURACY*)
  107 FORMAT (*0SECOND ORDER ACCURACY*)
  108 FORMAT (*0CLOSE=*E10.4/*  VS=*E10.4/)
  110 FORMAT (*0CAVITY OPENS AT TIME=*,E10.3/)
  111 FORMAT (*0CAVITY CLOSES AT TIME=*,E10.3/)
  112 FORMAT (* VALVE UPSTREAM*)
  113 FORMAT (* VALVE DOWNSTREAM*)
  115 FORMAT (2I10)

      CALL NOBLANK
      READ 115,IQU,MPLOT
      IF (MPLOT.EQ.0) GO TO 998
      CALL PLOTS (IBUF,257,IOU)
      CALL PLOPIT (45.0)
      CALL PLOT (0.5,0.5,-3)
  998 READ 100,L,D,TH,EP,C1,F,KL,RL,KS,P0,U0,B0,DT,TMAX,N,K,IT,TC,G,PATM
     1,IFLAG,HV,THETA,TEMP,P,THL,EPL,C2,LL,FL,NL,IPRINT,IVALVE,IPLOTAV,I
     1PLOTAM,IPLOTPV,IPLOTPM,TS,PS,GAM1,GAM2,GFACTOR,DSLVE
      IF (L.EQ.0.) GO TO 999
      PRINT 101,L,D,TH,EP,C1,F,KL,RL,KS,P0,U0,B0,DT,TMAX,N,K,IT,TC,G,PAT
     1M,HV,THETA,TEMP,THL,EPL,C2,LL,FL,NL,R
      PRINT 114,TS,PS,GAM1,GAM2,GFACTOR,DSLVE
      PRINT 103
       IF (IFLAG.EQ.0) PRINT 106
       IF (IFLAG.EQ.1) PRINT 107
      IF (IVALVE.EQ.0) PRINT 112
      IF (IVALVE.EQ.1) PRINT 113
      SLOPE=(GAM2-GAM1)/TS
      DX=L/N
      DXL=LL/NL
      THE=DT/DX
      THEL=DT/DXL
      CC=0.*C1/(EP*TH)
      CCL=0.*C2/(EPL*THL)
      DD=-F/(2.*D)
      DDL=-FL/(2.*D)
      T=0.
      KK=0
      NN=N+2*NL+1
      KKK=0
      IPV=NN
      IF (IVALVE.EQ.0) IPV=1
      IPM=NN/2
      READ 104,(EL(I),I=1,NN)
      PRINT 105,(EL(I),I=1,NN)
      N1=NN-1
      DO 498 I=1,NN
      VCAVP(I)=0.
      ICAVP(I)=0
```

```
      ICAV(I)=0
      UL(I)=0.
  498 VCAV(I)=0.
      AR=.7854*D*D
C     THIS  SECTION CALCULATES THE INITIAL STEADY-STATE
C     CONDITIONS IN THE PIPE
      IF (IVALVE) 600,601
  600 DO 200 I=1,NN
      IF (I.LE.(NL+1)) P(I)=P0-(FL*U0*U0/(2.*D*G)*(I-1)*DXL)
      IF (I.GT.(NL+1).AND.I.LE.(NN-NL)) P(I)=P(I-1)-(F*U0*U0/(2.*D*G)*DX
     1)
      IF (I.GT.(NN-NL)) P(I)=P(I-1)-(FL*U0*U0/(2.*D*G)*DXL)
      U(I)=U0
      UT(I)=U(I)
      C5=B0/(1.-B0)*((P(I)-EL(I))/PATM)**(-1./KS)*EXP((PATM-P(I)+EL(I))/
     1KL)
      B(I)=C5/(1.+C5)
      A(I)=WAVE(B(I),P(I),EL(I),I)
      PR(I)=(P(I)-EL(I))*RL*G/144.
      PI(I)=(P(I)-EL(I))
      TX(I)=0.0
      GAMMA(I)=GAM(P(I),EL(I),I,1,B(I))
  200 CONTINUE
      B0=B(1)
      C3=U(NL)*U(NN)/P(NN)
      GO TO 602
  601 DO 603 I=1,NN
      IF (I.LE.(NL+1)) P(I)=P0+F*U0*U0*L/(2.*D*G)+FL*U0*U0*(2*NL+1-I)*DX
     1/(2.*D*G)
      IF (I.GT.(NL+1).AND.I.LE.(NN-NL)) P(I)=P0+FL*U0*U0*LL/(2.*D*G)+F*U
     10*U0*(I-NL-1)*DX/(2.*D*G)
      IF (I.GT.(NN-NL)) P(I)=P0+FL*U0*U0*(NN-I)*DXL/(2.*D*G)
      U(I)=U0
      UT(I)=U(I)
      C5=B0/(1.-B0)*((P(I)-EL(I))/PATM)**(-1./KS)*EXP((PATM-P(I)+EL(I))/
     1KL)
      B(I)=C5/(1.+C5)
      A(I)=WAVE(B(I),P(I),EL(I),I)
      PR(I)=(P(I)-EL(I))*RL*G/144.
      PI(I)=(P(I)-EL(I))
      TX(I)=0.0
      GAMMA(I)=GAM(P(I),EL(I),I,1,B(I))
  603 CONTINUE
      C11=U(1)*U(1)/P(1)
      B00=B(1)
  602 NI=NL/6
  201 PRINT 102,T,(PR(I),I=1,NN,NI),(U(I),I=1,NN,NI),(B(I),I=1,NN,NI),(A
     3(I),I=1,NN,NI)
      IF (ICAV(NN).EQ.1.OR.ICAV(1).EQ.1) PRINT 109,(UL(I),I=1,NN,NI),(VC
     1AV(I),I=1,NN,NI)
  205 KKK=KKK+1
      PLOTPV(KKK)=PR(IPV)
      PLOTPM(KKK)=PR(IPM)
      PLOTAV(KKK)=B(IPV)
      PLOTAM(KKK)=B(IPM)
      TT(KKK)=T
  204 T=T+DT
      IF (T.GT.TMAX) GO TO 997
      KK=KK+1
      IF (IVALVE) 604,605
C     THIS SECTION CALULATES UNKNOWN PARAMETERS AT THE UPSTREAM
C     BOUNDARY NODE WHEN THE VALVE IS IN THE DOWNSTREAM LOCATION
  604 I=1
      IA=(DT*A(I))/DXL
      IB=IA+1
      UB=UT(I+IA)-(DT*A(I)/DXL-IA)*(UT(I+IA)-UT(I+IB))
      PB=P(I+IA)-(DT*A(I)/DXL-IA)*(P(I+IA)-P(I+IB))
      BB=B(I+IA)-(DT*A(I)/DXL-IA)*(B(I+IA)-B(I+IB))
      GAMB=GAMMA(I+IA)-(DT*A(I)/DXL-IA)*(GAMMA(I+IA)-GAMMA(I+IB))
      PIB=PI(I+IA)-(DT*A(I)/DXL-IA)*(PI(I+IA)-PI(I+IB))
      ELB=EL(I+IA)-(DT*A(I)/DXL-IA)*(EL(I+IA)-EL(I+IB))
      AB=WAVE(PB,PB,ELB,1)
      CALL COEFB(UB,PB,BB,GAMB,PIB,ELB,AB,CB,DB,EBFB,HB,I)
```

3

```
      PP(I)=P0
      BP(I)=B0
      UP(I)=UB+(CB/AB)*(PP(I)-PB+HB*DT)
      GAMMAP(I)=GAM(PP(I),EL(I),I,1,B(I))
      IF (IT.EQ.0) GO TO 800
C     BEGINNING OF SECOND-ORDER PROCESS
      DO 801 II=1,IT
      AP=WAVE(BP(I),PP(I),EL(I),1)
      ABP=0.5*(AB+AP)
      IAB=(DT*ABP)/DXL
      IBB=IAB+1
      UB=UT(I+IAB)-(DT*ABP/DXL-IAB)*(UT(I+IAB)-UT(I+IBB))
      BB=B(I+IAB)-(DT*ABP/DXL-IAB)*(B(I+IAB)-B(I+IBB))
      PB=P(I+IAB)-(DT*ABP/DXL-IAB)*(P(I+IAB)-P(I+IBB))
      GAMB=GAMMA(I+IAB)-(DT*ABP/DXL-IAB)*(GAMMA(I+IAB)-GAMMA(I+IBB))
      PIB=PI(I+IAB)-(DT*ABP/DXL-IAB)*(PI(I+IAB)-PI(I+IBB))
      ELB=EL(I+IAB)-(DT*ABP/DXL-IAB)*(EL(I+IAB)-EL(I+IBB))
      AB=WAVE(PB,PB,ELB,1)
      CALL COEFB(UB,PB,BB,GAMB,PIB,ELB,AB,CB,DB,EBFB,HB,I)
      AA=AP
      CALL COEFP(UP(I),PP(I),BP(I),GAMMAP(I),PI(I),EL(I),AP,AX,CP,DP,EBF
     1P,GP,HP,I)
      PP(I)=P0
      BP(I)=B0
      UP(I)=2.*(AB/CB+AP/CP)**(-1)*(PP(I)-PB+0.5*(HB+HP)*DT)+UB
      GAMMAP(I)=GAM(PP(I),EL(I),I+0,B(I))
  801 CONTINUE
  800 CONTINUE
C     THIS SECTION CALULATES UNKNOWN PARAMETERS AT THE DOWNSTREAM
C     BOUNDARY NODE WHEN THE VALVE IS IN THE DOWNSTREAM LOCATION
      I=NN
      IA=(DT*A(I))/DXL
      IB=IA+1
      UA=UT(I-IA)-(DT*A(I)/DXL-IA)*(UT(I-IA)-UT(I-IB))
      PA=P(I-IA)-(DT*A(I)/DXL-IA)*(P(I-IA)-P(I-IB))
      BA=B(I-IA)-(DT*A(I)/DXL-IA)*(B(I-IA)-B(I-IB))
      GAMA=GAMMA(I-IA)-(DT*A(I)/DXL-IA)*(GAMMA(I-IA)-GAMMA(I-IB))
      PIA=PI(I-IA)-(DT*A(I)/DXL-IA)*(PI(I-IA)-PI(I-IB))
      ELA=EL(I-IA)-(DT*A(I)/DXL-IA)*(EL(I-IA)-EL(I-IB))
      AA=WAVE(PA,PA,ELA,1)
      CALL COEFA(UA,PA,BA,GAMA,PIA,ELA,AA,CA,DA,EBFA,GA,I)
      TAU=0.0
      IF (TC.GT.0.0.AND.T.LT.TC) TAU=1.-T/TC
      IF (ICAV(I).EQ.1) GO TO 704
  308 C4=TAU*TAU*C3*(1-GA*DT*UA*AA/CA*PA)
      UP(I)=-.5*AA/CA*TAU*TAU*C3+.5*SQRT(TAU**4*C3*C3*(AA/CA)**2+4.*C4)
      PP(I)=PA*DT-AA/CA*(UP(I)-UA)+PA
      IF ((PP(I)-EL(I)).LT.HV) GO TO 705
      GO TO 703
C     CALCULATE VAPOR CAVITY
  705 PRINT 110,T
  704 ICAVP(I)=1
      PP(I)=HV+EL(I)
      UP(I)=-(PP(I)-PA)/(AA/CA)-GA*DT/(AA/CA)+UA
      VCAVP(I)=VCAV(I)-.5*DT*AR*(UP(I)+U(I))
      IF (VCAVP(I).GT.0.0) GO TO 703
      PRINT 111,T
      ICAVP(I)=0
      VCAVP(I)=0.
      UP(I)=0.
      PP(I)=PA-(AA/CA)*(UP(I)-UA)-GA*DT
      IF (PP(I)-EL(I).LE.HV) PP(I)=HV+EL(I)
  703 GAMMAP(I)=GAM(PP(I),EL(I),1,1,B(I))
      BP(I)=(PP(I)-EL(I))/(PP(I)-EL(I)))**(1./KS)*(B(I)+R/(P(I)-EL(I))*(
     1P(I)-EL(I))/PI(I))**(1.-1./KS)*TEMP*DT*0.5*(GAMMA(I)+GAMMAP(I)))
      IF (BP(I).LT.0.0) BP(I)=0.
      IF (IT.EQ.0) GO TO 802
C     BEGINNING OF SECOND-ORDER PROCESS
      DO 805 II=1,IT
```

4

```
      AP=WAVE(BP(I),PP(I),EL(I),1)
      AAP=0.5*(AA+AP)
      IAA=(DT*AAP)/DXL
      IBA=IAA+1
      UA=UT(I-IAA)-(DT*AAP/DXL-IAA)*(UT(I-IAA)-UT(I-IBA))
      PA=P(I-IAA)-(DT*AAP/DXL-IAA)*(P(I-IAA)-P(I-IBA))
      BA=B(I-IAA)-(DT*AAP/DXL-IAA)*(B(I-IAA)-B(I-IBA))
      GAMA=GAMMA(I-IAA)-(DT*AAP/DXL-IAA)*(GAMMA(I-IAA)-GAMMA(I-IBA))
      PIA=PI(I-IAA)-(DT*AAP/DXL-IAA)*(PI(I-IAA)-PI(I-IBA))
      ELA=EL(I-IAA)-(DT*AAP/DXL-IAA)*(EL(I-IAA)-EL(I-IBA))
      AA=WAVE(BA,PA,ELA,1)
      CALL COEFA(UA,PA,BA,GAMA,PIA,ELA,AA,CA,DA,EBFA,GA,I)
      AX=AP
      CALL COEFP(UP(I),PP(I),BP(I),GAMMAP(I),PI(I),EL(I),AP,AX,CP,DP,EBF
     1P,GP,HP,I)
      IF (ICAV(I).EQ.1) GO TO 803
      C4=TAU*TAU*C3*(-GA*DT*UA+AA/CA*PA)
      UP(I)=-.5*AA/CA*TAU+TAU*C3-.5*SQRT(TAU**4.*C3*C3*(AA/CA)**2+4.*C4)
      PP(I)=0.5*(AA/CA*AP/CP)*(UA-UP(I))-0.5*(GA*GP)*DT*PA
      IF ((PP(I)-EL(I)).LT.HV) GO TO 803
      GO TO 804

C     CALCULATE VAPOR CAVITY

  803 ICAVP(I)=1
      PP(I)=HV+EL(I)
      UP(I)=2.*(AA/CA*AP/CP)**(-1)*(-PP(I)+PA-.5*(GA*GP)*DT)+UA
      VCAVP(I)=VCAV(I)-.5*DT*AR*(UP(I)+U(I))
      IF (VCAVP(I).GT.0.0) GO TO 804
      ICAVP(I)=0
      VCAVP(I)=0.
      UP(I)=0.
      PP(I)=0.5*(AA/CA*AP/CP)*UA-.5*(GA*GP)*DT*PA
  804 GAMMAP(I)=GAM(PP(I),EL(I),I,0,B(I))
      BP(I)=((P(I)-EL(I))/(PP(I)-EL(I)))**(1./KS)*(B(I)+R/(P(I)-EL(I)))*(
     1(P(I)-EL(I))/PI(I))**(1.-1./KS)*TEMP*DT*.5*(GAMMA(I)+GAMMAP(I)))
      IF (BP(I).LT.0.0) BP(I)=0.
  805 CONTINUE
  802 CONTINUE
      GO TO 606

C   THIS SECTION CALULATES UNKNOWN PARAMETERS AT THE UPSTREAM
C   BOUNDARY NODE WHEN THE VALVE IS IN THE UPSTREAM LOCATION

  605 I=1
      IA=(DT*A(I))/DXL
      IB=IA+1
      UB=UT(I+IA)-(DT*A(I)/DXL-IA)*(UT(I+IA)-UT(I+IB))
      PB=P(I+IA)-(DT*A(I)/DXL-IA)*(P(I+IA)-P(I+IB))
      BB=B(I+IA)-(DT*A(I)/DXL-IA)*(B(I+IA)-B(I+IB))
      GAMB=GAMMA(I+IA)-(DT*A(I)/DXL-IA)*(GAMMA(I+IA)-GAMMA(I+IB))
      PIB=PI(I+IA)-(DT*A(I)/DXL-IA)*(PI(I+IA)-PI(I+IB))
      ELB=EL(I+IA)-(DT*A(I)/DXL-IA)*(EL(I+IA)-EL(I+IB))
      AB=WAVE(BB,PB,ELB,1)
      CALL COEFB(UB,PB,BB,GAMB,PIB,ELB,AB,CB,DB,EBFB,HB,I)
      TAU=0.0
      IF (TC.GT.0.0.AND.T.LT.TC) TAU=1.-T/TC
      IF (ICAV(I).EQ.1) GO TO 607
      C10=TAU*TAU*C11*(-AB*UB/CB-HB*DT*PB)
      UP(I)=TAU*TAU*C11*AB/CB*.5*.5*SQRT(TAU**4*C11*C11*AB*AB/(CB*CB)*4.
     1*C10)
      PP(I)=AB/CB*(UP(I)-UB)-HB*DT*PB
      IF ((PP(I)-EL(I)).LT.HV) GO TO 608
      GO TO 609

C     CALCULATE VAPOR CAVITY

  608 PRINT 110,T
  607 ICAVP(I)=1
      PP(I)=HV+EL(I)
      UP(I)=(CB/AB)*(HB*DT*PP(I)-PB)+UB
      VCAVP(I)=VCAV(I)+.5*DT*AR*(UP(I)+U(I))
      IF (VCAVP(I).GT.0.) GO TO 609
      PRINT 111,T
      ICAVP(I)=0
      VCAVP(I)=0.0
      UP(I)=0.
      PP(I)=AB/CB*(UP(I)-UB)-HB*DT*PB
  609 GAMMAP(I)=GAM(PP(I),EL(I),I,1,B(I))
      BP(I)=((P(I)-EL(I))/(PP(I)-EL(I)))**(1./KS)*(B(I)+R/(P(I)-EL(I)))*(
     1(P(I)-EL(I))/PI(I))**(1.-1./KS)*TEMP*DT*0.5*(GAMMA(I)+GAMMAP(I)))
      IF (BP(I).LT.0.0) BP(I)=0.
      IF (IT.EQ.0) GO TO 806

C     BEGINNING OF SECOND-ORDER PROCESS

      DO 807 II=1,IT
      AP=WAVE(BP(I),PP(I),EL(I),1)
      ABP=0.5*(AB+AP)
      IAB=(DT*ABP)/DXL
      IBB=IAB+1
      UB=UT(I+IAB)-(DT*ABP/DXL-IAB)*(UT(I+IAB)-UT(I+IBB))
      PB=P(I+IAB)-(DT*ABP/DXL-IAB)*(P(I+IAB)-P(I+IBB))
      BB=B(I+IAB)-(DT*ABP/DXL-IAB)*(B(I+IAB)-B(I+IBB))
      GAMB=GAMMA(I+IAB)-(DT*ABP/DXL-IAB)*(GAMMA(I+IAB)-GAMMA(I+IBB))
      PIB=PI(I+IAB)-(DT*ABP/DXL-IAB)*(PI(I+IAB)-PI(I+IBB))
      ELB=EL(I+IAB)-(DT*ABP/DXL-IAB)*(EL(I+IAB)-EL(I+IBB))
      AB=WAVE(BB,PB,ELB,1)
      AX=AP
      CALL COEFP(UP(I),PP(I),BP(I),GAMMAP(I),PI(I),EL(I),AP,AX,CP,DP,EBF
     1P,GP,HP,I)
      CALL COEFB(UB,PB,BB,GAMB,PIB,ELB,AB,CB,DB,EBFB,HB,I)
      IF (ICAV(I).EQ.1) GO TO 808
      C10=TAU*TAU*C11*(-AB*UB/CB-HB*DT*PB)
      UP(I)=TAU*TAU*C11*AB/CB*.5*.5*SQRT(TAU**4*C11*C11*AB*AB/(CB*CB)*4.
     1*C10)
      PP(I)=PB-.5*(HB+HP)*DT+.5*(AB/CB+AP/CP)*(UP(I)-UB)
      IF ((PP(I)-EL(I)).LT.HV) GO TO 808
      GO TO 809

C     CALCULATE VAPOR CAVITY

  808 ICAVP(I)=1
      PP(I)=HV+EL(I)
      UP(I)=UB-2.*(AB/CB+AP/CP)**(-1)*(PB-PP(I)-0.5*DT*(HB+HP))
      VCAVP(I)=VCAV(I)+.5*DT*AR*(UP(I)+U(I))
      IF (VCAVP(I).GT.0.0) GO TO 809
      ICAVP(I)=0
      VCAVP(I)=0.
      UP(I)=0.
      PP(I)=PB-.5*(HB+HP)*DT+.5*(AB/CB+AP/CP)*(UP(I)-UB)
  809 GAMMAP(I)=GAM(PP(I),EL(I),I,0,B(I))
      BP(I)=((P(I)-EL(I))/(PP(I)-EL(I)))**(1./KS)*(B(I)+R/(P(I)-EL(I)))*(
     1(P(I)-EL(I))/PI(I))**(1.-1./KS)*TEMP*DT*.5*(GAMMA(I)+GAMMAP(I)))
      IF (BP(I).LT.0.0) BP(I)=0.
  807 CONTINUE
  806 CONTINUE

C   THIS SECTION CALULATES UNKNOWN PARAMETERS AT THE DOWNSTREAM
C   BOUNDARY NODE WHEN THE VALVE IS IN THE UPSTREAM LOCATION

      I=NN
      IA=(DT*A(I))/DXL
      IB=IA+1
      UA=UT(I-IA)-(DT*A(I)/DXL-IA)*(UT(I-IA)-UT(I-IB))
      PA=P(I-IA)-(DT*A(I)/DXL-IA)*(P(I-IA)-P(I-IB))
      BA=B(I-IA)-(DT*A(I)/DXL-IA)*(B(I-IA)-B(I-IB))
      GAMA=GAMMA(I-IA)-(DT*A(I)/DXL-IA)*(GAMMA(I-IA)-GAMMA(I-IB))
      PIA=PI(I-IA)-(DT*A(I)/DXL-IA)*(PI(I-IA)-PI(I-IB))
      ELA=EL(I-IA)-(DT*A(I)/DXL-IA)*(EL(I-IA)-EL(I-IB))
      AA=WAVE(BA,PA,ELA,1)
      CALL COEFA(UA,PA,BA,GAMA,PIA,ELA,AA,CA,DA,EBFA,GA,I)
      PP(I)=PP
      BP(I)=BP
      UP(I)=CA-CA/AA*(PA-PP(I)-GA*DT)
      GAMMAP(I)=GAM(PP(I),EL(I),I,1,B(I))
      IF (IT.EQ.0) GO TO 810

C     BEGINNING OF SECOND-ORDER PROCESS

      DO 811 II=1,IT
      AP=WAVE(BP(I),PP(I),EL(I),1)
      AAP=0.5*(AA+AP)
      IAA=(DT*AAP)/DXL
```

```
      IBA=IAA-1
      UA=UT(I-IAA)-(DT*AAP/DXL-IAA)*(UT(I-IAA)-UT(I-IBA))
      PA=P(I-IAA)-(DT*AAP/DXL-IAA)*(P(I-IAA)-P(I-IBA))
      BA=B(I-IAA)-(DT*AAP/DXL-IAA)*(B(I-IAA)-B(I-IBA))
      GAMA=GAMMA(I-IAA)-(DT*AAP/DXL-IAA)*(GAMMA(I-IAA)-GAMMA(I-IBA))
      PIA=PI(I-IAA)-(DT*AAP/DXL-IAA)*(PI(I-IAA)-PI(I-IBA))
      ELA=EL(I-IAA)-(DT*AAP/DXL-IAA)*(EL(I-IAA)-EL(I-IBA))
      AA=WAVE(BA-PA-ELA-1)
      AX=AP
      CALL COEFP(UP(I),PP(I),BP(I),GAMMAP(I),PI(I),EL(I),AP,AX,CP,DP,EBF
     1P,GP,HP,I)
      CALL COEFA(UA,PA,BA,GAMA,PIA,ELA,AA,CA,DA,EBFA,GA,I)
      PP(I)=P0
      BP(I)=B00
      UP(I)=UA-2.*(AA/CA-AP/CP)**(-1)*(PA-PP(I)-.5*(GA-GP)*DT)
      GAMMAP(I)=GAM(PP(I),EL(I),I,0,B(I))
  811 CONTINUE
  810 CONTINUE
  606 CONTINUE

C   THIS SECTION CALCULATES THE UNKNOWN PARAMETERS
C   AT THE JUNCTIONS BETWEEN THE LUCITE AND COPPER PIPES

      DO 815 IXYZ=1,2
      IF (IXYZ.EQ.1) I=NL-1
      IF (IXYZ.EQ.2) I=NN-NL
      IF (IXYZ.EQ.1) A(I)=WAVE(B(I),P(I),EL(I),1)
      DXX=DX
      IF (IXYZ.EQ.1) DXX=DXL
      IA=(DT*A(I))/DXX
      IB=IA+1
      UA=UT(I-IA)-(DT*A(I)/DXX-IA)*(UT(I-IA)-UT(I-IB))
      PA=P(I-IA)-(DT*A(I)/DXX-IA)*(P(I-IA)-P(I-IB))
      BA=B(I-IA)-(DT*A(I)/DXX-IA)*(B(I-IA)-B(I-IB))
      GAMA=GAMMA(I-IA)-(DT*A(I)/DXX-IA)*(GAMMA(I-IA)-GAMMA(I-IB))
      PIA=PI(I-IA)-(DT*A(I)/DXX-IA)*(PI(I-IA)-PI(I-IB))
      ELA=EL(I-IA)-(DT*A(I)/DXX-IA)*(EL(I-IA)-EL(I-IB))
      IF (IXYZ.EQ.1) A(I)=WAVE(B(I),P(I),EL(I),1)
      IF (IXYZ.EQ.2) A(I)=WAVE(B(I),P(I),EL(I),1)
      IF (IXYZ.EQ.1) DXX=DX
      IF (IXYZ.EQ.2) DXX=DXL
      IA=(DT*A(I))/DXX
      IB=IA+1
      UB=UT(I-IA)-(DT*A(I)/DXX-IA)*(UT(I-IA)-UT(I-IB))
      PB=P(I-IA)-(DT*A(I)/DXX-IA)*(P(I-IA)-P(I-IB))
      BB=B(I-IA)-(DT*A(I)/DXX-IA)*(B(I-IA)-B(I-IB))
      GAMB=GAMMA(I-IA)-(DT*A(I)/DXX-IA)*(GAMMA(I-IA)-GAMMA(I-IB))
      PIB=PI(I-IA)-(DT*A(I)/DXX-IA)*(PI(I-IA)-PI(I-IB))
      ELB=EL(I-IA)-(DT*A(I)/DXX-IA)*(EL(I-IA)-EL(I-IB))
      IF (IXYZ.EQ.1) AA=WAVE(BA-PA-ELA-1)
      IF (IXYZ.EQ.1) AB=WAVE(BB-PB-ELB-1)
      IF (IXYZ.EQ.2) AA=WAVE(BA-PA-ELA-1)
      IF (IXYZ.EQ.2) AB=WAVE(BB-PB-ELB-1)
      CALL COEFA(UA,PA,BA,GAMA,PIA,ELA,AA,CA,DA,EBFA,GA,I)
      CALL COEFB(UB,PB,BB,GAMB,PIB,ELB,AB,CB,DB,EBFB,HB,I)
      IF (ICAV(I).EQ.1) GO TO 816
      PP(I)=(1.+AB*CA/(CB*AA))**(-1)*(PB-HB*DT+AB/CB*(UA-UB-CA/AA*GA*DT+
     1PA*CA/AA))
      IF ((PP(I)-EL(I)).LT.HV) GO TO 817
      UP(I)=(AA/CA*AB/CB)**(-1)*(AA/CA*UA+AB/CB*UB+PA-PB-(GA-HB)*DT)
      GO TO 818

C     CALCULATE VAPOR CAVITY

  817 ICAVP(I)=1
      UL(I)=U(I)
  816 PP(I)=HV+EL(I)
      UP(I)=CB/AB*(HB*DT-PB+PP(I))+UB
      ULP(I)=CA/AA*(PA-GA*DT-PP(I))+UA
      VCAVP(I)=VCAV(I)+.5*DT*AR*(U(I)+UP(I)-UL(I)-ULP(I))
      IF (II.EQ.0) UL(I)=ULP(I)
      IF (VCAVP(I).GT.0.) GO TO 818
      ICAVP(I)=0
      VCAVP(I)=0.0
      IF (II.EQ.0) UL(I)=0.
      UP(I)=(AA/CA+AB/CB)**(-1)*(AA/CA*UA+AB/CB*UB+PA-PB-(GA-HB)*DT)
      PP(I)=(1.+AR*CA/(CB*AA))**(-1)*(PB-HB*DT+AB/CB*(UA-UB-CA/AA*GA*DT+
     1PA*CA/AA))
      IF ((PP(I)-EL(I)).LT.HV) PP(I)=HV+EL(I)
  818 GAMMAP(I)=GAM(PP(I),EL(I),I,1,B(I))
      BP(I)=((P(I)-EL(I))/(PP(I)-EL(I)))**(1./KS)*(B(I)+R/(P(I)-EL(I)))*(
     1(P(I)-EL(I))/PI(I))**(1.-1./KS)*TEMP*DT*.5*(GAMMA(I)+GAMMAP(I)))
      IF (BP(I).LT.0.0) BP(I)=0.
      IF (IT.EQ.0) GO TO 819

C     BEGINNING OF SECOND-ORDER PROCESS

      DO 820 II=1,IT
      IF (ICAVP(I).EQ.1) UP(I)=(UP(I)+ULP(I))*.5
      AP1=WAVE(BP(I),PP(I),EL(I),1)
      AP2=WAVE(BP(I),PP(I),EL(I),1)
      IF (IXYZ.EQ.1) AAP=.5*(AP2+AA)
      IF (IXYZ.EQ.2) AAP=.5*(AP1+AA)
      DXX=DXL
      IF (IXYZ.EQ.2) DXX=DX
      IA=(DT*AAP)/DXX
      IB=IA+1
      UA=UT(I-IA)-(DT*AAP/DXX-IA)*(UT(I-IA)-UT(I-IB))
      PA=P(I-IA)-(DT*AAP/DXX-IA)*(P(I-IA)-P(I-IB))
      BA=B(I-IA)-(DT*AAP/DXX-IA)*(B(I-IA)-B(I-IB))
      GAMA=GAMMA(I-IA)-(DT*AAP/DXX-IA)*(GAMMA(I-IA)-GAMMA(I-IB))
      PIA=PI(I-IA)-(DT*AAP/DXX-IA)*(PI(I-IA)-PI(I-IB))
      ELA=EL(I-IA)-(DT*AAP/DXX-IA)*(EL(I-IA)-EL(I-IB))
      IF (IXYZ.EQ.1) APP=.5*(AB+AP1)
      IF (IXYZ.EQ.2) ABP=.5*(AB+AP2)
      DXX=DXL
      IF (IXYZ.EQ.1) DXX=DX
      IA=(DT*ABP)/DXX
      IB=IA+1
      UB=UT(I+IA)-(DT*ABP/DXX-IA)*(UT(I+IA)-UT(I+IB))
      PB=P(I+IA)-(DT*ABP/DXX-IA)*(P(I+IA)-P(I+IB))
      BB=B(I+IA)-(DT*ABP/DXX-IA)*(B(I+IA)-B(I+IB))
      GAMB=GAMMA(I+IA)-(DT*ABP/DXX-IA)*(GAMMA(I+IA)-GAMMA(I+IB))
      PIB=PI(I+IA)-(DT*ABP/DXX-IA)*(PI(I+IA)-PI(I+IB))
      ELB=EL(I+IA)-(DT*ABP/DXX-IA)*(EL(I+IA)-EL(I+IB))
      IF (IXYZ.EQ.1) AA=WAVE(BA,PA,ELA,1)
      IF (IXYZ.EQ.1) AB=WAVE(BB,PB,ELB,1)
      IF (IXYZ.EQ.2) AA=WAVE(BA,PA,ELA,1)
      IF (IXYZ.EQ.2) AB=WAVE(BB,PB,ELB,1)
      IF (IXYZ.EQ.1) APA=AP2
      IF (IXYZ.EQ.1) APB=AP2
      IF (IXYZ.EQ.2) APA=AP1
      IF (IXYZ.EQ.2) APB=AP2
      CALL COEFA(UA,PA,BA,GAMA,PIA,ELA,AA,CA,DA,EBFA,GA,I)
      CALL COEFB(UB,PB,BB,GAMB,PIB,ELB,AB,CB,DB,EBFB,HB,I)
      CALL COEFP(UP(I),PP(I),BP(I),GAMMAP(I),PI(I),EL(I),APA,APB,CP,DP,E
     1BFP,GP,HP,I)
      IF (ICAVP(I).EQ.1) GO TO 821
      UP(I)=(AA/CA*APA/CP+APB/CP+AB/CB)**(-1)*((AA/CA+APA/CP)*UA+(AB/CB+
     1APB/CP)*UB+2.*(PA-PB)-DT*(GA+GP-HB-HP))
      PP(I)=PB+0.5*(AB/CB+APB/CP)*(UP(I)-UB)-.5*(HB+HP)*DT
      IF ((PP(I)-EL(I)).LT.HV) GO TO 822
      GO TO 823

C     CALCULATE VAPOR CAVITY

  822 UL(I)=UT(I)
  821 PP(I)=HV+EL(I)
      ICAVP(I)=1
      UP(I)=2.*(AB/CB+APB/CP)**(-1)*(PP(I)-PB+.5*(HB+HP)*DT)+UB
      ULP(I)=2.*(AA/CA+APA/CP)**(-1)*(-PP(I)+PA-.5*(GA+GP)*DT)+UA
      VCAVP(I)=VCAV(I)+.5*DT*AR*(U(I)+UP(I)-UL(I)-ULP(I))
      IF (II.EQ.IT) UL(I)=ULP(I)
      IF (VCAVP(I).GT.0.0) GO TO 823
      ICAVP(I)=0
      VCAVP(I)=0
      IF (II.EQ.IT) UL(I)=0.
      UP(I)=(AA/CA+APA/CP+APB/CP+AB/CB)**(-1)*((AA/CA+APA/CP)*UA+(AB/CB+
     1APB/CP)*UB+2.*(PA-PB)-DT*(GA+GP-HB-HP))
      PP(I)=PB+0.5*(AB/CB+APB/CP)*(UP(I)-UB)-.5*(HB+HP)*DT
      IF ((PP(I)-EL(I)).LT.HV) PP(I)=HV+EL(I)
  823 GAMMAP(I)=GAM(PP(I),EL(I),I,0,B(I))
      BP(I)=((P(I)-EL(I))/(PP(I)-EL(I)))**(1./KS)*(B(I)+R/(P(I)-EL(I)))*(
     1(P(I)-EL(I))/PI(I))**(1.-1./KS)*TEMP*DT*.5*(GAMMA(I)+GAMMAP(I)))
```

```
      IF (BP(I).LT.0.0) BP(I)=0.
  820 CONTINUE
  819 CONTINUE
  815 CONTINUE

C     THIS SECTION CALCULATES THE UNKNOWN PARAMETERS AT THE INTERIOR
C     NODES OF THE COPPER AND LUCITE PIPES

      DO 850 KXYZ=1,3
      I1=1
      I2=NL+1
      IF (KXYZ.EQ.2) I1=NL+1
      IF (KXYZ.EQ.2) I2=NN-NL
      IF (KXYZ.EQ.3) I1=NN-NL
      IF (KXYZ.EQ.3) I2=NN
      KSTR=I1+1
      KEND=I2-1
      DXX=DX
      IF (KSTR.LE.NL.OR.KEND.GE.NN-NL) DXX=DXL
      DO 720 I=KSTR,KEND
      IA=(DT*A(I))/DXX
      IB=IA+1
      KINT=0
      IF (DT*A(I)/DXX.GE.I-I1) KINT=KINT+1
      IF (DT*A(I)/DXX.GE.I2-I) KINT=KINT+3
      IF (KINT.EQ.1) GO TO 852
      IF (KINT.EQ.3) GO TO 855
      IF (KINT.EQ.4) GO TO 852
  855 UA=UT(I-IA)-(DT*A(I)/DXX-IA)*(UT(I-IA)-UT(I-IB))
      PA=P(I-IA)-(DT*A(I)/DXX-IA)*(P(I-IA)-P(I-IB))
      BA=B(I-IA)-(DT*A(I)/DXX-IA)*(B(I-IA)-B(I-IB))
      GAMMA=GAMMA(I-IA)-(DT*A(I)/DXX-IA)*(GAMMA(I-IA)-GAMMA(I-IB))
      PIA=PI(I-IA)-(DT*A(I)/DXX-IA)*(PI(I-IA)-PI(I-IB))
      ELA=EL(I-IA)-(DT*A(I)/DXX-IA)*(EL(I-IA)-EL(I-IB))
      DT1=DT
      IF (KINT.EQ.3) GO TO 853
  857 UB=UT(I-IA)-(DT*A(I)/DXX-IA)*(UT(I+IA)-UT(I+IB))
      PB=P(I+IA)-(DT*A(I)/DXX-IA)*(P(I+IA)-P(I+IB))
      BB=B(I+IA)-(DT*A(I)/DXX-IA)*(B(I+IA)-B(I+IB))
      GAMMB=GAMMA(I+IA)-(DT*A(I)/DXX-IA)*(GAMMA(I+IA)-GAMMA(I+IB))
      PIB=PI(I+IA)-(DT*A(I)/DXX-IA)*(PI(I+IA)-PI(I+IB))
      ELB=EL(I+IA)-(DT*A(I)/DXX-IA)*(EL(I+IA)-EL(I+IB))
      DT2=DT
      GO TO 856
  852 UA=UP(I1)-DXX*(I-I1)/(DT*A(I))*(UP(I1)-UT(I1))
      PA=PP(I1)-DXX*(I-I1)/(DT*A(I))*(PP(I1)-P(I1))
      BA=BP(I1)-DXX*(I-I1)/(DT*A(I))*(BP(I1)-B(I1))
      GAMA=GAMMAP(I1)-DXX*(I-I1)/(DT*A(I))*(GAMMAP(I1)-GAMMA(I1))
      PIA=PI(I1)
      ELA=EL(I1)
      DT1=DXX*(I-I1)/A(I)
      IF (KINT.EQ.4) GO TO 853
      GO TO 857
  853 UB=UP(I2)-DXX*(I2-I)/(DT*A(I))*(UP(I2)-UT(I2))
      PB=PP(I2)-DXX*(I2-I)/(DT*A(I))*(PP(I2)-P(I2))
      BB=BP(I2)-DXX*(I2-I)/(DT*A(I))*(BP(I2)-B(I2))
      GAMB=GAMMAP(I2)-DXX*(I2-I)/(DT*A(I))*(GAMMAP(I2)-GAMMA(I2))
      PIB=PI(I2)
      ELB=EL(I2)
      DT2=DXX*(I2-I)/A(I)
  856 CONTINUE
      AA=WAVE(BA,PA,ELA,I)
      AB=WAVE(BB,PB,ELB,I)
      CALL COEFA(UA,PA,BA,GAMA,PIA,ELA,AA,CA,DA,EBFA,GA,I)
      CALL COEFB(UB,PB,BB,GAMB,PIB,ELB,AB,CB,DB,EBFB,HB,I)
      IF (ICAV(I).EQ.1) GO TO 500
      PP(I)=(1.+AB*CA/(CB*AA))**(-1)*(PB-HB*DT2*AB/CB*(UA-UB-CA/AA*GA*DT
     1)*PA*CA/AA))
      IF ((PP(I)-EL(I)).LT.HV) GO TO 501
      UP(I)=(AA/CA*AB/CB)**(-1)*(AA/CA*UA+AB/CB*UB+PA-PB-GA*DT1+HB*DT2)
      GO TO 502

C     CALCULATE VAPOR CAVITY

  501 ICAVP(I)=1
      UL(I)=U(I)
  500 PP(I)=HV+EL(I)
      UP(I)=CB/AB*(HB*DT2-PB+PP(I))+UB
      ULP(I)=CA/AA*(PA-GA*DT1-PP(I))+UA
      VCAVP(I)=VCAV(I)+.5*DT*AR*(U(I)+UP(I)-UL(I)-ULP(I))
      IF (IT.EQ.0) UL(I)=ULP(I)
      IF (VCAVP(I).GT.0.0) GO TO 502
      ICAVP(I)=0
      VCAVP(I)=0.
      IF (IT.EQ.0) UL(I)=0.
      UP(I)=(AA/CA+AB/CB)**(-1)*(AA/CA*UA+AB/CB*UB+PA-PB-GA*DT1+HB*DT2)
      PP(I)=(1.+AB*CA/(CB*AA))**(-1)*(PB-HB*DT2+AB/CB*(UA-UB-CA/AA*GA*DT
     1)*PA*CA/AA))
      IF ((PP(I)-EL(I)).LT.HV) PP(I)=HV+EL(I)
  502 GAMMAP(I)=GAM(PP(I),EL(I),I,1,B(I))
      BP(I)=((P(I)-EL(I))/(PP(I)-EL(I)))**(1./KS)*(B(I)+R/(P(I)-EL(I)))*(
     1(P(I)-EL(I))/PI(I))**(1.-1./KS)*TEMP*DT*0.5*(GAMMA(I)+GAMMAP(I)))
      IF (BP(I).LT.0.0) BP(I)=0.
      IF (IT.EQ.0) GO TO 859

C     BEGINNING OF SECOND-ORDER PROCESS

      DO 860 II=1,IT
      IF (ICAVP(I).EQ.1) UP(I)=(UP(I)+ULP(I))*.5
      AP=WAVE(PP(I),PP(I),EL(I),I)
      ABP=.5*(AB+AP)
      AAP=.5*(AA+AP)
      IAB=(DT*ABP)/DXX
      IBB=IAB+1
      IAA=(DT*AAP)/DXX
      IBA=IAA+1
      KINT=0
      IF (DT*AAP/DXX.GE.I-I1) KINT=KINT+1
      IF (DT*AAP/DXX.GE.I2-I) KINT=KINT+3
      IF (KINT.EQ.1) GO TO 870
      IF (KINT.EQ.3) GO TO 872
      IF (KINT.EQ.4) GO TO 870
  872 UA=UT(I-IAA)-(DT*AAP/DXX-IAA)*(UT(I-IAA)-UT(I-IBA))
      BA=B(I-IAA)-(DT*AAP/DXX-IAA)*(B(I-IAA)-B(I-IBA))
      PA=P(I-IAA)-(DT*AAP/DXX-IAA)*(P(I-IAA)-P(I-IBA))
      GAMA=GAMMA(I-IAA)-(DT*AAP/DXX-IAA)*(GAMMA(I-IAA)-GAMMA(I-IBA))
      PIA=PI(I-IAA)-(DT*AAP/DXX-IAA)*(PI(I-IAA)-PI(I-IBA))
      ELA=EL(I-IAA)-(DT*AAP/DXX-IAA)*(EL(I-IAA)-EL(I-IBA))
      DT1=DT
      IF (KINT.EQ.3) GO TO 871
  874 UB=UT(I+IAB)-(DT*ABP/DXX-IAB)*(UT(I+IAB)-UT(I+IBB))
      PB=P(I+IAB)-(DT*ABP/DXX-IAB)*(P(I+IAB)-P(I+IBB))
      BB=B(I+IAB)-(DT*ABP/DXX-IAB)*(B(I+IAB)-B(I+IBB))
      GAMB=GAMMA(I+IAB)-(DT*ABP/DXX-IAB)*(GAMMA(I+IAB)-GAMMA(I+IBB))
      PIB=PI(I+IAB)-(DT*ABP/DXX-IAB)*(PI(I+IAB)-PI(I+IBB))
      ELB=EL(I+IAB)-(DT*ABP/DXX-IAB)*(EL(I+IAB)-EL(I+IBB))
      DT2=DT
      GO TO 873
  870 UA=UP(I1)-DXX*(I-I1)/(DT*AAP)*(UP(I1)-UT(I1))
      BA=BP(I1)-DXX*(I-I1)/(DT*AAP)*(BP(I1)-B(I1))
      PA=PP(I1)-DXX*(I-I1)/(DT*AAP)*(PP(I1)-P(I1))
      GAMA=GAMMAP(I1)-DXX*(I-I1)/(DT*AAP)*(GAMMAP(I1)-GAMMA(I1))
      PIA=PI(I1)
      ELA=EL(I1)
      DT1=DXX*(I-I1)/AAP
      IF (KINT.EQ.4) GO TO 871
      GO TO 874
  871 UB=UP(I2)-DXX*(I2-I)/(DT*ABP)*(UP(I2)-UT(I2))
      PB=PP(I2)-DXX*(I2-I)/(DT*ABP)*(PP(I2)-P(I2))
      BB=BP(I2)-DXX*(I2-I)/(DT*ABP)*(BP(I2)-B(I2))
      GAMB=GAMMAP(I2)-DXX*(I2-I)/(DT*ABP)*(GAMMAP(I2)-GAMMA(I2))
      PIB=PI(I2)
      ELB=EL(I2)
      DT2=DXX*(I2-I)/ABP
  873 CONTINUE
      AA=WAVE(BA,PA,ELA,I)
      AB=WAVE(BB,PB,ELB,I)
      AX=AP
      CALL COEFP(UP(I),PP(I),BP(I),GAMMAP(I),PI(I),EL(I),AP,AX,CP,DP,EBF
     1P,GP,HP,I)
      CALL COEFA(UA,PA,BA,GAMA,PIA,ELA,AA,CA,DA,EBFA,GA,I)
      CALL COEFB(UB,PB,BB,GAMB,PIB,ELB,AB,CB,DB,EBFB,HB,I)
      IF (ICAV(I).EQ.1) GO TO 840
      UP(I)=(AA/CA+2.*AP/CP+AB/CB)**(-1)*((AA/CA+AP/CP)*UA+(AB/CB+AP/CP)
```

```
     1*UB*2.*(PA-PB)-DT1*(GA+GP)*DT2*(HB+HP))
      PP(I)=PB+.5*(AB/CB*AP/CP)*(UP(I)-UB)-.5*(HB+HP)*DT2
            IF ((PP(I)-EL(I)).LT.HV) GO TO 841
      GO TO 842

C     CALCULATE VAPOR CAVITY

  841 UL(I)=UT(I)
  840 PP(I)=HV+EL(I)
      ICAVP(I)=1
      UP(I)=2.*(AB/CB*AP/CP)**(-1)*(PP(I)-PB+.5*(HB+HP)*DT2)+UB
      ULP(I)=2.*(AA/CA*AP/CP)**(-1)*(-PP(I)+PA-.5*(GA+GP)*DT1)+UA
      VCAVP(I)=VCAV(I)+.5*DT*AR*(U(I)+UP(I)-UL(I)-ULP(I))
      IF (II.EQ.IT) UL(I)=ULP(I)
      IF (VCAVP(I).GT.0.0) GO TO 842
      ICAVP(I)=0
      VCAVP(I)=0.
      IF (II.EQ.IT) UL(I)=0.
      UP(I)=(AA/CA*2.*AP/CP*AB/CB)**(-1)*((AA/CA*AP/CP)*UA+(AB/CB*AP/CP)
     1*UB*2.*(PA-PB)-DT1*(GA+GP)*DT2*(HB+HP))
      PP(I)=PB+.5*(AB/CB*AP/CP)*(UP(I)-UB)-.5*(HB+HP)*DT2
      IF ((PP(I)-EL(I)).LT.HV) PP(I)=HV+EL(I)
  842 GAMMAP(I)=GAM(PP(I),EL(I),I,0,B(I))
      BP(I)=((P(I)-EL(I))/(PP(I)-EL(I)))**(1./KS)*(B(I)+R/(P(I)-EL(I))*(
     1(P(I)+EL(I))/PI(I))**(1.-1./KS)*TEMP*DT*.5*(GAMMA(I)+GAMMAP(I)))
      IF (BP(I).LT.0.0) BP(I)=0.
  860 CONTINUE
  859 CONTINUE
  702 CONTINUE
  850 CONTINUE

C     THIS SECTION ADVANCES THE PARAMETERS AND RETURNS CONTROL TO
C     THE BODY OF THE PROGRAM SUCH THAT VALUES AT A NEW TIME-STEP
C     CAN BE CALCULATED

      DO 203 I=1,NN
      P(I)=PP(I)
      B(I)=BP(I)
      U(I)=UP(I)
      VCAV(I)=VCAVP(I)
      ICAV(I)=ICAVP(I)
      A(I)=WAVE(B(I),P(I),EL(I),I)
      PR(I)=(P(I)-EL(I))*RL*G/144.
      UT(I)=U(I)
      IF (ICAV(I).EQ.1.AND.I.NE.NN) UT(I)=(U(I)+UL(I))*.5
      IF (I.EQ.1) UT(I)=U(I)
      GAMMA(I)=GAMMAP(I)
  203 CONTINUE
      IF (IPRINT.EQ.1.AND.KK/K*K.EQ.KK) GO TO 205
      IF (KK/K*K.EQ.KK) GO TO 201
      GO TO 204
  997 IF (IPLOTAV.EQ.1) CALL PLOTG(PLOTAV,TT,KKK,IBUF)
      IF (IPLOTAM.EQ.1) CALL PLOTG(PLOTAM,TT,KKK,IBUF)
      IF (IPLOTPV.EQ.1) CALL PLOTG(PLOTPV,TT,KKK,IBUF)
      IF (IPLOTPM.EQ.1) CALL PLOTG(PLOTPM,TT,KKK,IBUF)
      GO TO 998
  999 CONTINUE
      IF (MPLOT.NE.0) CALL PLOT(2.0,0.0,999)
      END
```

11

```
      FUNCTION WAVE(B,P,EL,I)

C     THIS SUBPROGRAM CALCULATES  EXISTING WAVESPEEDS

      COMMON /A/RL,KS,KL,CC,G,CCL,NN,NL
      REAL KS,KL
      C=CC
      IF (I.LE.NL.OR.I.GT.(NN-NL)) C=CCL
      WAVE=SQRT(1./(RL*(1.-B)*(1.-B)/KL+B/(KS*(P-EL)*G*RL*(1.-B))*C))
      END


      FUNCTION GAM(P,E,I,IX,B)

C     THIS SUBPROGRAM CALCULATES THE GAS PRODUCTION RATE AT A NODE
C     GIVEN THE PRESSURE.  THE TOTAL TIME OF SUPERSATURATED CONDITIONS
C     AT THE NODES ARE STORED IN THE ARRAY TX.

      COMMON/B/TS,PS,GAM2,SLOPE,DT,TX(45),GAM1,GFACTOR,HV,DSLVE
      IF ((P-E).GT.PS) GO TO 50
      IF (IX.EQ.1) TX(I)=TX(I)+DT
      GAM=(SLOPE*TX(I)+GAM1)*(PS-(P-E))
      IF (TX(I).GT.TS) GAM=GAM2*(PS-(P-E))
      IF ((P-E).LE.HV) GAM=GAM*GFACTOR
      RETURN
   50 IF (B.GT.0.0) GO TO 51
      GAM=0.0
      RETURN
   51 IF (IX.EQ.1.AND.DSLVE.NE.0.0) TX(I)=TX(I)-DT
      GAM=-(SLOPE*TX(I)+GAM1)*(PS-P+E)*DSLVE
      IF (TX(I).GT.TS) GAM=-GAM2*(PS-P+E)*DSLVE
      RETURN
      END


      SUBROUTINE COEFA(UA,PA,BA,GAMA,PIA,ELA,AA,CA,DA,EBFA,GA,I)

C     THIS SUBROUTINE CALCULATES THE COEFFICIENTS USED IN THE
C     COMPATIBILITY RELATIONS TRANSMITTED ALONG THE C PLUS CHARACTERISTIC

      COMMON /A/RL,KS,KL,CC,G,CCL,NN,NL
      COMMON/C/DD,DDL,R,TEMP,THETA
      REAL KS,KL
      DDD=DD
      IF (I.LE.NL+1.OR.I.GT.NN-NL) DDD=DDL
      CA=G*RL/(RL*(1.-BA))
      DA=UA*ABS(UA)*DDD*G*SIN(THETA)*(1.-RL/(RL*(1.-BA)))
      EBFA=-GAMA*AA*AA*R*TEMP*((PA-ELA)/PIA)**(1.-1./KS)/(G*(PA-ELA))*(1
     1.-BA)+UA*SIN(THETA)
      GA=EBFA-AA*DA/CA
      RETURN
      END
```

12

```
      SUBROUTINE COEFB(UB,PB,BB,GAMB,PIB,ELB,AB,CB,DB,EBFB,HB,I)
C     THIS SUBROUTINE CALCULATES THE COEFFICIENTS USED IN THE
C     COMPATIBILITY RELATIONS WHICH ARE TRANSMITTED ALONG THE
C     C MINUS CHARACTERISTIC
      COMMON /A/RL,KS,KL,CC,G,CCL,NN,NL
      COMMON/C/DD,DDL,R,TEMP,THETA
      REAL KS,KL
      DDB=DD
      IF (I.LT.NL+1.OR.I.GE.NN-NL) DDB=DDL
      CB=G*RL/(RL*(1.-BB))
      DB=UB*ABS(UB)*DDB+G*SIN(THETA)*(1.-RL/(RL*(1.-BB)))
      EBFB=-GAMB*AB*AB*R*TEMP*((PB-ELB)/PIB)**(1.-1./KS)/(G*(PB-ELB))*(1
     1.-BB)*UB*SIN(THETA)
      HB=EBFB*AB*DB/CB
      RETURN
      END


      SUBROUTINE COEFP(UP,PP,BP,GAMP,PIP,ELP,APA,APB,CP,DP,EBFP,GP,HP,I)
C     THIS SUBROUTINE CALCULATES THE COEFFICIENTS USED IN THE
C     COMPATIBILITY EQUATIONS OF THE NODE BEING SOLVED DURING THE
C     SECOND-ORDER PROCESS
      COMMON /A/RL,KS,KL,CC,G,CCL,NN,NL
      COMMON/C/DD,DDL,R,TEMP,THETA
      REAL KS,KL
      DDA=DD
      DDB=DD
      IF (I.LE.NL+1.OR.I.GT.NN-NL) DDA=DDL
      IF (I.LT.NL+1.OR.I.GE.NN-NL) DDB=DDL
      CP=G*RL/(RL*(1.-BP))
      DPA=UP*ABS(UP)*DDA+G*SIN(THETA)*(1.-RL/(RL*(1.-BP)))
      DPB=UP*ABS(UP)*DDB+G*SIN(THETA)*(1.-RL/(RL*(1.-BP)))
      EBFPA=-GAMP*APA*APA*R*TEMP*((PP-ELP)/PIP)**(1.-1./KS)/(G*(PP-ELP))
     1*(1.-BP)*UP*SIN(THETA)
      EBFPB=-GAMP*APB*APB*R*TEMP*((PP-ELP)/PIP)**(1.-1./KS)/(G*(PP-ELP))
     1*(1.-BP)*UP*SIN(THETA)
      GP=EBFPA-APA*DPA/CP
      HP=EBFPB-APB*DPB/CP
      EBFP=EBFPA
      RETURN
      END


      SUBROUTINE PLOTG (P,T,K,IBUF)
C     THIS SUBROUTINE HANDLES THE CALCOMP PLOTTING OF DESIRED VARIABLES
      DIMENSION P(250),T(250),IBUF(257)
      CALL SCALE (T,8.0,K,1)
      CALL SCALE (P,5.0,K,1)
      CALL AXIS (0.0,0.0,15HTIME IN SECONDS,-15,8.0,0.0,T(K+1),T(K+2))
      CALL AXIS (0.0,0.0,2H  ,2,5.0,90.0,P(K+1),P(K+2))
      CALL LINE (T,P,K,1,0,0)
      CALL PLOT (10.0,0.0,-3)
      RETURN
      END
```

13

COPPER LENGTH	L	.4020E+03
PIPE DIAMETER	D	.8290E-01
PIPE WALL THICKNESS	TH	.5320E-02
PIPE MODULUS	EP	.244AE+10
PIPE CONSTRAINT PARAMETER	C1	.9000E+00
COPPER FRICTION COEFF	F	.2900E-01
FLUID MODULUS OF ELASTICITY	KL	.4470E+08
FLUID DENSITY	RL	.1938E+01
POLYTROPIC GAS CONSTANT	KS	.1000E+01
REFERENCE PRESSURE	P0	.5820E+02
REFERENCE VELOCITY	U0	.2500E+01
REFERENCE VOID FRACTION	B0	0.
TIME INCREMENT	DT	.4937E-02
MAXIMUM TIME	TMAX	.4000E+01
REACHES OF COPPER	N	38
NO. OF TIME INCREMENTS PER PRINTOUT	K	10
NO. OF ITERATIONS IN 2ND ORDER PROCESS	IT	1
TIME OF CLOSURE	TC	0.
GRAVITY	G	.322E+02
ATMOSPHERE PRESSURE	PATM	.324E+02
VAPOR PRESSURE	HV	.570E+00
PIPE ANGLE	THETA	.650E-02
TEMPERATURE	TEMP	.519E+03
LUCITE WALL THICKNESS	THL	.211E-01
LUCITE PIPE MODULUS	EPL	.511E+08
LUCITE CONSTRAINT PARAMETER	C2	.860E+00
LENGTH OF LUCITE	LL	.122E+02
LUCITE FRICTION FACTOR	FL	.270E-01
NUMBER OF LUCITE REACHES	NL	2
GAS CONSTANT	R	.181E+02
GAMMA TIME PARAMETER	TS	.400E+01
SATURATION PRESSURE	PS	.1875E+02
INITIAL GAMMA	GAM1	.3500E-07
GAMMA AT TS	GAM2	.1000E-06
GAMMA FACTOR	GFACTOR	.1000E+01
SOLUTION FACTOR	DSLVE	0.

COMPUTED VALUES OF PRESSURE, VELOCITY, VOID FRACTION AND WAVE SPEED

UNITS - PRESSURE LB/SQ.IN. ABSOLUTE
- VELOCITY FT/SEC
-WAVE SPEED FT/SEC

SECOND ORDER ACCURACY
VALVE UPSTREAM

ELEVATIONS ALONG PIPE

0.00	0.00	0.00	.11	.22	.33	.44	.55	.66	.77
.88	.99	1.10	1.21	1.32	1.43	1.54	1.65	1.76	1.87
1.98	2.09	2.20	2.30	2.41	2.52	2.63	2.74	2.85	2.96
3.07	3.18	3.29	3.40	3.51	3.62	3.73	3.84	3.95	4.06
4.17	4.17	0.00							

T=0.
P= .3147E+02 .3029E+02 .2886E+02 .2744E+02 .2602E+02 .2460E+02 .2522E+02
U= .2500E+01 .2500E+01 .2500E+01 .2500E+01 .2500E+01 .2500E+01 .2500E+01
B=0. 0. 0. 0. 0. 0. 0.
A= .2415E+04 .4285E+04 .4285E+04 .4285E+04 .4285E+04 .4285E+04 .2415E+04

CAVITY OPENS AT TIME= .494E-02

T= .4937E-01
P= .2470E+00 .2525E+01 .3298E+01 .2744E+02 .2602E+02 .2460E+02 .2522E+02
U= .1491E+01 .1977E+01 .2039E+01 .2500E+01 .2500E+01 .2500E+01 .2500E+01
B= .4974E-03 .1562E-04 .2977E-050. 0. 0. 0.
A= .1915E+03 .2695E+04 .3875E+04 .4285E+04 .4285E+04 .4285E+04 .2415E+04

UL=0. 0. 0. 0. 0. 0. 0.
V= .3730E-030. 0. 0. 0. 0. 0.

```
T= .9874E-01
P= .2470E+00 .1489E+01 .2530E+01 .2800E+01 .2995E+01 .3627E+01 .2522E+02
U= .1501E+01 .1860E+01 .1969E+01 .2023E+01 .2072E+01 .2125E+01 .2500E+01
B= .1032E-02 .9512E-04 .3911E-04 .2316E-04 .1160E-04 .2220E-050.
A= .1331E+03 .1046E+04 .1952E+04 .2456E+04 .3063E+04 .3994E+04 .2415E+04

UL=0.        0.        0.        0.        0.        0.        0.
 V= .7741E-030.        0.        0.        0.        0.        0.

T= .1481E+00
P= .2470E+00 .1143E+01 .2088E+01 .2642E+01 .2009E+02 .2070E+02 .2522E+02
U= .1462E+01 .1744E+01 .1883E+01 .1961E+01 .1591E+01 .1641E+01 .1640E+01
B= .1579E-02 .2254E-03 .9451E-04 .5869E-04 .5362E-05 .1840E-050.
A= .1077E+03 .6077E+03 .1228E+04 .1682E+04 .4151E+04 .4239E+04 .2415E+04

UL=0.        0.        0.        0.        0.        0.        0.
 V= .1169E-020.        0.        0.        0.        0.        0.


T= .1975E+00
P= .2470E+00 .1036E+01 .1856E+01 .1490E+02 .1836E+02 .2099E+02 .2522E+02
U= .1413E+01 .1649E+01 .1801E+01 .1462E+01 .1473E+01 .1464E+01 .1468E+01
B= .2138E-02 .1468E-03 .1635E-03 .1387E-04 .5867E-05 .1815E-050.
A= .9256E+02 .4555E+03 .8981E+03 .3864E+04 .4125E+04 .4240E+04 .2415E+04

UL=0.        0.        0.        0.        0.        0.        0.
 V= .1552E-020.        0.        0.        0.        0.        0.

T= .2469E+00
P= .2470E+00 .9953E+00 .1004E+02 .1374E+02 .1639E+02 .1978E+02 .2522E+02
U= .1358E+01 .1565E+01 .1245E+01 .1265E+01 .1271E+01 .1280E+01 .1282E+01
B= .2709E-02 .5082E-03 .3322E-04 .1505E-04 .6573E-05 .1926E-050.
A= .8226E+02 .3800E+03 .3178E+04 .3801E+04 .4087E+04 .4235E+04 .2415E+04

UL=0.        0.        0.        0.        0.        0.        0.
 V= .1922E-020.        0.        0.        0.        0.        0.

T= .2962E+00
P= .2470E+00 .5639E+01 .8636E+01 .1225E+02 .1633E+02 .2008E+02 .2522E+02
U= .1299E+01 .1036E+01 .1063E+01 .1061E+01 .1056E+01 .1059E+01 .1072E+01
B= .3292E-02 .1039E-03 .3862E-04 .1688E-04 .6598E-05 .1897E-050.
A= .7464E+02 .1818E+04 .2954E+04 .3701E+04 .4086E+04 .4236E+04 .2415E+04

UL=0.        0.        0.        0.        0.        0.        0.
 V= .2276E-020.        0.        0.        0.        0.        0.

T= .3456E+00
P= .2470E+00 .5195E+01 .9083E+01 .1237E+02 .1634E+02 .2000E+02 .2522E+02
U= .1204E+01 .8578E+00 .8505E+00 .8559E+00 .8476E+00 .8466E+00 .8448E+00
B= .3884E-02 .1229E-03 .3671E-04 .1672E-04 .6591E-05 .1905E-050.
A= .6870E+02 .1638E+04 .3031E+04 .3710E+04 .4086E+04 .4236E+04 .2415E+04

UL=0.        0.        0.        0.        0.        0.        0.
 V= .2611E-020.        0.        0.        0.        0.        0.

T= .3950E+00
P= .2470E+00 .5515E+01 .9248E+01 .1299E+02 .1669E+02 .2028E+02 .2522E+02
U= .8699E+00 .6579E+00 .6506E+00 .6660E+00 .6458E+00 .6457E+00 .6451E+00
B= .4492E-02 .1250E-03 .3604E-04 .1592E-04 .6457E-05 .1878E-050.
A= .6390E+02 .1668E+04 .3058E+04 .3754E+04 .4094E+04 .4237E+04 .2415E+04

UL=0.        0.        0.        0.        0.        0.        0.
 V= .2904E-020.        0.        0.        0.        0.        0.

T= .4443E+00
P= .2470E+00 .5453E+01 .9516E+01 .1310E+02 .1657E+02 .2020E+02 .2522E+02
U= .5913E-01 .4313E+00 .4492E+00 .4505E+00 .4495E+00 .4497E+00 .4484E+00
B= .5114E-02 .1354E-03 .3505E-04 .1578E-04 .6502E-05 .1865E-050.
A= .5991E-02 .1604E+04 .3101E+04 .3762E+04 .4091E+04 .4237E+04 .2415E+04

UL=0.        0.        0.        0.        0.        0.        0.
 V= .3028E-020.        0.        0.        0.        0.        0.
```

```
T= .4937E+00
P= .2470E+00 .4245E+01 .8520E+01 .1263E+02 .1655E+02 .2030E+02 .2522E+02
U=-.2529E+00 .1840E+00 .2333E+00 .2463E+00 .2531E+00 .2551E+00 .2560E+00
B= .5740E-02 .1869E-03 .3914E-04 .1437E-04 .6509E-05 .1676E-050.
A= .5653E+02 .1237E+04 .2933E+04 .3729E+04 .4091E+04 .4237E+04 .2415E+04

UL=0.        0.        0.        0.        0.        0.        0.
 V= .3000E-020.        0.        0.        0.        0.        0.

T= .5431E+00
P= .2470E+00 .3365E+01 .7281E+01 .1125E+02 .1528E+02 .1952E+02 .2522E+02
U=-.4427E+00-.3909E-01 .1400E-01 .2754E-01 .3846E-01 .4502E-01 .4719E-01
B= .6382E-02 .2642E-03 .4658E-04 .1838E-04 .7050E-05 .1951E-050.
A= .5361E+02 .9468E+03 .2667E+04 .3617E+04 .4060E+04 .4233E+04 .2415E+04

UL=0.        0.        0.        0.        0.        0.        0.
 V= .2905E-020.        0.        0.        0.        0.        0.

T= .5924E+00
P= .2470E+00 .2943E+01 .6544E+01 .1059E+02 .1492E+02 .1939E+02 .2522E+02
U=-.5902E+00-.2390E+00-.1904E+00-.1591E+00-.1920E+00-.1944E+00-.1953E+00
B= .7034E-02 .3366E-03 .5531E-04 .1953E-04 .7222E-05 .1965E-050.
A= .5106E+02 .7921E+03 .2436E+04 .3551E+04 .4050E+04 .4232E+04 .2415E+04

UL=0.        0.        0.        0.        0.        0.        0.
 V= .2767E-020.        0.        0.        0.        0.        0.

T= .6418E+00
P= .2470E+00 .2759E+01 .6954E+01 .1122E+02 .1550E+02 .1970E+02 .2522E+02
U=-.7294E+00-.4241E+00-.4114E+00-.4184E+00-.4226E+00-.4249E+00-.4256E+00
B= .7701E-02 .3988E-03 .5695E-04 .1842E-04 .6950E-05 .1934E-050.
A= .4881E+02 .7071E+03 .2454E+04 .3614E+04 .4066E+04 .4234E+04 .2415E+04

UL=0.        0.        0.        0.        0.        0.        0.
 V= .2592E-020.        0.        0.        0.        0.        0.

T= .6912E+00
P= .2470E+00 .2968E+01 .7343E+01 .1155E+02 .1568E+02 .1978E+02 .2522E+02
U=-.8431E+00-.6327E+00-.6410E+00-.6426E+00-.6425E+00-.6421E+00-.6419E+00
B= .8237E-02 .4683E-03 .5560E-04 .1790E-04 .6870E-05 .1926E-050.
A= .4679E+02 .7244E+03 .2529E+04 .3644E+04 .4071E+04 .4235E+04 .2415E+04

UL=0.        0.        0.        0.        0.        0.        0.
 V= .2344E-020.        0.        0.        0.        0.        0.

T= .7405E+00
P= .2470E+00 .3388E+01 .7484E+01 .1153E+02 .1561E+02 .1973E+02 .2522E+02
U=-.9639E+00-.8607E+00-.8569E+00-.8571E+00-.8572E+00-.8573E+00-.8573E+00
B= .9058E-02 .3869E-03 .5634E-04 .1793E-04 .6899E-05 .1931E-050.
A= .4498E+02 .7908E+03 .2534E+04 .3642E+04 .4069E+04 .4234E+04 .2415E+04

UL=0.        0.        0.        0.        0.        0.        0.
 V= .2143E-020.        0.        0.        0.        0.        0.

T= .7899E+00
P= .2470E+00 .3630E+01 .7622E+01 .1167E+02 .1573E+02 .1979E+02 .2522E+02
U=-.1089E+01-.1070E+01-.1064E+01-.1067E+01-.1068E+01-.1069E+01-.1069E+01
B= .9769E-02 .3905E-03 .5681E-04 .1772E-04 .6849E-05 .1925E-050.
A= .4334E+02 .8159E+03 .2542E+04 .3654E+04 .4072E+04 .4235E+04 .2415E+04

UL=0.        0.        0.        0.        0.        0.        0.
 V= .1870E-020.        0.        0.        0.        0.        0.

T= .8393E+00
P= .2470E+00 .3819E+01 .7859E+01 .1188E+02 .1588E+02 .1987E+02 .2522E+02
U=-.1225E+01-.1271E+01-.1269E+01-.1271E+01-.1272E+01-.1273E+01-.1273E+01
B= .1044E-01 .3966E-03 .5608E-04 .1746E-04 .6782E-05 .1917E-050.
A= .4184E+02 .8297E+03 .2578E+04 .3672E+04 .4076E+04 .4235E+04 .2415E+04

UL=0.        0.        0.        0.        0.        0.        0.
 V= .1562E-020.        0.        0.        0.        0.        0.
```

```
T= .8887E+00
P= .2470E+00 .4031E+01 .8036E+01 .1200E+02 .1595E+02 .1989E+02 .2522E+02
U=-.1400E+01-.1470E+01-.1467E+01-.1468E+01-.1469E+01-.1469E+01-.1469E+01
B= .1121E-01 .3994E-03 .5527E-04 .1723E-04 .6755E-05 .1915E-050.
A= .4046E+02 .8489E+03 .2608E+04 .3681E+04 .4077E+04 .4235E+04 .2415E+04

UL=0.          0.        0.        0.        0.        0.        0.
 V= .1213E-020.          0.        0.        0.        0.        0.

T= .9390E+00
P= .2470E+00 .4184E+01 .8137E+01 .1207E+02 .1599E+02 .1991E+02 .2522E+02
U=-.1622E+01-.1665E+01-.1658E+01-.1659E+01-.1659E+01-.1659E+01-.1659E+01
B= .1194E-01 .4057E-03 .5467E-04 .1713E-04 .6737E-05 .1913E-050.
A= .3920E+02 .8567E+03 .2627E+04 .3687E+04 .4078E+04 .4235E+04 .2415E+04

UL=0.          0.        0.        0.        0.        0.        0.
 V= .8111E-030.          0.        0.        0.        0.        0.

T= .9874E+00
P= .2470E+00 .4243E+01 .8201E+01 .1213E+02 .1604E+02 .1994E+02 .2522E+02
U=-.1667E+01-.1853E+01-.1842E+01-.1843E+01-.1843E+01-.1843E+01-.1843E+01
B= .1265E-01 .4225E-03 .5429E-04 .1705E-04 .6718E-05 .1911E-050.
A= .3802E+02 .8468E+03 .2640E+04 .3692E+04 .4079E+04 .4235E+04 .2415E+04

UL=0.          0.        0.        0.        0.        0.        0.
 V= .3443E-030.          0.        0.        0.        0.        0.

CAVITY CLOSES AT TIME=  .102E+01

T= .1037E+01
P= .1871E+02 .4221E+01 .8200E+01 .1213E+02 .1604E+02 .1994E+02 .2522E+02
U=0.          -.2037E+01-.2021E+01-.2021E+01-.2020E+01-.2020E+01-.2020E+01
B= .1747E-03 .4469E-03 .5428E-04 .1705E-04 .6716E-05 .1910E-050.
A= .1835E+04 .8225E+03 .2640E+04 .3692E+04 .4079E+04 .4235E+04 .2415E+04

T= .1084E+01
P= .7102E+02 .6751E+02 .8111E+01 .1206E+02 .1599E+02 .1992E+02 .2522E+02
U=0.          -.3408E+00-.2194E+01-.2193E+01-.2192E+01-.2192E+01-.2192E+01
B= .4601E-04 .2896E-04 .5489E-04 .1715E-04 .6737E-05 .1912E-050.
A= .2356E+04 .4075E+04 .2622E+04 .3686E+04 .4078E+04 .4235E+04 .2415E+04

T= .1136E+01
P= .1104E+03 .1107E+03 .1087E+03 .1028E+03 .1591E+02 .1988E+02 .2522E+02
U=0.          -.3258E+00-.5126E+00-.7485E+00-.2360E+01-.2359E+01-.2359E+01
B= .2950E-04 .1767E-04 .4096E-05 .2012E-05 .6770E-05 .1916E-050.
A= .2390E+04 .4203E+04 .4265E+04 .4275E+04 .4076E+04 .4235E+04 .2415E+04

T= .1185E+01
P= .1425E+03 .1413E+03 .1390E+03 .1318E+03 .1267E+03 .1106E+03 .2522E+02
U=0.          -.1378E+00-.2577E+00-.4611E+00-.6191E+00-.6070E+00 .1378E+01
B= .2293E-04 .1364E-04 .3204E-05 .1566E-05 .8504E-06 .3444E-060.
A= .2400E+04 .4234E+04 .4273E+04 .4279E+04 .4282E+04 .4284E+04 .2415E+04

T= .1234E+01
P= .1574E+03 .1568E+03 .1557E+03 .5715E+02 .5257E+02 .3835E+02 .2522E+02
U=0.          -.9846E-01-.1814E+00 .1426E+01 .1358E+01 .1399E+01 .1438E+01
B= .2076E-04 .1247E-04 .2859E-05 .3618E-05 .2047E-05 .9933E-060.
A= .2402E+04 .4244E+04 .4275E+04 .4252E+04 .4265E+04 .4272E+04 .2415E+04

T= .1284E+01
P= .5727E+02 .8070E+02 .6286E+02 .5074E+02 .3930E+02 .2983E+02 .2522E+02
U=0.          .1679E+01 .1706E+01 .1814E+01 .1907E+01 .1960E+01 .1968E+01
B= .5706E-04 .2423E-04 .7082E-05 .4075E-05 .2741E-05 .1277E-050.
A= .2326E+04 .4135E+04 .4227E+04 .4243E+04 .4249E+04 .4263E+04 .2415E+04
```

```
T= .1333E+01
P= .6045E+01 .6198E+01 .9480E+01 .3668E+02 .3841E+02 .2873E+02 .2522E+02
U=0.         .7145E+00 .1430E+01 .2138E+01 .2292E+01 .2232E+01 .2234E+01
B= .5419E-03 .3161E-03 .4696E-04 .5636E-05 .2804E-05 .1326E-050.
A= .8519E+03 .1162E+04 .2873E+04 .4206E+04 .4247E+04 .4261E+04 .2415E+04

T= .1382E+01
P= .3101E+01 .2460E+01 .2180E+01 .2337E+01 .2639E+01 .4069E+01 .2522E+02
U=0.         .7205E+00 .1330E+01 .1581E+01 .1795E+01 .2040E+01 .2579E+01
B= .1087E-02 .8402E-03 .2458E-03 .1093E-03 .5044E-04 .1109E-040.
A= .4523E+03 .4637E+03 .7975E+03 .1209E+04 .1791E+04 .3312E+04 .2415E+04

T= .1432E+01
P= .2073E+01 .1659E+01 .1442E+01 .1451E+01 .1298E+01 .1664E+02 .2522E+02
U=0.         .7321E+00 .1289E+01 .1544E+01 .1759E+01 .1378E+01 .1341E+01
B= .1693E-02 .1339E-02 .4720E-03 .2531E-03 .1870E-03 .5316E-050.
A= .2993E+03 .3022E+03 .4736E+03 .6452E+03 .7004E+03 .4125E+04 .2415E+04

T= .1481E+01
P= .1582E+01 .1316E+01 .1197E+01 .1220E+01 .1418E+02 .1892E+02 .2522E+02
U=0.         .7292E+00 .1252E+01 .1508E+01 .1068E+01 .1066E+01 .1056E+01
B= .2317E-02 .1813E-02 .6997E-03 .4013E-03 .1950E-04 .4675E-050.
A= .2243E+03 .2319E+03 .3554E+03 .4724E+03 .3702E+04 .4160E+04 .2415E+04

T= .1530E+01
P= .1304E+01 .1128E+01 .1082E+01 .1081E+02 .1535E+02 .1941E+02 .2522E+02
U=0.         .7179E+00 .1217E+01 .8203E+00 .8151E+00 .8095E+00 .8069E+00
B= .2937E-02 .2272E-02 .9666E-03 .4933E-04 .1801E-04 .4558E-050.
A= .1913E+03 .1919E+03 .2940E+03 .2937E+04 .3773E+04 .4166E+04 .2415E+04

T= .1580E+01
P= .1134E+01 .1011E+01 .5287E+01 .1193E+02 .1600E+02 .2005E+02 .2522E+02
U=0.         .7015E+00 .6633E+00 .5898E+00 .5880E+00 .5861E+00 .5895E+00
B= .3541E-02 .2719E-02 .2183E-03 .4475E-04 .1728E-04 .4412E-050.
A= .1599E+03 .1662E+03 .1280E+04 .3087E+04 .3807E+04 .4173E+04 .2415E+04

T= .1629E+01
P= .1019E+01 .9329E+00 .7338E+01 .1143E+02 .1544E+02 .1959E+02 .2522E+02
U=0.         .6818E+00 .3520E+00 .3594E+00 .3665E+00 .3714E+00 .3718E+00
B= .4124E-02 .3143E-02 .1603E-03 .4668E-04 .1791E-04 .4515E-050.
A= .1353E+03 .1484E+03 .1694E+04 .3023E+04 .3778E+04 .4168E+04 .2415E+04

T= .1679E+01
P= .9378E+00 .8921E+00 .7402E+01 .1123E+02 .1529E+02 .1956E+02 .2522E+02
U=0.         .6513E+00 .1504E+00 .1490E+00 .1438E+00 .1415E+00 .1442E+00
B= .4681E-02 .3502E-02 .1614E-03 .4752E-04 .1804E-04 .4522E-050.
A= .1219E+03 .1375E+03 .1695E+04 .2996E+04 .3770E+04 .4168E+04 .2415E+04

T= .1728E+01
P= .8779E+00 .1268E+01 -.7746E+01 -.1165E+02 -.1594E+02 -.1985E+02 -.2522E+02
U=0.         .4244E+00-.5618E-01-.7173E-01-.7685E-01-.8004E-01-.7857E-01
B= .5212E-02 .2616E-02 .1563E-03 .4505E-04 .1734E-04 .4497E-050.
A= .1119E+03 .1896E+03 .1752E+04 .3077E+04 .3804E+04 .4171E+04 .2415E+04

T= .1777E+01
P= .8368E+00 .3629E+01 .8478E+01 .1243E+02 .1627E+02 .2003E+02 .2522E+02
U=0.        -.1395E+00-.2755E+00-.2835E+00-.2863E+00-.2864E+00-.2879E+00
B= .5716E-02 .4605E-03 .1431E-03 .4294E-04 .1699E-04 .4417E-050.
A= .1042E+03 .5252E+03 .1865E+04 .3147E+04 .3820E+04 .4173E+04 .2415E+04

T= .1827E+01
P= .8055E+00 .5007E+01 .8962E+01 .1267E+02 .1636E+02 .2010E+02 .2522E+02
U=0.        -.4296E+00-.4411E+00-.4851E+00-.4872E+00-.4873E+00-.4880E+00
B= .6189E-02 .7149E-03 .1353E-03 .4212E-04 .1690E-04 .4401E-050.
A= .9625E+02 .7114E+03 .1970E+04 .3175E+04 .3825E+04 .4174E+04 .2415E+04

T= .1876E+01
P= .7854E+00 .5711E+01 .9331E+01 .1295E+02 .1653E+02 .2019E+02 .2522E+02
U=0.        -.6405E+00-.6740E+00-.6796E+00-.6820E+00-.6834E+00-.6835E+00
B= .6609E-02 .6402E-03 .1300E-03 .4121E-04 .1673E-04 .4382E-050.
A= .9389E+02 .7995E+03 .2033E+04 .3206E+04 .3833E+04 .4175E+04 .2415E+04
```